(2)

Naval Oceanographic and
Atmospheric Research Laboratory

Technical Note 79
October 1990

Computer Modeling of Direct Path, Backscattered Bottom Reverberations for the Acoustic Reverberation Special Research Program (ARSRP)

A. K. Kalra
Ocean Acoustics Division
Ocean Acoustics and Technology Directorate

ABSTRACT

Quasi-monostatic reverberations, in the general vicinity of the Atlantic natural laboratory area for the Acoustic Reverberation Special Research Program (ARSRP), are simulated using RASP (Range-dependent Active System Performance) modeling code. They are discussed in the context of the bathymetric profiles and lithology, and the short range experiment planned in FY93.

ACKNOWLEDGMENTS

This work was supported by the Office of Naval Research under the Program Element 601153N and the Program Manager Marshall Orr. I also want to acknowledge the helpful assistance received from Jim Fulford at NOARL in the running of the RASP modeling program.

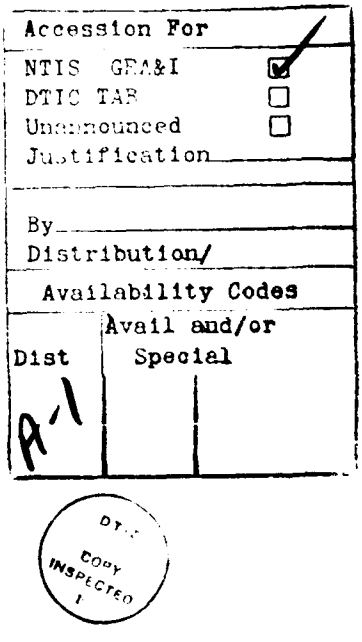

Computer Modeling of Direct Path, Backscattered Bottom Reverberations for the Acoustic Reverberation Special Research Program (ARSRP)

INTRODUCTION

The Bottom/Subbottom Special Research Project of the Acoustic Reverberation Special Research Program (ARSRP) is planning to collect, and later interpret the low-frequency (50-500 Hz), low-grazing angle (±15°) backscattered bottom/subbottom reverberation data in the Atlantic natural laboratory. Although the specific location of the natural laboratory has not been decided, it will be located between the Bermuda Rise and the Mid-Atlantic Ridge (MAR). We have modeled the quasi-monostatic, bottom surface reverberation responses for different bathymetric profiles, within the above mentioned general area of the Atlantic natural laboratory, in order to facilitate the design of the reverberation experiment planned in FY93.

The study of the reverberation field for the ARSRP objectives has been divided into three distinct ranges: long, intermediate, and short. The intermediate scale is set at a range of approximately 1/2 of a convergence zone distance. The long ranges are of the order of 1000 km, and the short range is close enough to the scattering region (5x5 km^2) to study the scattering processes as close to its source as possible. The short range studies correspond to the direct or pure path reverberations. The direct path defines the propagation paths that preclude interaction with the sea surface and minimize the effect of bulk variability within the water column.

The modeled reverberation studies described here are for the short range situations. Consequently, the bottom reverberations are simulated for the sensors located close to the reverberation patch (5x5 km area).

THE PROPOSED EXPERIMENT

The bottom reverberation data are to be acquired with four identical, high resolution, vertical hydrophone arrays moored at the bottom, about 150 m from the seafloor. Each array consists of 64

elements, is cut for 300 Hz, and has a 3-dB beamwidth of approximately 2°. The exact locations of the four vertical arrays with respect to the 5x5 km scattering area has not been determined.

The reverberation data simulated here are for only one receiver array located at the end of the bathymetric profiles. The responses are simulated for receiver-array steering angles of 2, 6, and 10°. They will correspond to the grazing angles for the horizontal interface in a constant velocity medium. This is not the case here.

THE SIMULATION EXAMPLES

The modeling program used for the simulations of the backscattered reverberation data was RASP (Range-dependent Active System Performance). It was originally coded at the Naval Research Laboratory (NRL), and the Naval Oceanographic and Atmospheric Research Laboratory (NOARL) has a useable version of this program.

As suggested above, RASP can handle a range-dependent environment but only for the monostatic and quasi-monostatic situations. Quasi-monostatic implies the source and receiver at different depths but at the same areal location. This code can also generate the reverberation data for bistatic configurations but, at the time of this writing, for the range-independent environments only.

Figure 1 is the flow diagram of the RASP modeling program.

The quasi-monostatic (different source/receiver depths) backscattered reverberations were simulated for three different bathymetric profiles and two different lithologies (rock and clay). These simulations were for the short range experiment (receivers close to the scattering area). The responses for the sand-type lithologies were also generated but the reverberation levels for sands were close, and similar to those of rock types, and consequently are not included here.

The three bathymetric profiles used for simulations were the flat/dipping interfaces, bathymetric depression and bathymetric high. These profiles were located as follows (see Figure 2):

1. Flat/Dipping Interface: the constant bathymetry and sound speed profiles were those located at (27,-48). The dipping

interfaces considered were ±1° and -3° only (+ is downdip and - is updip when viewed from receiver location).

2. Bathymetric Depression: this profile runs N-S with the corresponding extreme points located at (26.5,-48) and (27.5,-48). The vertical receiver array was situated at the south and north ends of this profile, simulating two sets of the data.

3. Bathymetric high: this profile runs W-E with the extreme points located at (26.7,-48.5) and (26.7,-47.5). The vertical receiver array was situated at the east and west ends of this profile, simulating two sets of the data.

The bathymetry profiles were approximately 50 to 60 nmi (92.6 to 111.12 km) in length. The sound profiles used were 'summer profiles' strictly valid during months of July, August, and September.

An identical bottom loss profile (required input to the RAYACT module in Figure 1) was used for all simulation runs.

For all simulation examples below, the source is a deep towed omnidirectional pulse with the center frequency of 450 Hz, bandwidth of 400 Hz, pulse length of 0.125 s and the source level of 205 dB. This is different from the DTAGS (Deep Towed Acoustical and Geophysical System) source which radiates a frequency modulated signal. Consequently, the responses generated here are broadband responses that are not match filtered with the source. The match filtered response, which will be the case for the DTAGS source, will have higher gains than those reported here. The receiver is the 64-element vertical array moored at the bottom, as discussed earlier.

The ambient noise indicated on the simulation results are underestimated by about 10 dB from the true values.

All the simulated (reverberation level) responses show the bottom, surface, and ambient noise reverberation levels separately on the same plot, although only the bottom reverberation characteristics, in terms of the bathymetry and rock types, are discussed. In actuality, a summation of these responses are observed. Whereas no suggestion is made on how to filter out the surface reverberation

from the bottom, it is assumed that the air/water (surface) reverberation will be eliminated (or greatly reduced) in processing so that only the direct path bottom reverberations are discussed further.

1. Horizontal/Dipping Interfaces:

The first example is the simple case of a flat horizon with an identical sound profile for all ranges, as indicated in Figure 3. The source is located at a distance of 300 m and the center of the receiver array is at 150 m from the seafloor (indicated by S, R). These locations were chosen to generate backscattered reverberations within the ±15° grazing angles. The constant water depth is 4978 m. The simulated direct path reverberations (surface and bottom) for rock-type bottom and the receiver beam steering angles of +2, +6 and +10° (towards the bottom) are respectively shown in Figures 4, 5, and 6. As mentioned earlier, these beam or steering angles will be identical to the grazing angles for the horizontal interface in a constant velocity medium.

It is hard to identify any well defined features of the bottom reverberation response for the receiver array beam angle of +2° in Figure 4, but those of Figures 5 and 6 (corresponding to the receiver beam angles of +6° and +10°, respectively) appear to represent the projection (on the flat horizon) of the unshaded receiver responses for steering angles of +6° and +10°. It is easier to recognize such a projection for the beam angle of 10° (Figure 6). The main lobe of the response in Figure 6 is located at about 1.19 s (two-way time); this is somewhat greater than the calculated time of 1.17 s, based on the straight line path. The higher time of 1.19 s is due to the curved propagation path in actuality, for the sound profile used. The first sidelobe at about 0.9 s is approximately 13 dB less than the peak value of 104 dB (at 1.19 s). This agrees with the expected beam pattern of an unshaded receiver array, as is the case here.

The set of Figures 7, 8, and 9 are the corresponding reverberation levels for the bottom sediments of clay-type lithology. They are very much similar to those of rock, as discussed above, but the reverberation levels are much reduced for the clays. They are about 5 to 15 dB less in comparison to those due to the sands. This is due to the reduced scattering strengths for the clay lithologies as compared to the rocks.

Figures 10, 11, and 12 are reverberation levels simulated for the inclined rock bottom interface with an up-dip gradient of 1°, for the receiver array beam angles of +2, +6 and +10°. These are very similar to the patterns of Figures of 4, 5, and 6 (for horizontal interface) except that the reverberation peaks now are narrower in width and somewhat higher in their magnitudes (dB levels). The same is true for the 3° up-dip rock-bottom interface case (Figures 13, 14, and 15). Note that the maximum dB scale for the updip cases is higher (110 dB) than that for the horizontal interface simulations (Figures 4, 5, and 6).

Figures 16, 17, and 18 are the corresponding reverberation levels simulated for the 1° down-dip rock interface. As can be expected, these responses are somewhat distorted (flattened out) as compared to the horizontal interface (Figures 4, 5, and 6). This is again an expected result due to the projection of the receiver array beam patterns onto a down dipping interface.

2. Bathymetric Depression Profile:

This profile (Figure 19) is the true dBdB5 bathymetry profile running N-S between the end points located at (27.5,-48) at the north and (26.5,-48) at the south. There are two sets of simulations generated for this profile; one with the source and receiver array located at the south end (26.5,-48) and second located at the north end (27.7,-48). The omnidirectional source and the center of the receiver array for both of these cases are located at water depths of 3700 and 3850 m respectively, once at the south end and then at the north end of this profile. They are at the vertical distance of 317 and 167 m from the shallowest point in the bathymetry profile (the south most point).

We will first consider the case with the source and receiver located at the south end of the profile. The bathymetric profile, as shown in Figure 19, represents a depression in the middle of the profile.

Figures 20, 21, and 22 are the bottom and surface reverberation responses for the receiver beam angles of +2, +6 and +10° (towards the seafloor) for the rock lithology. The bottom reverberation for all the receiver beam angles (2, 6, and 10°) are very similar to that for the flat cases of Figures 4, 5, and 6, respectively. This should not be surprising as all these beams (2, 6, and 10°) do traverse the flat portion of the bathymetry in Figure 19.

The corresponding responses for the clay lithology are shown in Figures 23, 24, and 25. They are lower by about 15 dB in magnitude in comparison to the responses for the rock lithology but otherwise are quite similar.

Next we consider the responses for the identical bathymetric profile to that of Figure 19 but now the omnidirectional source and receiver array are located at the north end of this profile. Although the source and receiver are at the same water depths, the steered receiver array senses the reverberations from an entirely different patch. Consequently, we will expect the responses to be very different. The bathymetry profile along with the source/receiver locations (S,R) are indicated in Figure 26.

Figures 27, 28, and 29 are the reverberation responses at 2, 6, and 10° receiver-array beam angles for the rock-type material. Only the 10° (Figure 29) response indicates the recognizable projection of the beam pattern of the receiver array; the 2 and 6° responses bear no resemblance to the receiver beam pattern. This is principally due to the fact that the direct-path returns from 2 and 6° angles take longer than the 10 s two-way time plotted on these figures. The responses at times less than the 10 s (in Figures 27 and 28) are the side-lobe returns of the array receiver beam patterns. For example, the reverberation return time for the main lobe of 6° beam is calculated to be around 12 s, and consequently we do not observe its return within the 10 s time window plotted in Figure 28.

The reverberation response of Figure 29 (steering angle of 10°) is still the projection of the receiver beam pattern on the bathymetry but now the receiver, although located at the same water depth, is farther from the illuminated footprint due to depression in the bathymetric profile. In addition, the illuminated patch is sloping away (downdip) from the receiver array. This results in a response which is somewhat wider than can be expected from a horizontal interface (compare Figure 29 with that of Figure 6).

The reverberation response is then characteristic of the specific bathymetry as seen by the receiver beam pattern. This is so because the source is considered to be an omnidirectional. If the source was also an array then the response will be the combination of the projections of the two beam patterns on the bathymetric surface.

The corresponding reverberation plots for the clay-type sediments are shown in Figures 30, 31, and 32. Their interpretations are similar to that of the rock-type material given above except that these are lower in their magnitude by approximately 17 dB.

3. Bathymetric High Profiles:

Figure 33 is the plot of another bathymetric profile. This is an E-W profile; the east point of this profile is located at (26.7,-47.5) and the west end is at (26.7,-48.5). This profile is almost flat at its east end with the water depth of 4042 m, a topographic high towards west of the center and becomes gradually deeper at the west most point with the water depth of 4868 m.

Again, we have simulated the responses for the quasi-monostatic cases for the source/receiver located at the two extremes of the profile; once at the east end and later at the west end. The source and center of the receiver array are now located at the water depths of 3365 and 3515 m, respectively. These depths are 300 and 150 m from the shallowest water depth (of 3665 m) within the bathymetric profile so as to provide enough clearance for the towed source. For this reason, the receiver is now located at a distance of 527 m from the seafloor at the east-point location but at 1353 m at the west-point location. We expect the two responses to be very different based on the different bathymetry seen by the steered receiver beams at the two extreme locations.

For the quasi-monostatic case with both the omnidirectional source and the receiver array located at the east end of the profile (Figure 33), the reverberation responses, for the receiver beam steering angles of 2, 6, and 10°, for the rock lithology, are shown in Figures 34, 35, and 36. The receiver array for all these steering angles is sampling the flat portion of the bathymetry as indicated in Figure 33, and consequently we should expect the responses to be similar to those of the horizontal interface in Figures 4, 5, and 6 except the receiver array is now 527 m from the seafloor instead of 150 m earlier (for figures 4, 5, and 6).

Out of these responses, only the 10° response (Figure 36) has some similarities to that of Figure 6; it indicates the existence of two anomalous peaks although they are much broader in nature. These are the projections of the receiver beam patterns on to the flat bathymetry but now from the receiver located at 527 m from the

seafloor. This was verified by simulating the horizontal interface response for the 10° receiver beam angle for the source/receiver location identical to that of Figure 33 (source at 677 and receiver at 527 m from seafloor); this is shown in Figure 37. The two responses (Figures 36 and 37) are similar in character and magnitude especially the first peak at about 4.5 s. The second peak around 7.5 s in Figure 36 arrives earlier than that in Figure 37. This second peak is the bottom reverberation of the signal that has once been scattered from the air/water surface. Because the receiver is located closer to the water surface for the bathymetry of Figure 33 than that of Figure 3, the surface reverberation signal arrives earlier in Figure 36 than in Figure 37 (as indicated in these Figures). Consequently, its bottom bounce (the second peak in Figures 36) is also correspondingly earlier than that in Figure 37. This is easily verified by aligning the surface reverberation peaks in Figures 36 and 37; it aligns the second bottom peaks too.

The responses of Figures 34 and 35 are the results of the projection of the respective receiver beams (steered downwards at 2 and 6°) on the almost flat bathymetry. These simulations look different from those in Figures 4 and 5 (horizontal interface) due to the differences in their source/receiver distances from the seafloor. The two-way time for the direct path for the main lobe of the 2° receiver beam pattern is calculated to be around 19.77 s (based on the straight ray path) and is beyond the 10 seconds plotted in Figure 34. The 2° response (Figure 34) is the backscattered energy received by the side lobes of the receiver beam pattern. The 6° response (Figure 35) is somewhat similar to that of the 2° (Figure 34) but indicates the start of the main-lobe energy return around 6 s. This agrees with the two-way-return time calculations of about 6.2 s, based on straight line propagation.

Figures 38, 39, and 40 are the corresponding responses for the clay-type lithology. Again their reverberation levels are reduced by about 17 dB in comparison to the rock lithology but otherwise are similar to those of Figures 34, 35, and 36.

Now we consider the reverberation responses for this bathymetry when the source and receiver array are located at the west end of the profile but at the same water depths. The source/receiver distances are now much greater from the reverberating surfaces. The bathymetry surface insonified is also very different as seen in Figure 41. Consequently, the vertical array interacts with an

entirely different bathymetric patch. The steering angles of 2° and higher, sample a different topographic region. It receives the scattered energy from different patches (with different slopes) in comparison to the horizontal interface on the east end. The main lobes interact with the interface at different distances and at different reverberation times.

Figures 42, 43, and 44 are the simulated responses for the 2, 6, and 10° receiver-steering angles. The first observation for these responses is tne late first arrivals of the reverberation energy, around 1.8 s, in comparison to all the previous cases. This is indicative of the larger travel distances between the scattering surfaces and the source/receiver locations. In addition, these responses do not indicate any definite reverberation pattern. This is, again, due to the relatively larger distances between the source/receiver locations and the insonified patches. Consequently the two-way-travel times are greater than or at the most equal to the 10 s (the total time plotted in Figures 42, 43, and 44). For example, the two-way time for the 2° grazing angle for the main lobe is calculated to be about 29.6 s. Only for the 10° grazing angle, the two-way time is about 10 s and the Figure 44 (refering to the 10° beam angle) does indicate a higher magnitude of the simulated response around 10 s. The simulated reverberations of Figures 42, 43, and 44 are then the scattered energies received by the side lobes of the steered beams, within the 10 s time interval.

Figure 45 is the simulated response for the 10° grazing angle plotted to 100 s. It does indicate a two-peak response from 12 to 20 s. The two-way time calculated for the 10° beam is about 10 s for the straight ray paths and it samples the bathymetric surface at the junction of two differing slopes (point A in Figure 41). The two peaks are due to the reverberations received from two different slopes simultaneously.

Note that the reverberation field of Figure 45 is corrupted by the air/water surface reverberation i.e., it is not the direct path reverberation. The true direct path reverberation lasts only 4.5 s as indicated in Figure 44. In order to record the uncorrupted direct path reverberations, the receiver needs to be located quite close to the sea bottom. It may still be necessary to locate the towed source at a much higher level from the seafloor, to stay clear of the rough bathymetry in the vicinity. The receiver also needs to be farther

from the air/water surface to avoid its interference with the bottom reverberations.

The set of Figures 46, 47, and 48 are the corresponding reverberation responses for the clay lithology. The conclusions are similar to those for the rock lithology except the magnitude of these responses are lower by about 20 dB.

DISCUSSION

The RASP program employed in simulating the bottom reverberation is a ray-tracing modeling program and is strictly valid for the high frequency approximations or for the observations in the far field regions. Although this is not quite true for the frequencies used and the recording configurations considered in the modeling studies here, RASP program generates correct time histories of the reverberation events and the results are adequate for the purposes of designing the field experiment.

The air/water and bottom reverberations are simulated independent of each other, although plotted on the same figures. This is acceptable if the objectives are to record and interpret only the direct path bottom reverberations that are free from the interference from the air/water surface reverberations. This is true of the ARSRP objectives for the short range experiment. However, in general we record the combined effects of these two reverberations. It will then be necessary to isolate (or filter) the bottom reverberation from the surface, before making an attempt to interpret the reverberation anomalies in the present context. It is assumed that this can be achieved in processing.

It is necessary that the source/receiver be located in the proximity to the seafloor so as to record the direct path reverberation responses. This is why these distances were kept relatively close to the bottom surface i.e., around 300 and 150 m in most cases. In order to record the bottom reverberations free of the air/water surface reverberations, it is also necessary to perform the experiment in relatively deep waters. These requirements were met in our simulation geometry.

The simulations clearly indicate that the reverberations are very much dependent on the bottom lithologies; the rocks (or sands) generate stronger reverberation levels than the clays by about 15 to

20 dB for the bathymetries considered here. For clay lithologies then, it may be necessary to employ a stronger pulse source, or the frequency modulated source such as DTAGS, in order to produce observable levels of reverberations.

A comparison of Figures 6 and 37 (receiver locations at 150 and 527 m from the horizontal interface) indicates that it is important to locate the receivers closer to the scattering patch in order to generate well recognized arrivals even if the active source is required to be towed at higher elevations from the seafloor, to accommodate the rough seafloor topography in the vicinity.

The simulations generated here are strictly for the central frequency of 450 Hz pulse source with the bandwidth of 400 Hz, the use of the chirp source signal such as that generated by DTAGS (from 250 to 650 Hz) should have an improved S/N, after matched filtering, by a factor of 50. RASP does not account for the reverberations produced by the subbottom inhomogeneities or refracted arrivals within the bottom layer. These become important at low frequencies.

The quasi-monostatic configuration considered in simulating the reverberation levels is similar to the vertical seismic profiling techniques used to look ahead of the drill bit in geophysical exploration. In seismics, they study the specular reflection events as opposed to the scattering phenomenon here. The bistatic reverberation studies (with the vertical array as the receiver) in acoustics, although not considered here, are similar to the offset vertical seismic profilings in geophysics.

CONCLUSIONS

The quasi-monostatic reverberation levels for three different bathymetric profiles and two lithologies (rock and clay) are simulated using the RASP program. The three bathymetry profiles range from the horizontal interface to true bathymetry in the deep water area, between the Bermuda rise and the MAR. This area is designated as the Atlantic natural laboratory for the bottom/subbottom special research project experiment within the ARSRP.

The reverberation levels are simulated for a deep towed 450 Hz, omnidirectional pulse source (center frequency of 450 Hz, bandwidth

of 400 Hz and source level of 205 dB), and a 64-element receiver array, cut at 300 Hz with the 3 dB beamwidth of approximately 2°, moored at the seafloor.

The simulation studies indicate that the scattering patterns can be characterized as the projection of the receiver-array beam patterns onto the scattering area. These patterns are easily recognized for the simple bathymetry such as the horizontal or dipping interfaces, but difficult to interpret for the more complicated surface roughnesses. They are also dependent on the location of the receiver array from the scattering patch; the closer the receiver array to the scattering surface the stronger the reverberation anomalies.

The lithology controls the magnitude of the backscattered reverberation levels; the rocks (or sands) generate higher levels by about 15 to 20 dB than the clay-type lithologies.

Based on the simulation studies, it is concluded that the receiver-array location of 150 m from the seafloor is adequate to study the direct path backscattered reverberations. The beam steering the received signal does emphasize the reverberation patterns from selected angular scattering patches.

FIGURE CAPTIONS

Figure 1: Flow diagram of the modeling program RASP

Figure 2: Location map of bathymetric profiles within the ARSRP Atlantic natural laboratory area

Figure 3: Horizontal bathymetry and sound profile located at (27,-48)

Figure 4: Quasi-monostatic response, for the bathymetric profile of Figure 3 and rock-type lithology, at receiver steering angle of 2°

Figure 5: Quasi-monostatic response, for the bathymetric profile of Figure 3 and rock-type lithology, at receiver steering angle of 6°

Figure 6: Quasi-monostatic response, for the bathymetric profile of Figure 3 and rock-type lithology, at receiver steering angle of 10°

Figure 7: Quasi-monostatic response, for the bathymetric profile of Figure 3 and clay-type lithology, at receiver steering angle of 2°

Figure 8: Quasi-monostatic response, for the bathymetric profile of Figure 3 and clay-type lithology, at receiver steering angle of 6°

Figure 9: Quasi-monostatic response, for the bathymetric profile of Figure 3 and clay-type lithology, at receiver steering angle of 10°

Figure 10: Quasi-monostatic response, for the 1° updipping bathymetric profile of Figure 3 and rock-type lithology, at receiver steering angle of 2°

Figure 11: Quasi-monostatic response, for the 1° updipping bathymetric profile of Figure 3 and rock-type lithology, at receiver steering angle of 6°

Figure 12: Quasi-monostatic response, for the 1° updipping bathymetric profile of Figure 3 and rock-type lithology, at receiver steering angle of 10°

Figure 13: Quasi-monostatic response, for the 3° updipping bathymetric profile of Figure 3 and rock-type lithology, at receiver steering angle of 2°

Figure 14: Quasi-monostatic response, for the 3° updipping bathymetric profile of Figure 3 and rock-type lithology, at receiver steering angle of 6°

Figure 15: Quasi-monostatic response, for the 3° updipping bathymetric profile of Figure 3 and rock-type lithology, at receiver steering angle of 10°

Figure 16: Quasi-monostatic response, for the 1° downdipping bathymetric profile of Figure 3 and rock-type lithology, at receiver steering angle of 2°

Figure 17: Quasi-monostatic response, for the 1° downdipping bathymetric profile of Figure 3 and rock-type lithology, at receiver steering angle of 6°

Figure 18: Quasi-monostatic response, for the 1° downdipping bathymetric profile of Figure 3 and rock-type lithology, at receiver steering angle of 10°

Figure 19: S-N bathymetric profile located between the end points S(26.5,-48) and N(27.5,-48), with the source and receiver array located at the S-end.

Figure 20: Quasi-monostatic response, for the bathymetric profile of Figure 19 and sand-type lithology, at receiver steering angle of 2°

Figure 21: Quasi-monostatic response, for the bathymetric profile of Figure 19 and sand-type lithology, at receiver steering angle of 6°

Figure 22: Quasi-monostatic response, for the bathymetric profile of Figure 19 and sand-type lithology, at receiver steering angle of 10°

Figure 23: Quasi-monostatic response, for the bathymetric profile of Figure 19 and clay-type lithology, at receiver steering angle of 2°

Figure 24: Quasi-monostatic response, for the bathymetric profile of Figure 19 and clay-type lithology, at receiver steering angle of 6°

Figure 25: Quasi-monostatic response, for the bathymetric profile of Figure 19 and clay-type lithology, at receiver steering angle of 10°

Figure 26: N-S bathymetric profile located between the end points N(27.5,-48) and S(26.5,-48), with the source and receiver array located at the N-end.

Figure 27: Quasi-monostatic response, for the bathymetric profile of Figure 26 and sand-type lithology, at receiver steering angle of 2°

Figure 28: Quasi-monostatic response, for the bathymetric profile of Figure 26 and sand-type lithology, at receiver steering angle of 6°

Figure 29: Quasi-monostatic response, for the bathymetric profile of Figure 26 and sand-type lithology, at receiver steering angle of 10°

Figure 30: Quasi-monostatic response, for the bathymetric profile of Figure 26 and clay-type lithology, at receiver steering angle of 2°

Figure 31: Quasi-monostatic response, for the bathymetric profile of Figure 26 and clay-type lithology, at receiver steering angle of 6°

Figure 32: Quasi-monostatic response, for the bathymetric profile of Figure 26 and clay-type lithology, at receiver steering angle of 10°

Figure 33: E-W bathymetric profile located between the end points E(26.7,-47.5) and W(26.7,-48.5), with the source and receiver array located at the E-end.

Figure 34: Quasi-monostatic response, for the bathymetric profile of Figure 33 and sand-type lithology, at receiver steering angle of 2°

Figure 35: Quasi-monostatic response, for the bathymetric profile of Figure 33 and sand-type lithology, at receiver steering angle of 6°

Figure 36: Quasi-monostatic response, for the bathymetric profile of Figure 33 and sand-type lithology, at receiver steering angle of 10°

Figure 37: Quasi-monostatic response for the horizontal bathymetric profile of Figure 3, for the source and receiver located at 677 and 527 m from the seafloor, and sand-type lithology at receiver steering angle of 10°

Figure 38: Quasi-monostatic response, for the bathymetric profile of Figure 33 and clay-type lithology, at receiver steering angle of 2°

Figure 39: Quasi-monostatic response, for the bathymetric profile of Figure 33 and clay-type lithology, at receiver steering angle of 6°

Figure 40: Quasi-monostatic response, for the bathymetric profile of Figure 33 and sand-type lithology, at receiver steering angle of 10°

Figure 41: W-E bathymetric profile located between the end points W(26.7,-48.5) and E(26.7,-47.5), with the source and receiver array located at the W-end.

Figure 42: Quasi-monostatic response, for the bathymetric profile of Figure 41 and sand-type lithology, at receiver steering angle of 2°

Figure 43: Quasi-monostatic response, for the bathymetric profile of Figure 41 and sand-type lithology, at receiver steering angle of 6°

Figure 44: Quasi-monostatic response, for the bathymetric profile of Figure 41 and sand-type lithology, at receiver steering angle of 10°

Figure 45: Quasi-monostatic response, for the bathymetric profile of Figure 41 and sand-type lithology, at receiver steering angle of 10°, plotted to 100 s.

Figure 46: Quasi-monostatic response, for the bathymetric profile of Figure 41 and clay-type lithology, at receiver steering angle of 2°

Figure 47: Quasi-monostatic response, for the bathymetric profile of Figure 41 and clay-type lithology, at receiver steering angle of 6°

Figure 48: Quasi-monostatic response, for the bathymetric profile of Figure 41 and clay-type lithology, at receiver steering angle of 10°

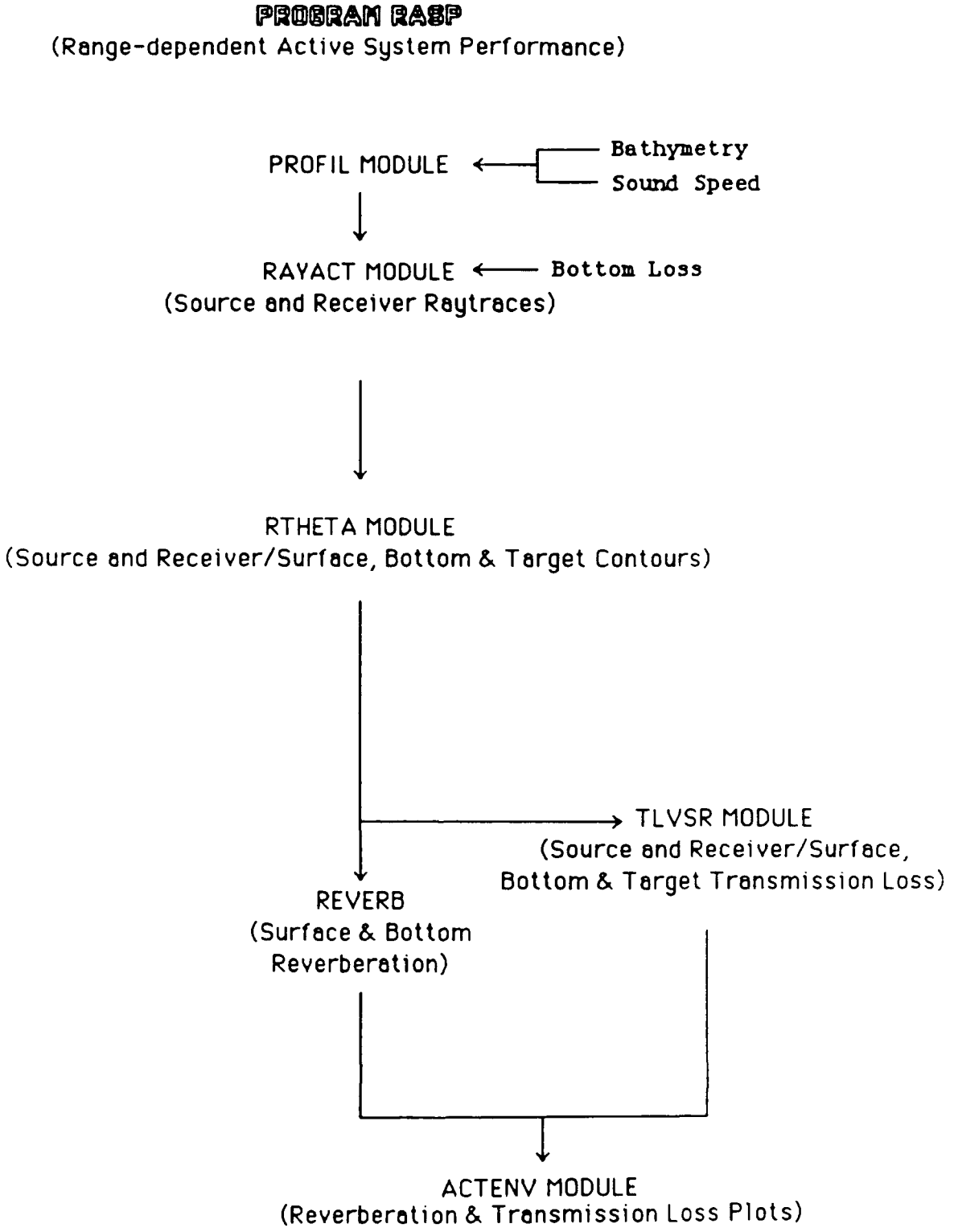
PROGRAM RASP
(Range-dependent Active System Performance)
PROFIL MODULE
Bathymetry
Sound Speed
RAYACT MODULE
Bottom Loss
(Source and Receiver Raytraces)
RTHETA MODULE
(Source and Receiver/Surface, Bottom & Target Contours)
TLVSR MODULE
(Source and Receiver/Surface, Bottom & Target Transmission Loss)
REVERB
(Surface & Bottom Reverberation)
ACTENV MODULE
(Reverberation & Transmission Loss Plots)

Figure 1

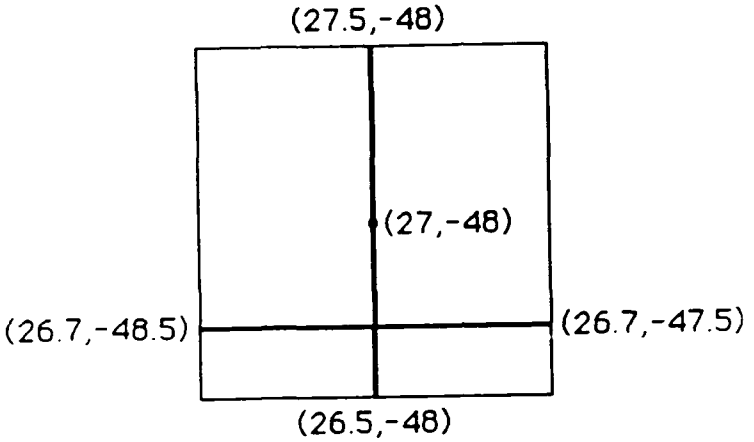

Location of Bathymetric Profiles

Figure 2

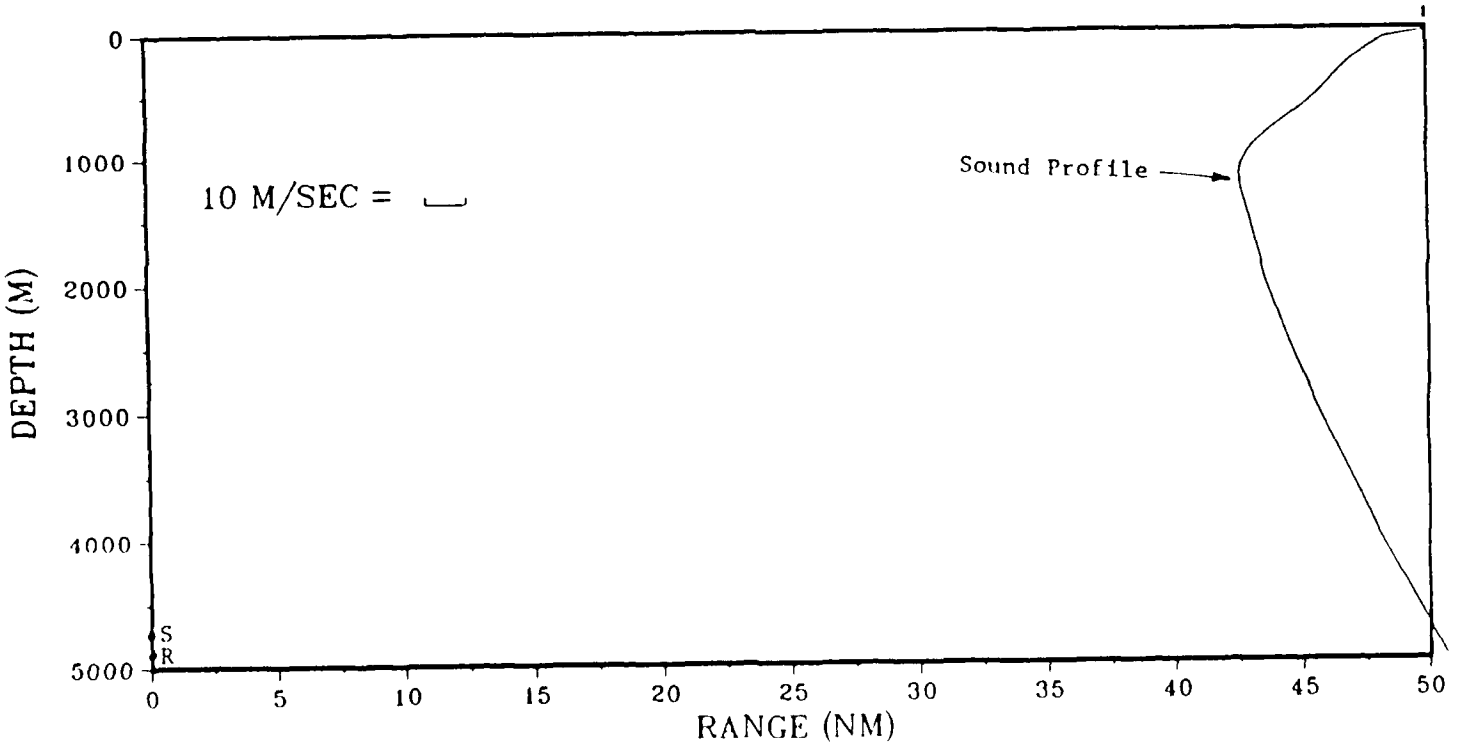
Atlantic Bottom/Subbottom Site at (27,-48)
0
1000
2000
3000
4000
5000
DEPTH (M)
10 M/SEC =
Sound Profile
S
R
0
5
10
15
20
25
30
35
40
45
50
RANGE (NM)

Figure 3

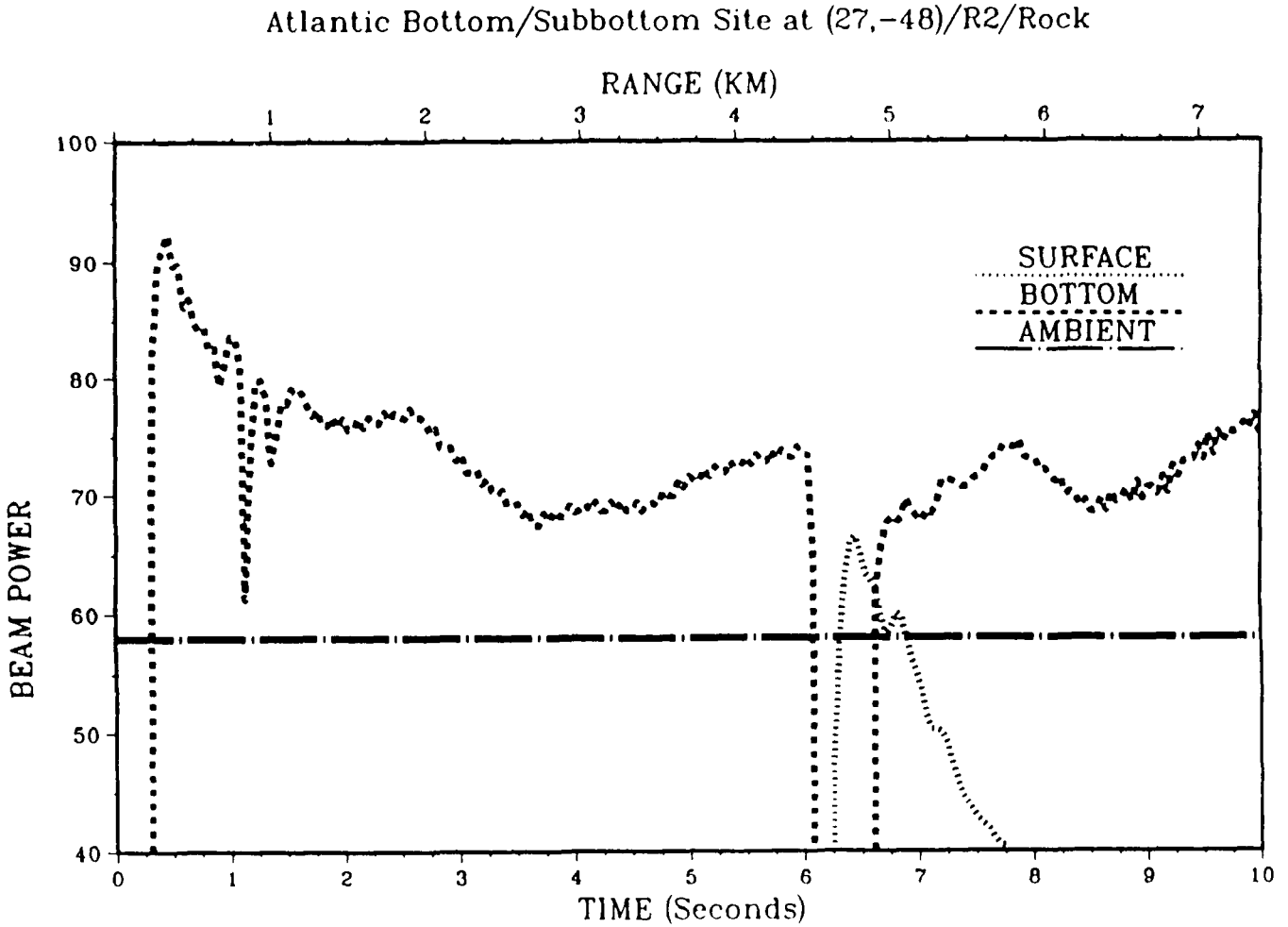
Atlantic Bottom/Subbottom Site at (27,-48)/R2/Rock
RANGE (KM)
1
2
3
4
5
6
7
100
90
80
70
60
50
40
BEAM POWER
SURFACE
BOTTOM
AMBIENT
0
1
2
3
4
5
6
7
8
9
10
TIME (Seconds)

Figure 4

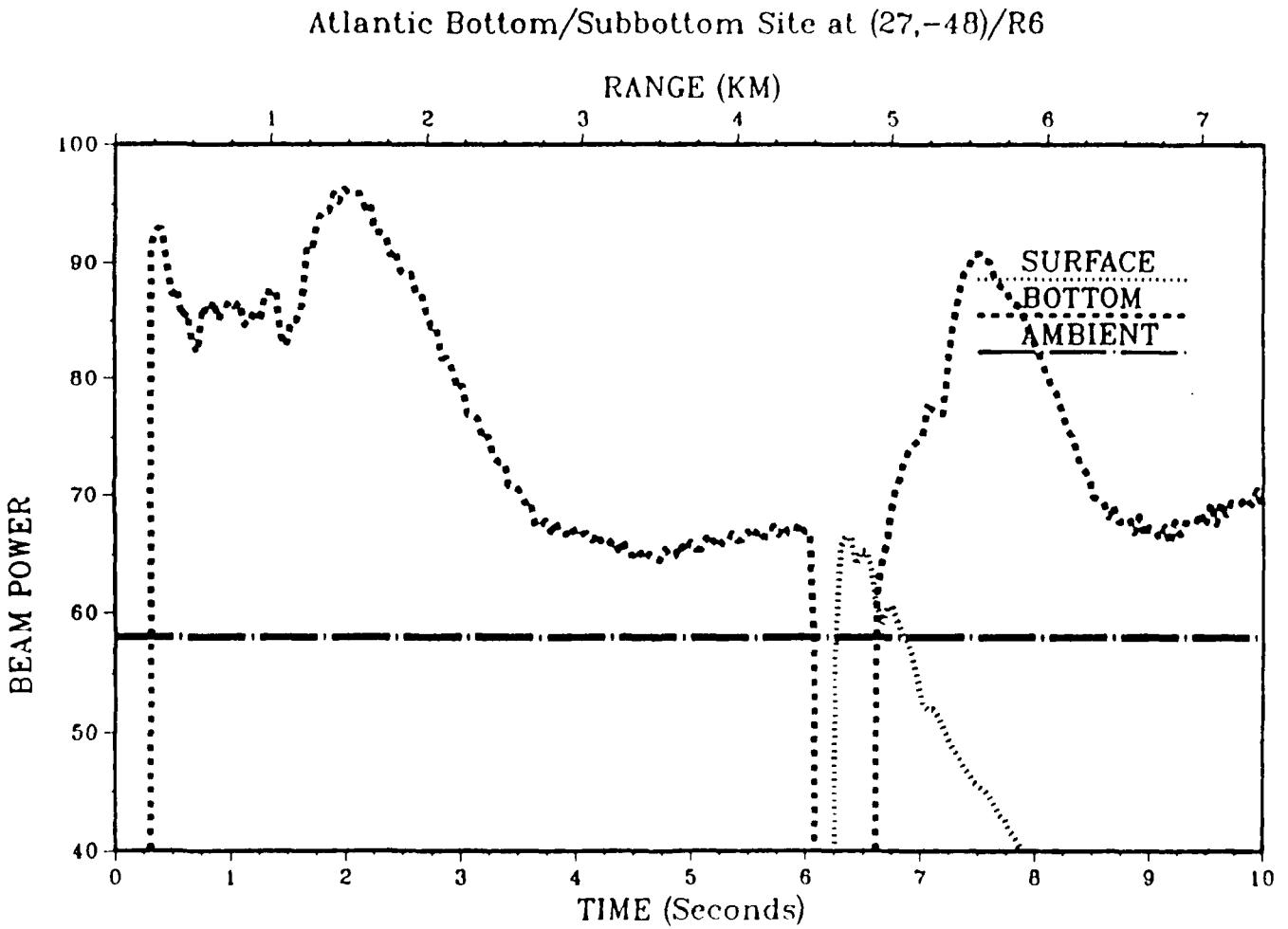
Atlantic Bottom/Subbottom Site at (27,-48)/R6
RANGE (KM)
1
2
3
4
5
6
7
100
90
80
70
60
50
40
BEAM POWER
SURFACE
BOTTOM
AMBIENT
0
1
2
3
4
5
6
7
8
9
10
TIME (Seconds)

Figure 5

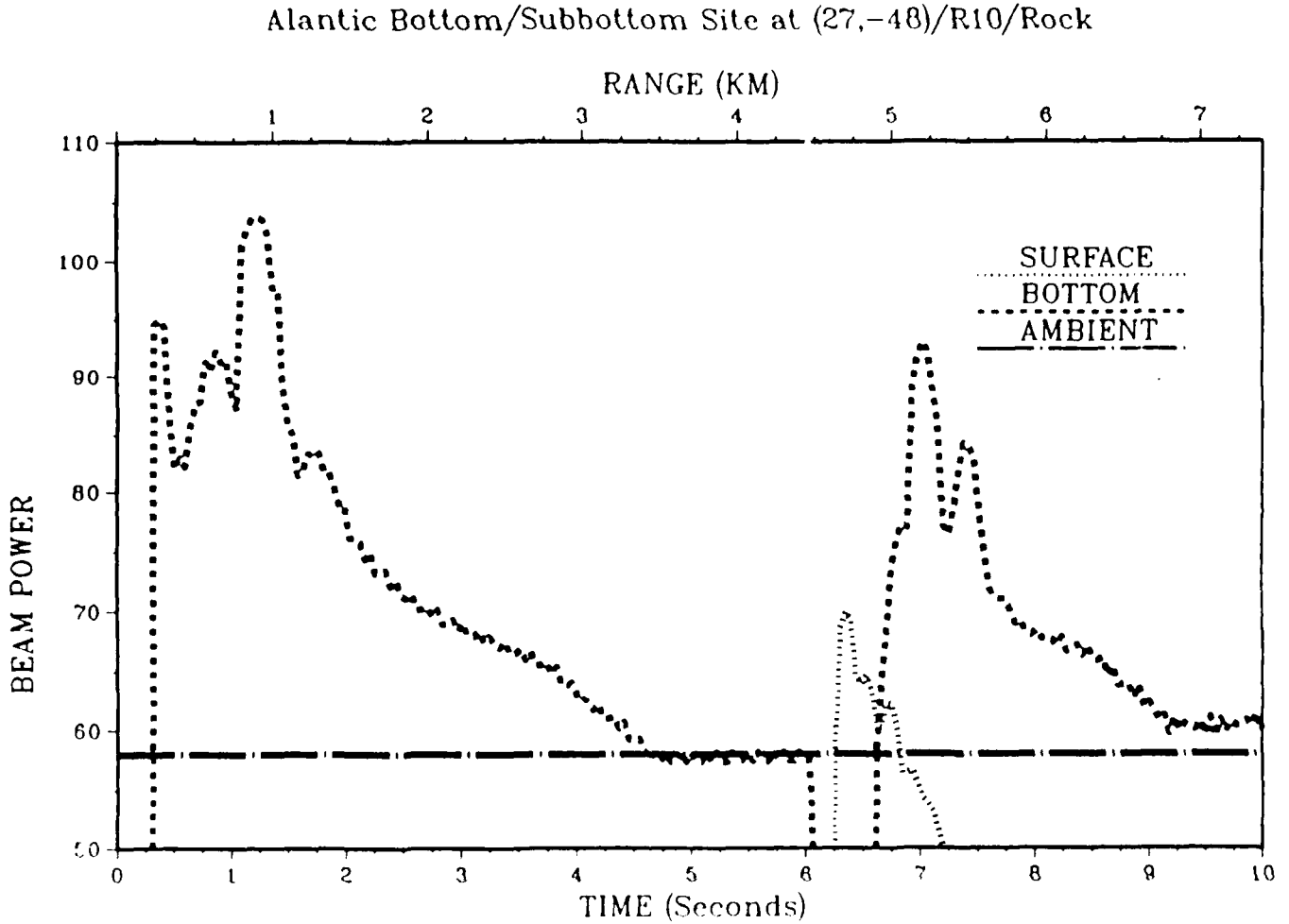
Alantic Bottom/Subbottom Site at (27,-48)/R10/Rock
RANGE (KM)
1
2
3
4
5
6
7
110
100
90
80
70
60
50
BEAM POWER
SURFACE
BOTTOM
AMBIENT
0
1
2
3
4
5
6
7
8
9
10
TIME (Seconds)

Figure 6

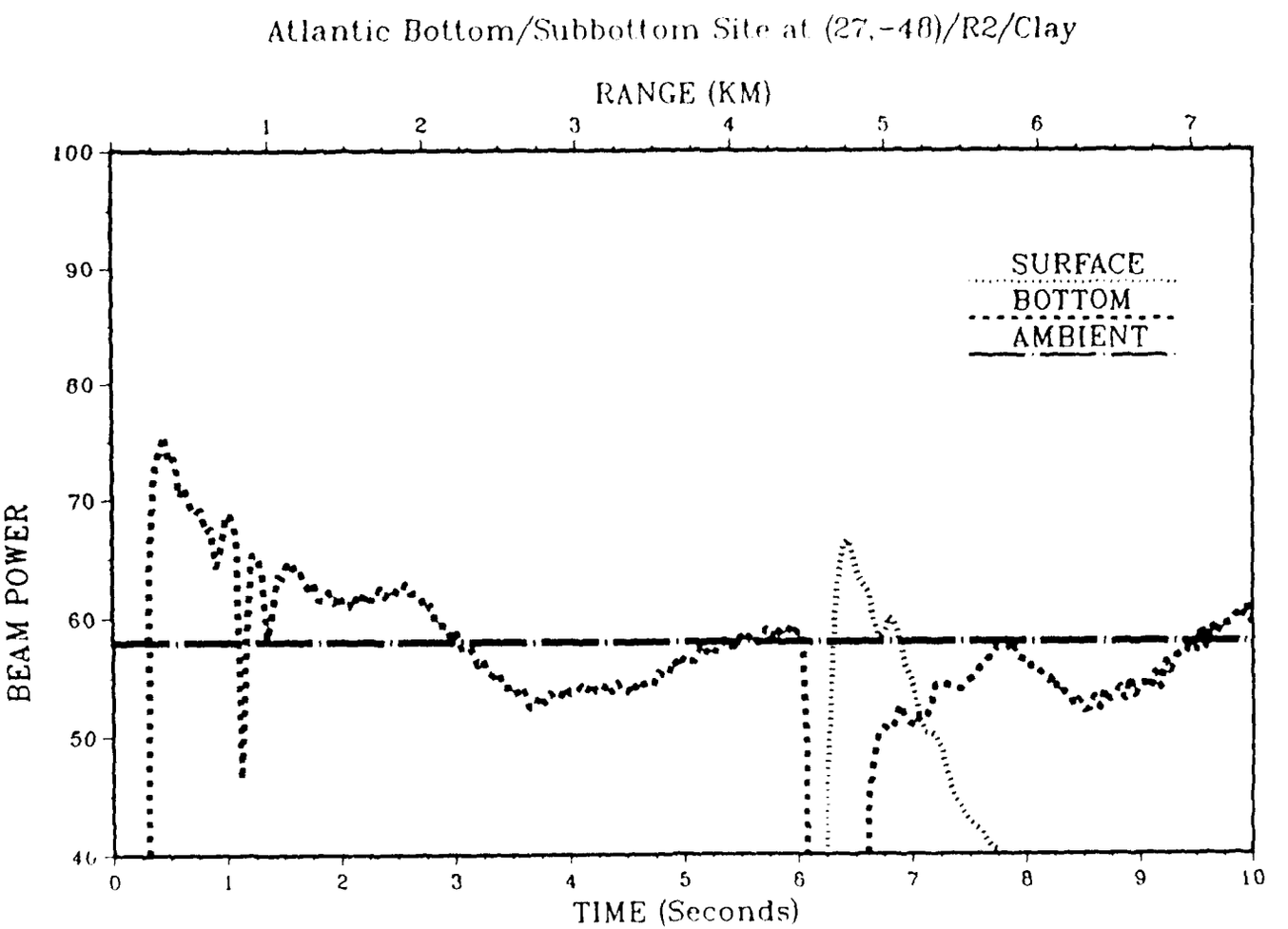
Atlantic Bottom/Subbottom Site at (27,-48)/R2/Clay
RANGE (KM)
1
2
3
4
5
6
7
100
90
80
70
60
50
40
BEAM POWER
SURFACE
BOTTOM
AMBIENT
0
1
2
3
4
5
6
7
8
9
10
TIME (Seconds)

Figure 7

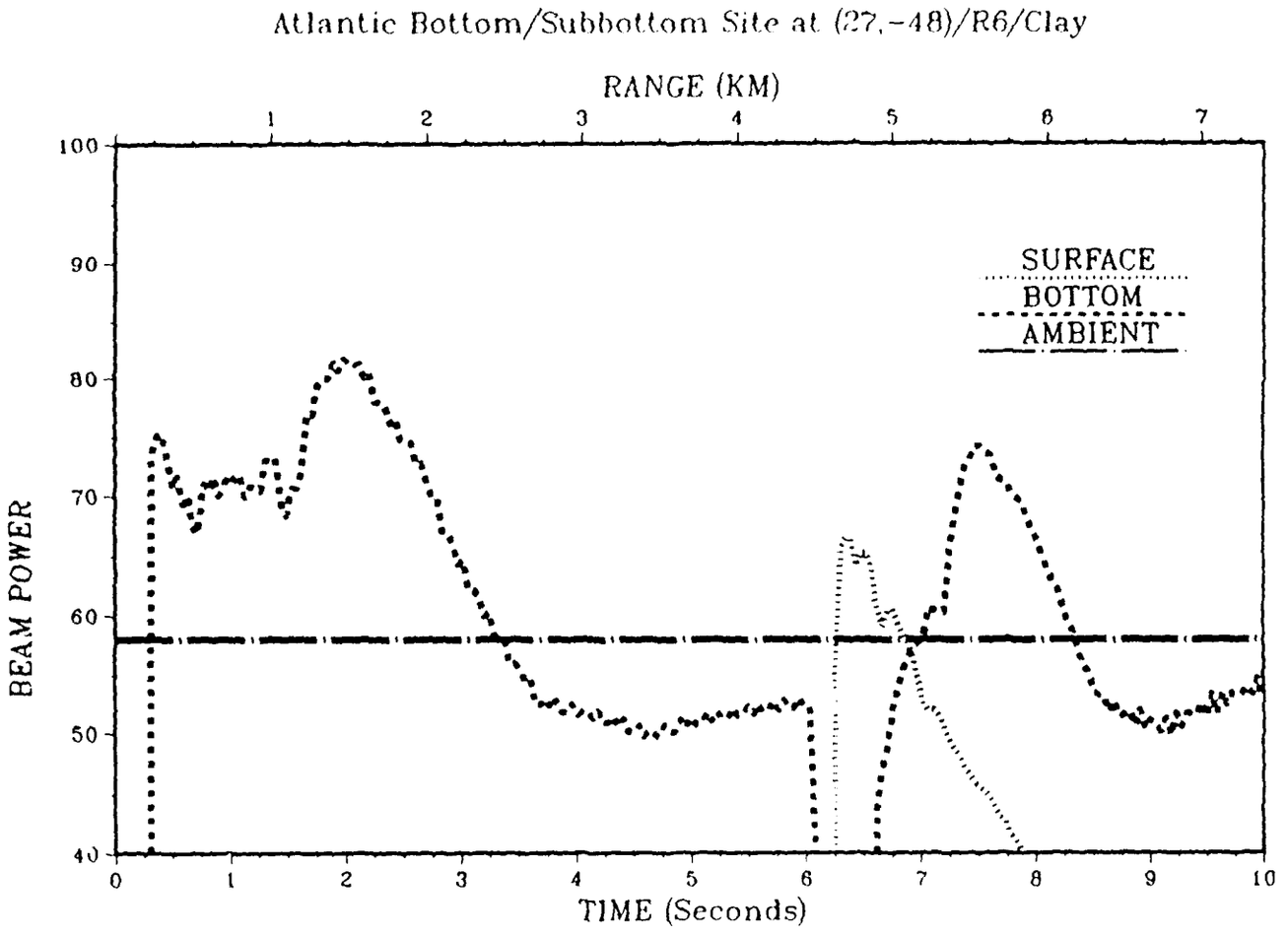
Atlantic Bottom/Subbottom Site at (27,-48)/R6/Clay
RANGE (KM)
1
2
3
4
5
6
7
100
90
80
70
60
50
40
BEAM POWER
SURFACE
BOTTOM
AMBIENT
0
1
2
3
4
5
6
7
8
9
10
TIME (Seconds)

Figure 8

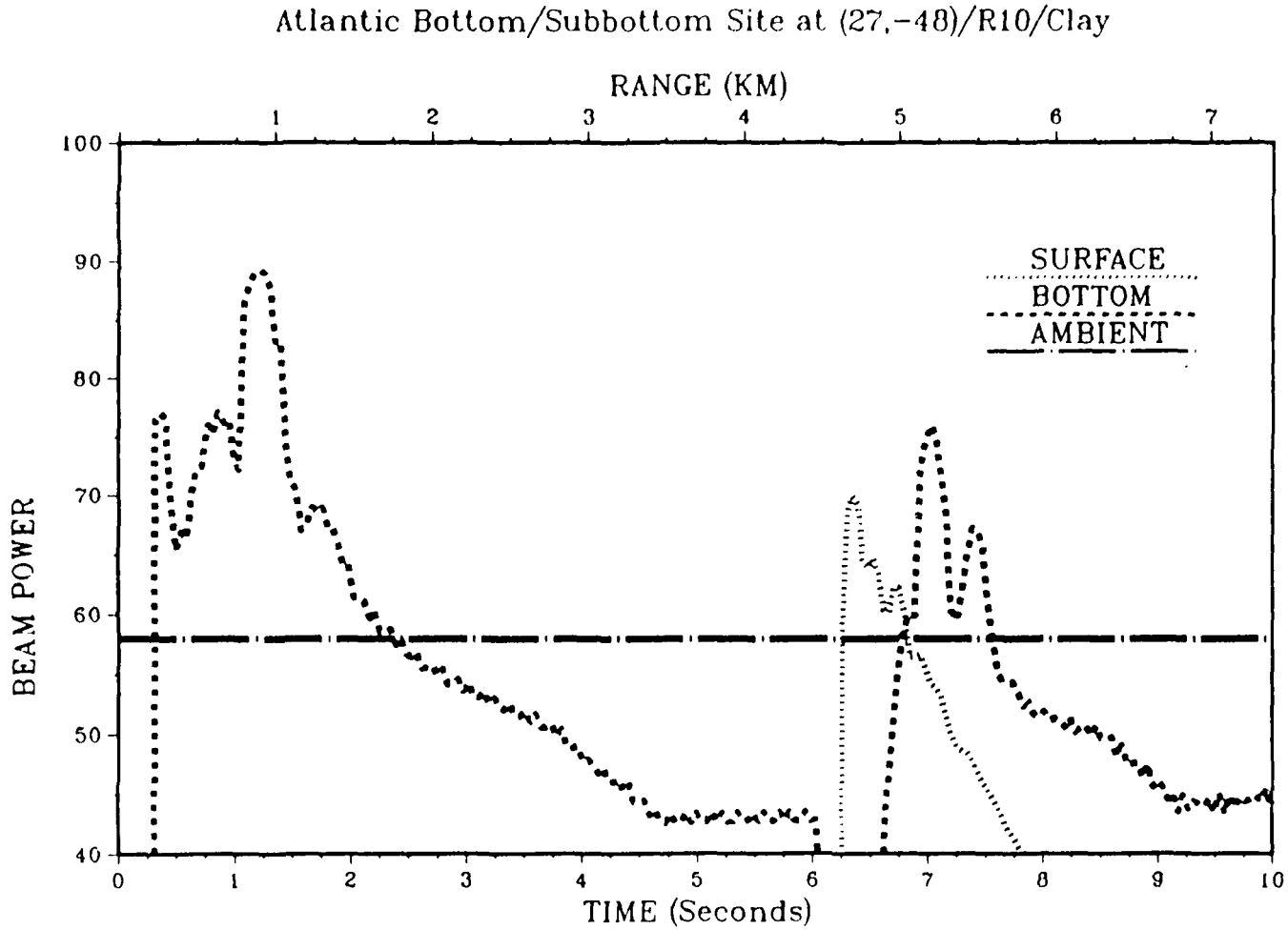
Atlantic Bottom/Subbottom Site at (27,-48)/R10/Clay
RANGE (KM)
1
2
3
4
5
6
7
100
90
80
70
60
50
40
BEAM POWER
SURFACE
BOTTOM
AMBIENT
0
1
2
3
4
5
6
7
8
9
10
TIME (Seconds)

Figure 9

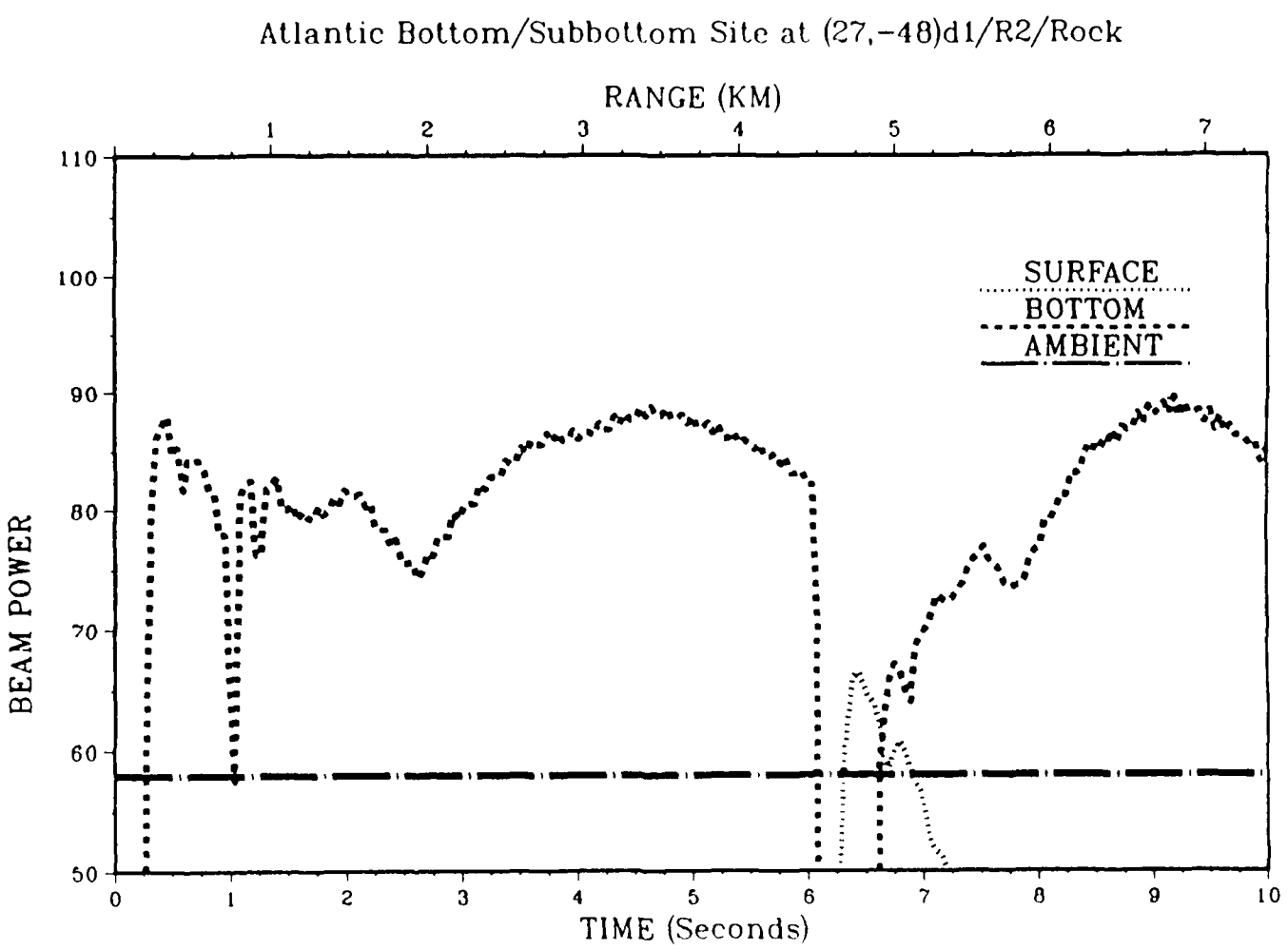
Atlantic Bottom/Subbottom Site at (27,-48)d1/R2/Rock
RANGE (KM)
1
2
3
4
5
6
7
110
100
90
80
70
60
50
BEAM POWER
SURFACE
BOTTOM
AMBIENT
0
1
2
3
4
5
6
7
8
9
10
TIME (Seconds)

Figure 10

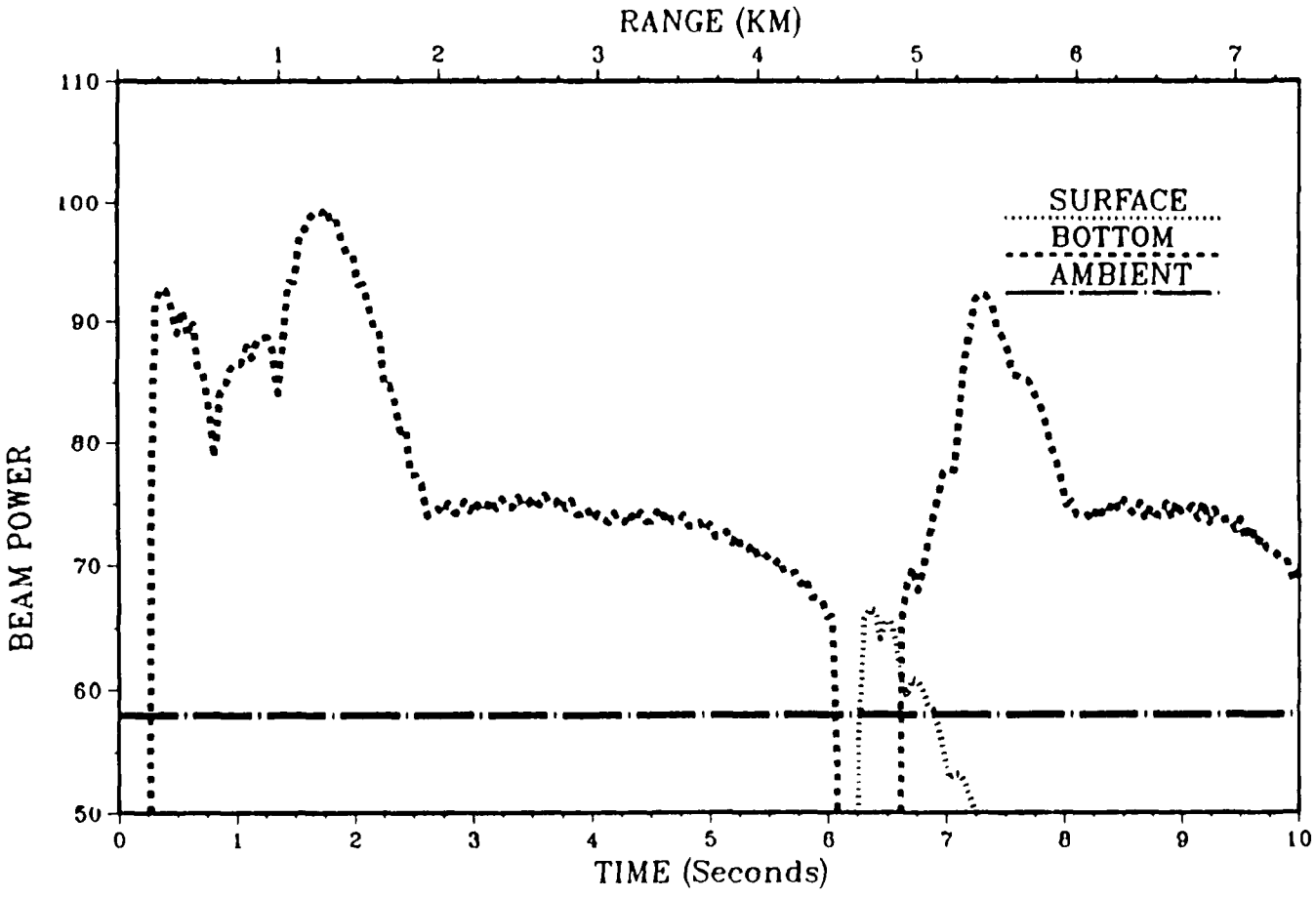
Atlantic Bottom/Subbottom Site at (27,-48)d1/R6/Rock
RANGE (KM)
1
2
3
4
5
6
7
110
100
90
80
70
60
50
BEAM POWER
SURFACE
BOTTOM
AMBIENT
0
1
2
3
4
5
6
7
8
9
10
TIME (Seconds)

Figure 11

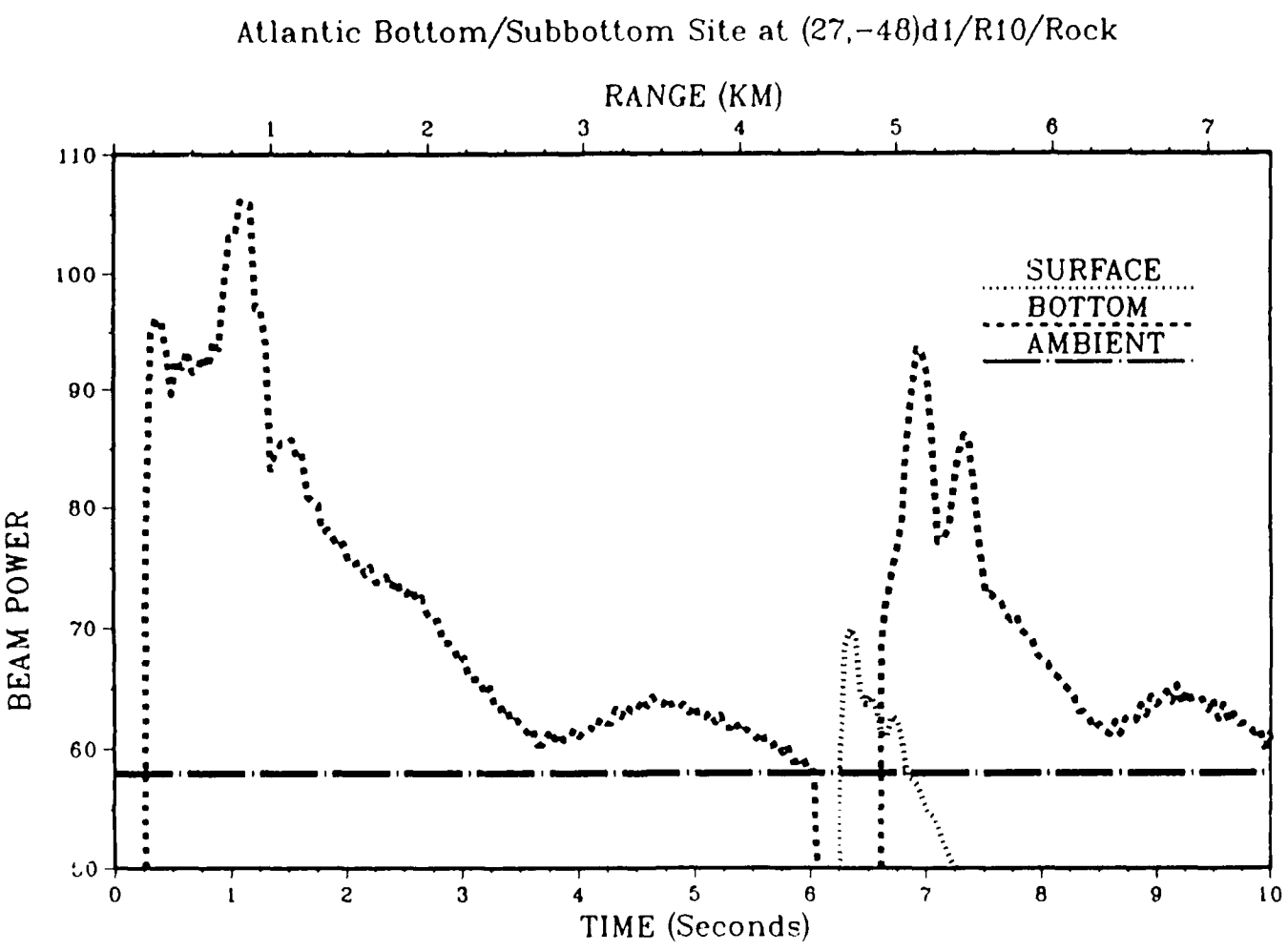
Atlantic Bottom/Subbottom Site at (27,-48)d1/R10/Rock
RANGE (KM)
1
2
3
4
5
6
7
110
100
90
80
70
60
50
BEAM POWER
SURFACE
BOTTOM
AMBIENT
0
1
2
3
4
5
6
7
8
9
10
TIME (Seconds)

Figure 12

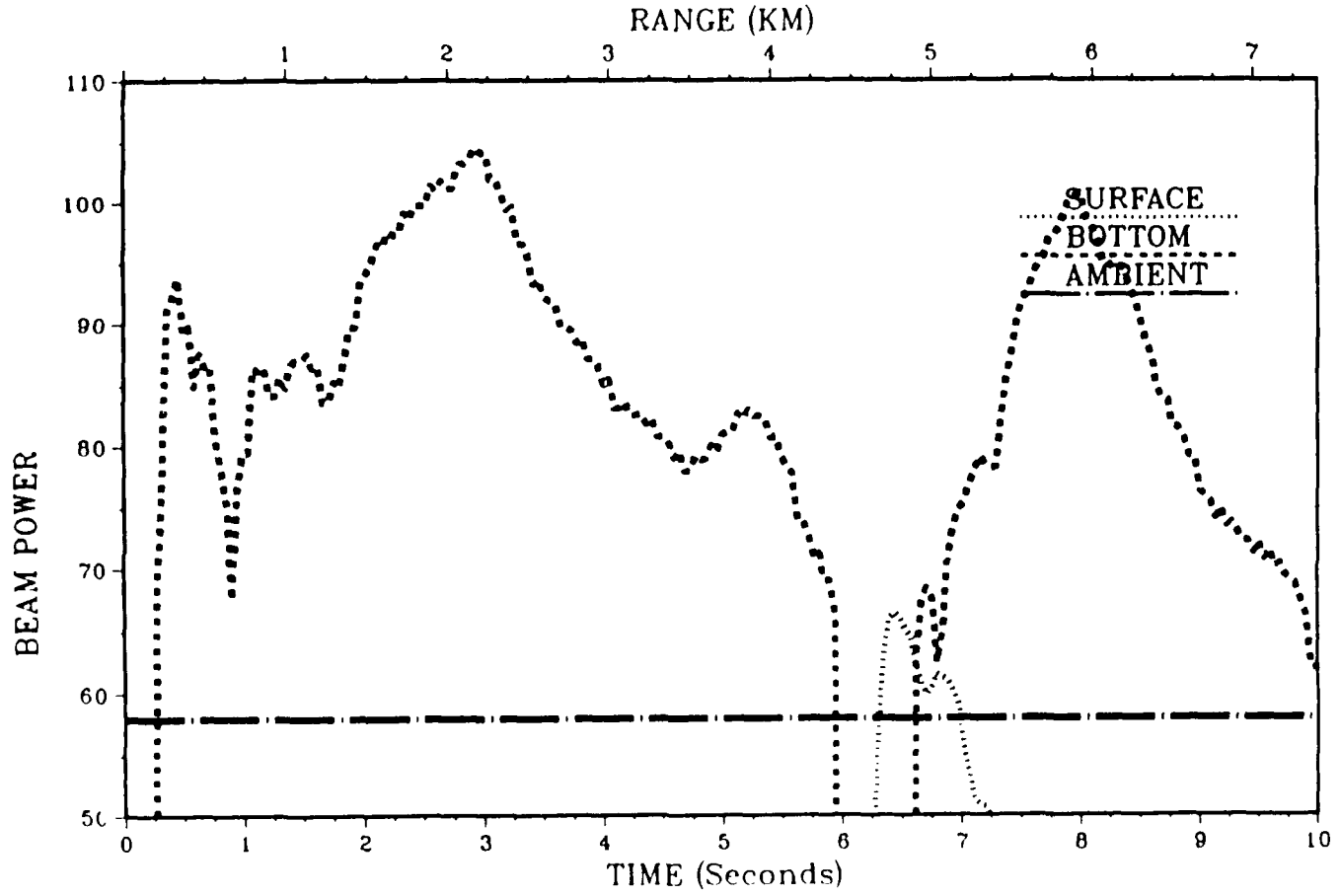
Atlantic Bottom/Subbottom Site at (27,-48)d3/R2/Rock
RANGE (KM)
1
2
3
4
5
6
7
110
100
90
80
70
60
50
BEAM POWER
SURFACE
BOTTOM
AMBIENT
0
1
2
3
4
5
6
7
8
9
10
TIME (Seconds)

Figure 13

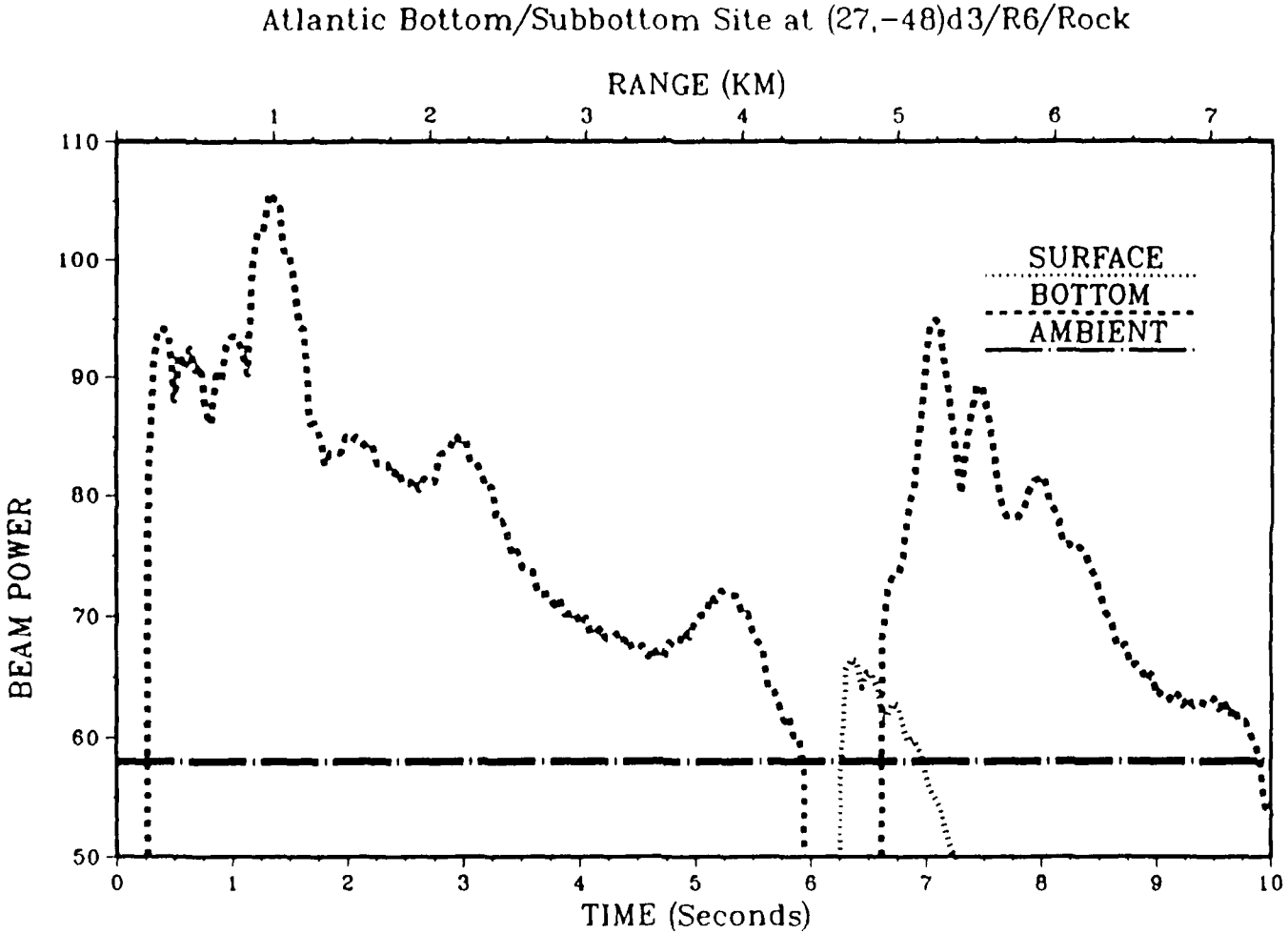
Atlantic Bottom/Subbottom Site at (27,-48)d3/R6/Rock
RANGE (KM)
1
2
3
4
5
6
7
110
100
90
80
70
60
50
BEAM POWER
SURFACE
BOTTOM
AMBIENT
0
1
2
3
4
5
6
7
8
9
10
TIME (Seconds)

Figure 14

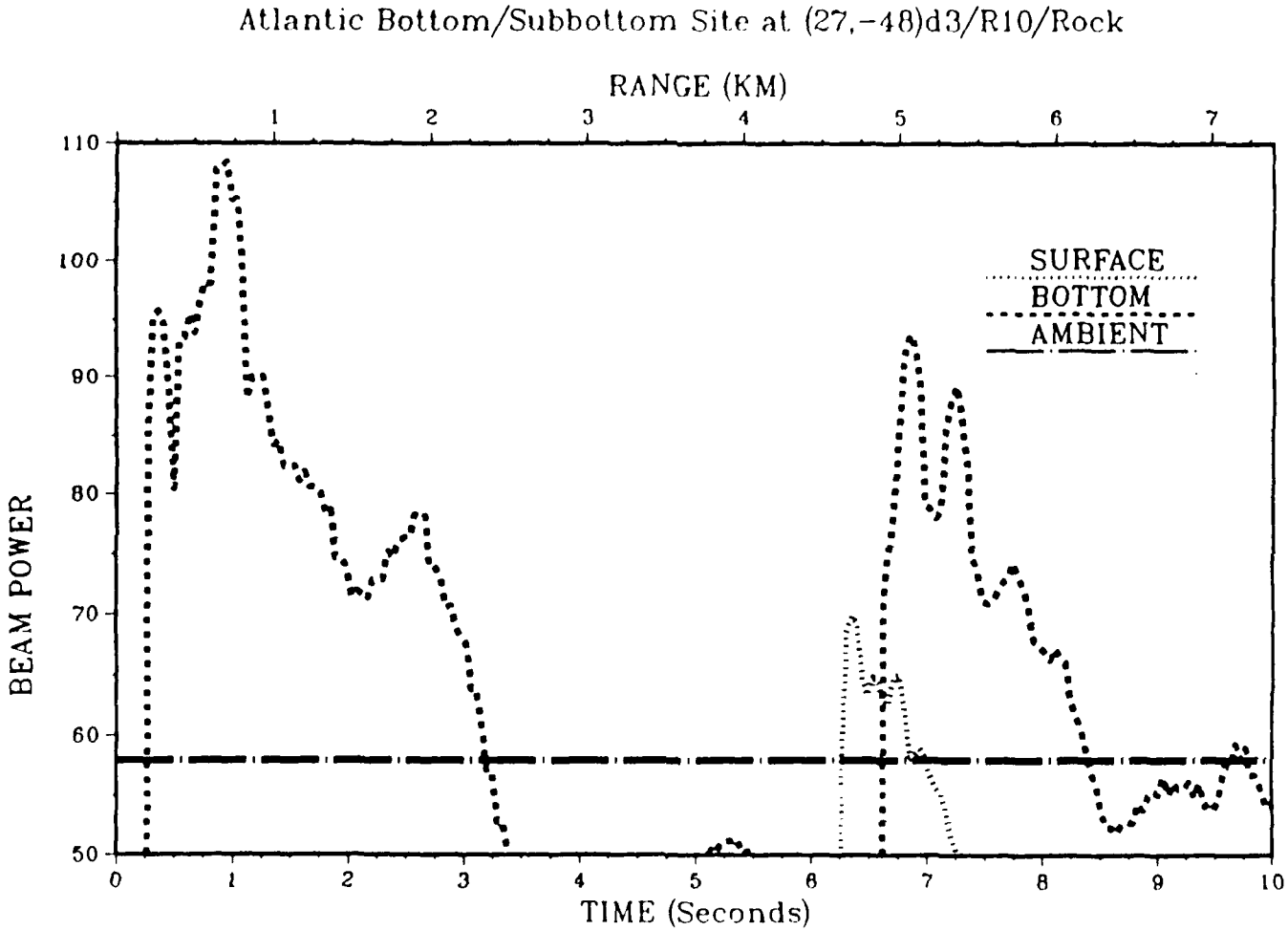
Atlantic Bottom/Subbottom Site at (27,-48)d3/R10/Rock
RANGE (KM)
1
2
3
4
5
6
7
110
100
90
80
70
60
50
BEAM POWER
SURFACE
BOTTOM
AMBIENT
0
1
2
3
4
5
6
7
8
9
10
TIME (Seconds)

Figure 15

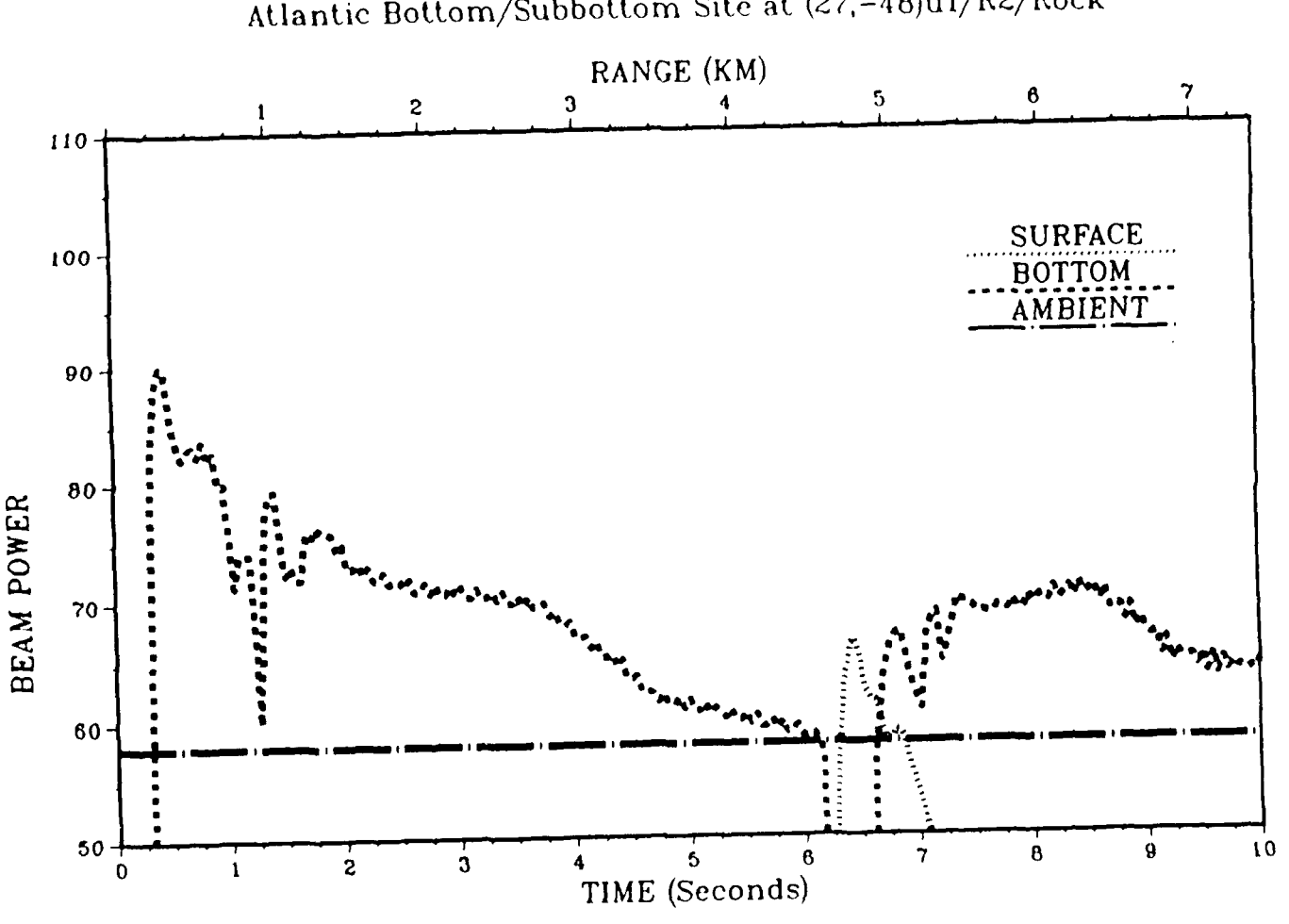
Atlantic Bottom/Subbottom Site at (27,-48)u1/R2/Rock
RANGE (KM)
1
2
3
4
5
6
7
110
100
90
80
70
60
50
BEAM POWER
SURFACE
BOTTOM
AMBIENT
0
1
2
3
4
5
6
7
8
9
10
TIME (Seconds)

Figure 16

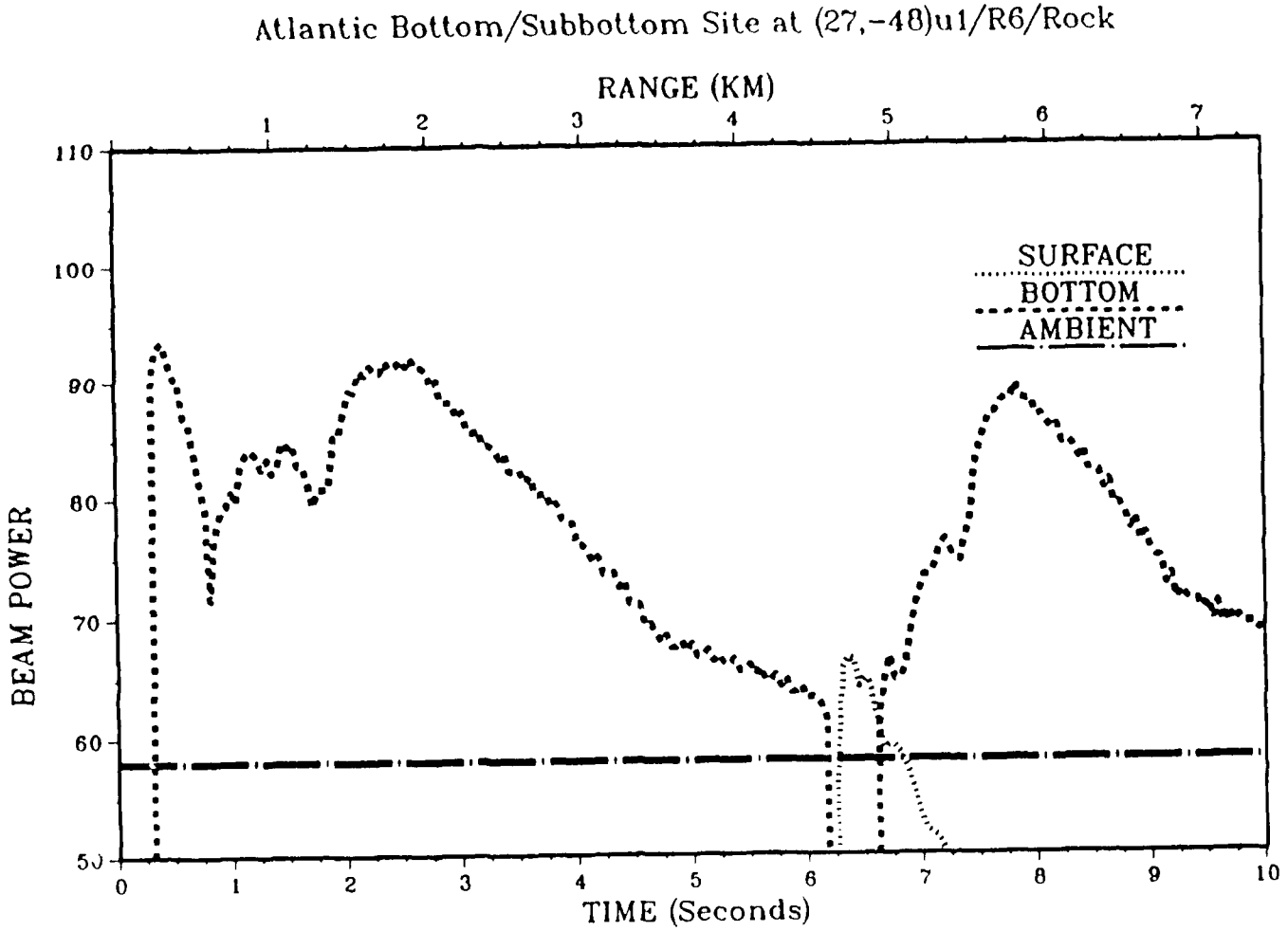
Atlantic Bottom/Subbottom Site at (27,-48)u1/R6/Rock
RANGE (KM)
1
2
3
4
5
6
7
110
100
90
80
70
60
50
BEAM POWER
SURFACE
BOTTOM
AMBIENT
0
1
2
3
4
5
6
7
8
9
10
TIME (Seconds)

Figure 17

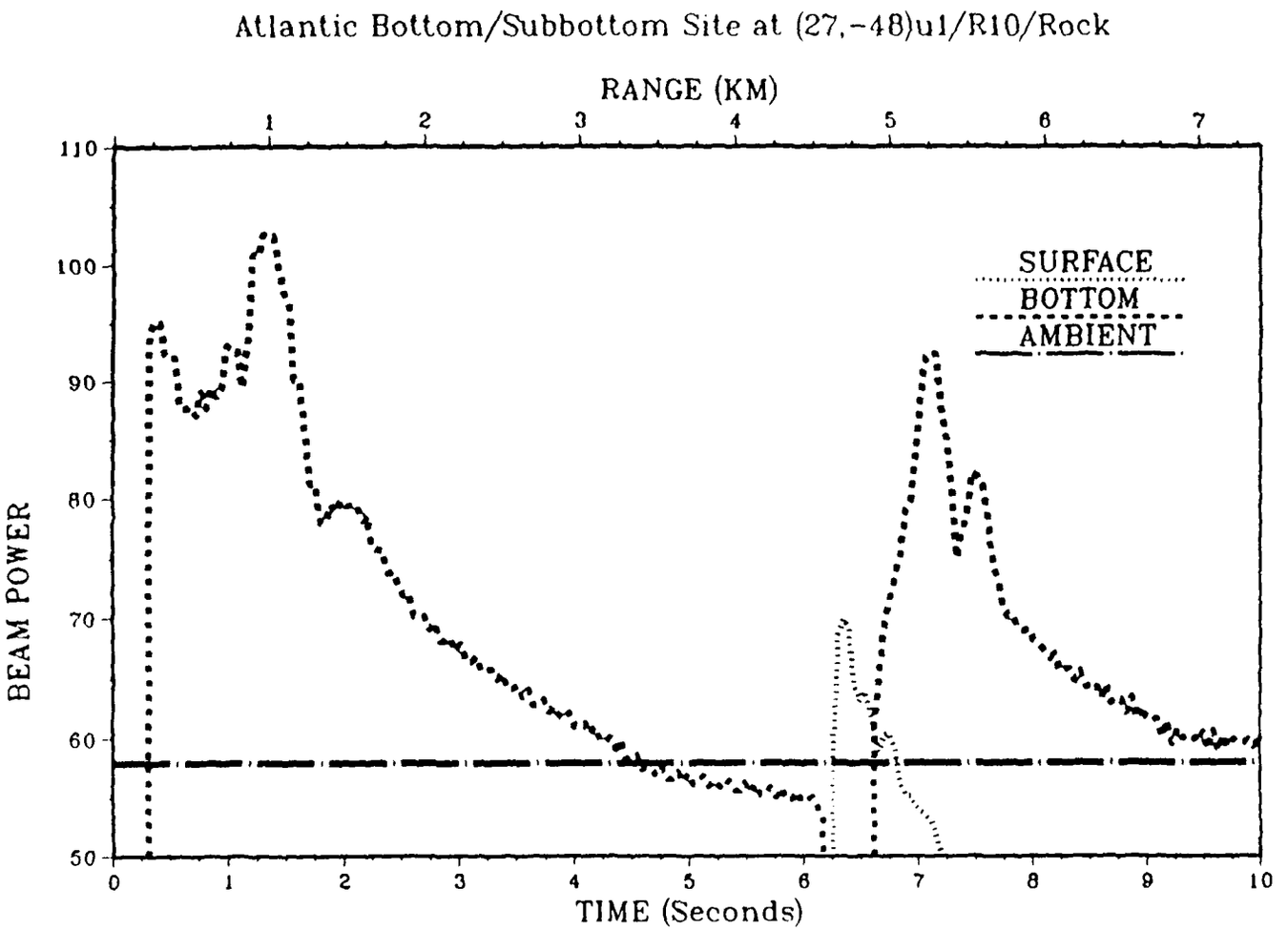
Atlantic Bottom/Subbottom Site at (27,-48)u1/R10/Rock
RANGE (KM)
1
2
3
4
5
6
7
110
100
90
80
70
60
50
BEAM POWER
SURFACE
BOTTOM
AMBIENT
0
1
2
3
4
5
6
7
8
9
10
TIME (Seconds)

Figure 18

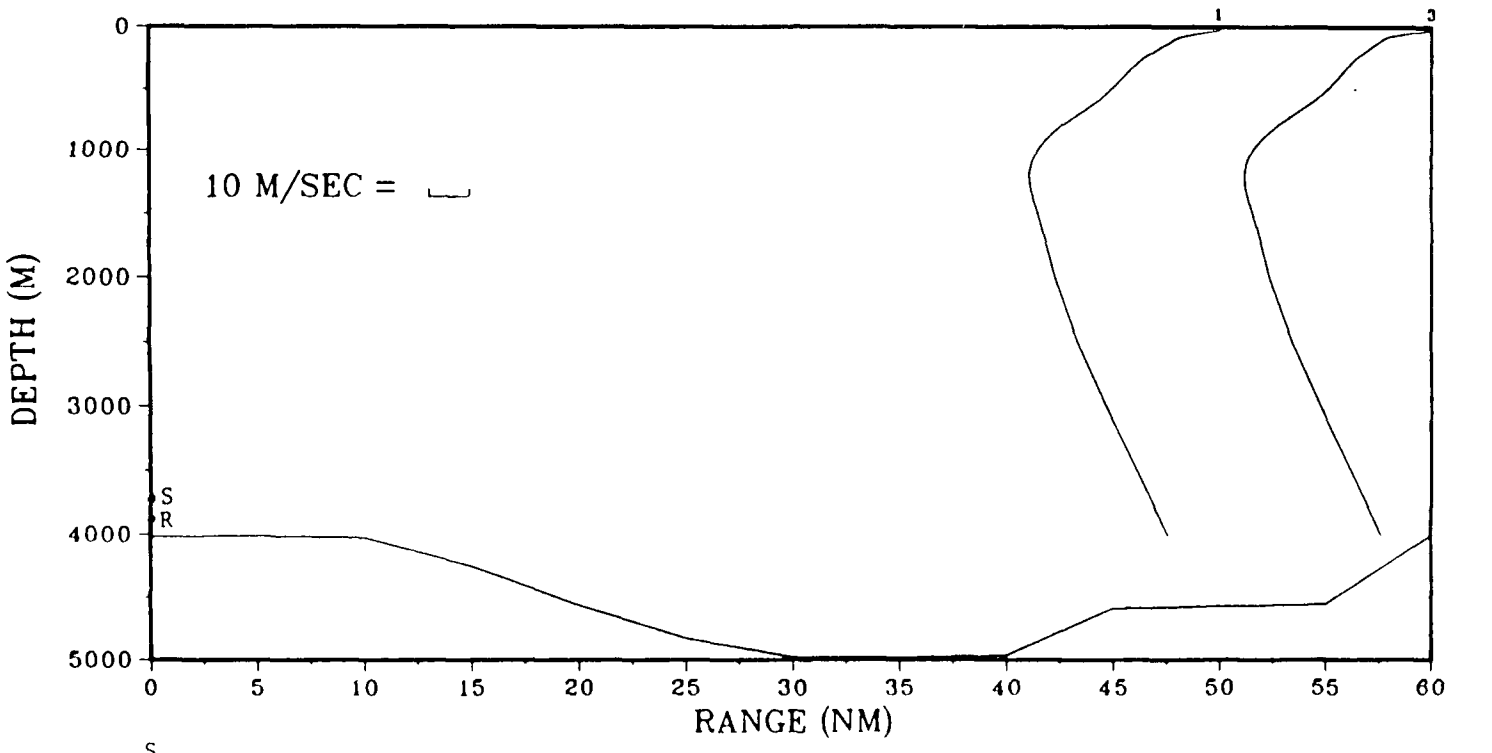
Atlantic Bottom/Subbottom Site at (26.5,-48)N
0
1000
2000
3000
4000
5000
DEPTH (M)
10 M/SEC =
S
R
1
3
0
5
10
15
20
25
30
35
40
45
50
55
60
RANGE (NM)
S
(26.5,-48)
N
(27.5,-48)

Figure 19

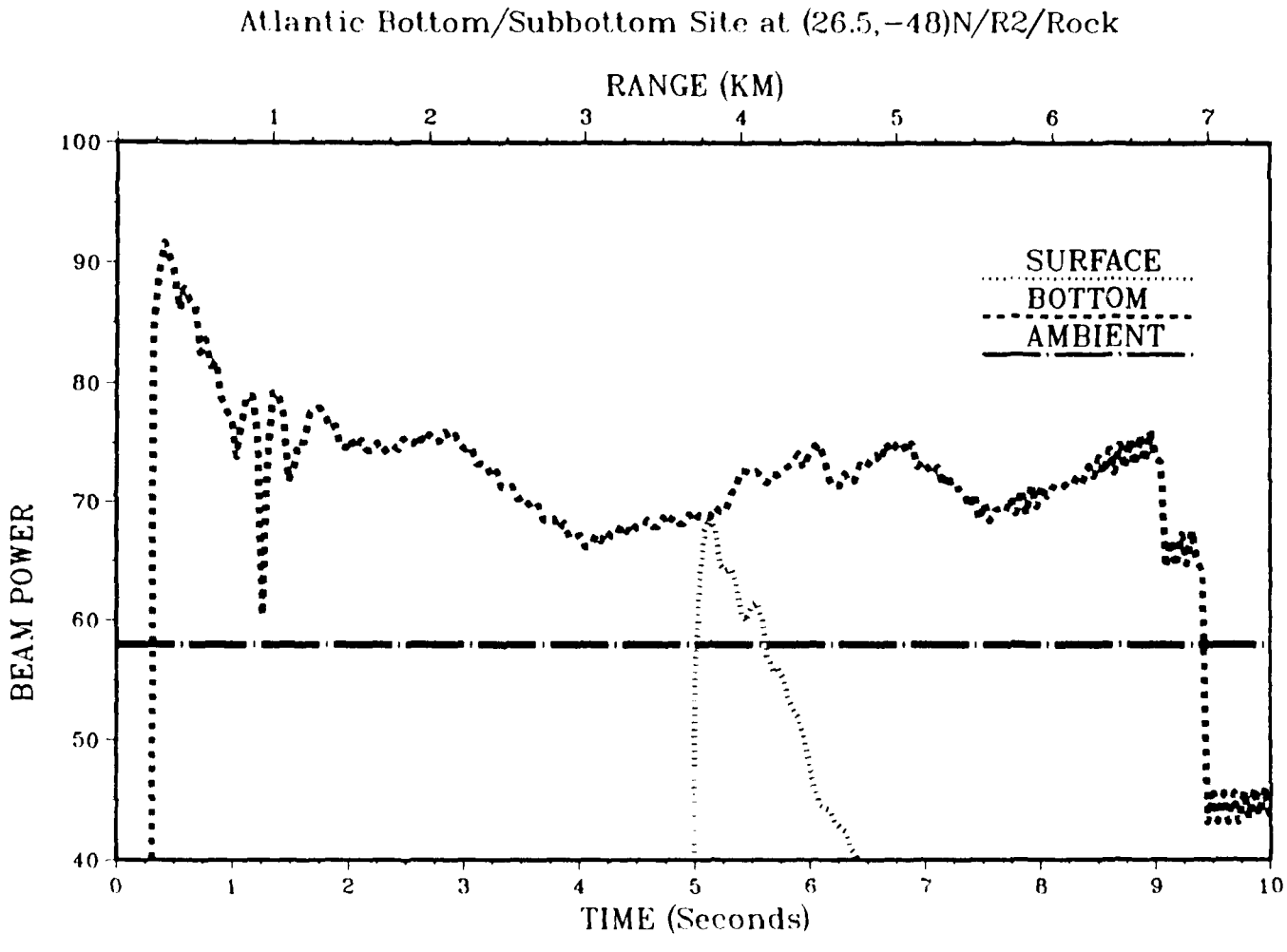
Atlantic Bottom/Subbottom Site at (26.5,−48)N/R2/Rock
RANGE (KM)
1
2
3
4
5
6
7
100
90
80
70
60
50
40
BEAM POWER
SURFACE
BOTTOM
AMBIENT
0
1
2
3
4
5
6
7
8
9
10
TIME (Seconds)

Figure 20

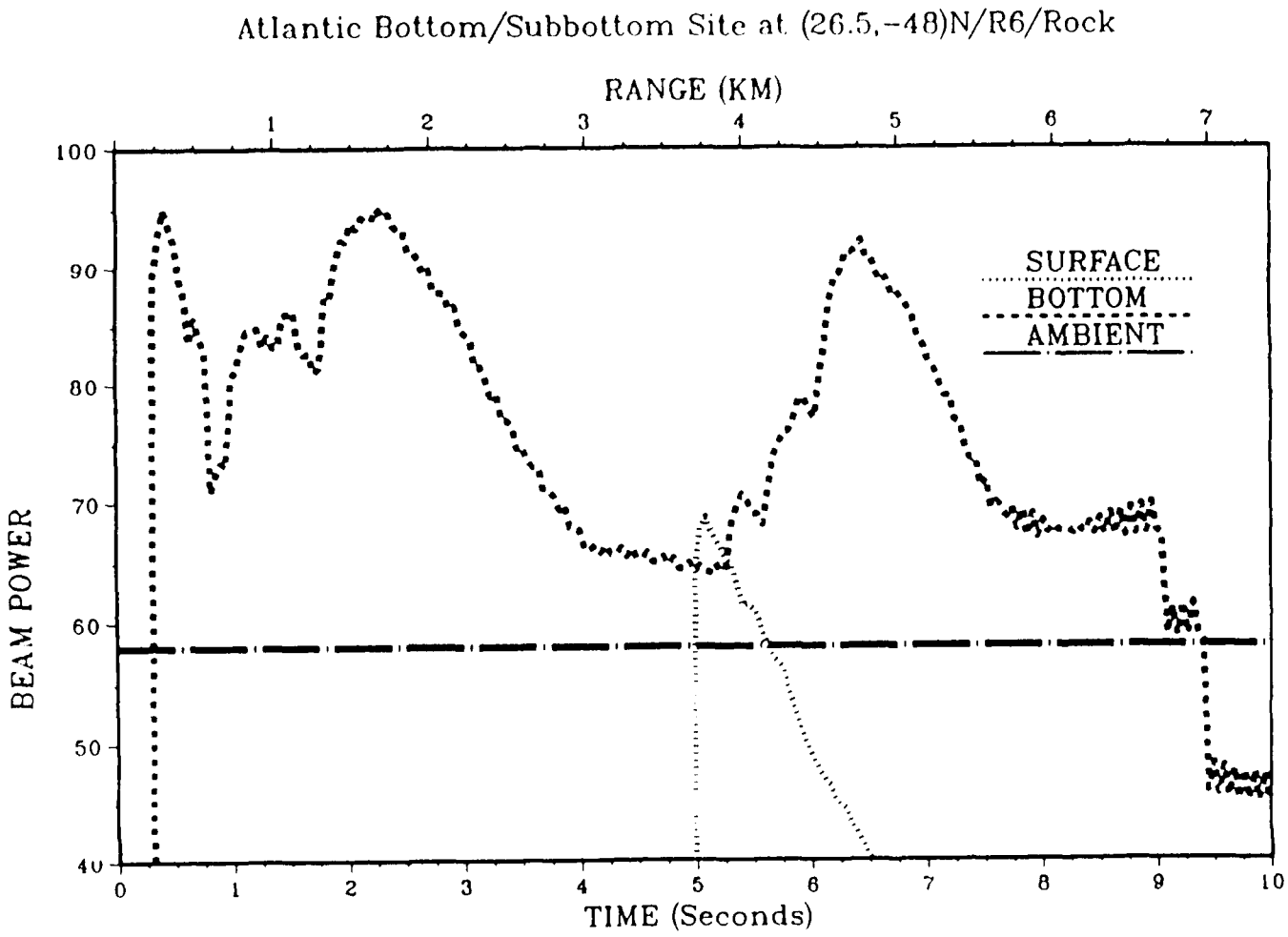
Atlantic Bottom/Subbottom Site at (26.5,-48)N/R6/Rock
RANGE (KM)
1
2
3
4
5
6
7
100
90
80
70
60
50
40
BEAM POWER
SURFACE
BOTTOM
AMBIENT
0
1
2
3
4
5
6
7
8
9
10
TIME (Seconds)

Figure 21

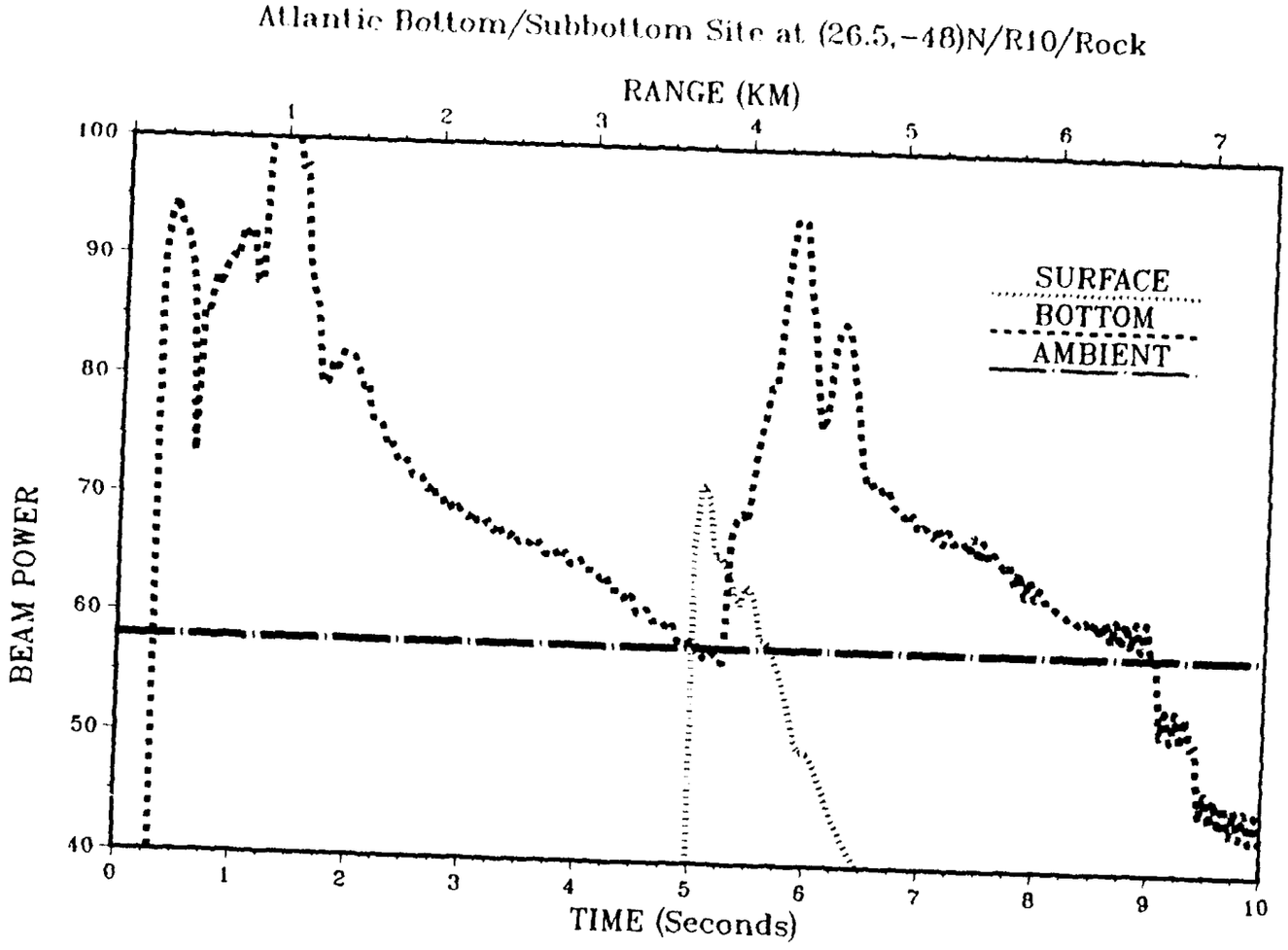
Atlantic Bottom/Subbottom Site at (26.5,-48)N/R10/Rock
RANGE (KM)
1
2
3
4
5
6
7
100
90
80
70
60
50
40
BEAM POWER
SURFACE
BOTTOM
AMBIENT
0
1
2
3
4
5
6
7
8
9
10
TIME (Seconds)

Figure 22

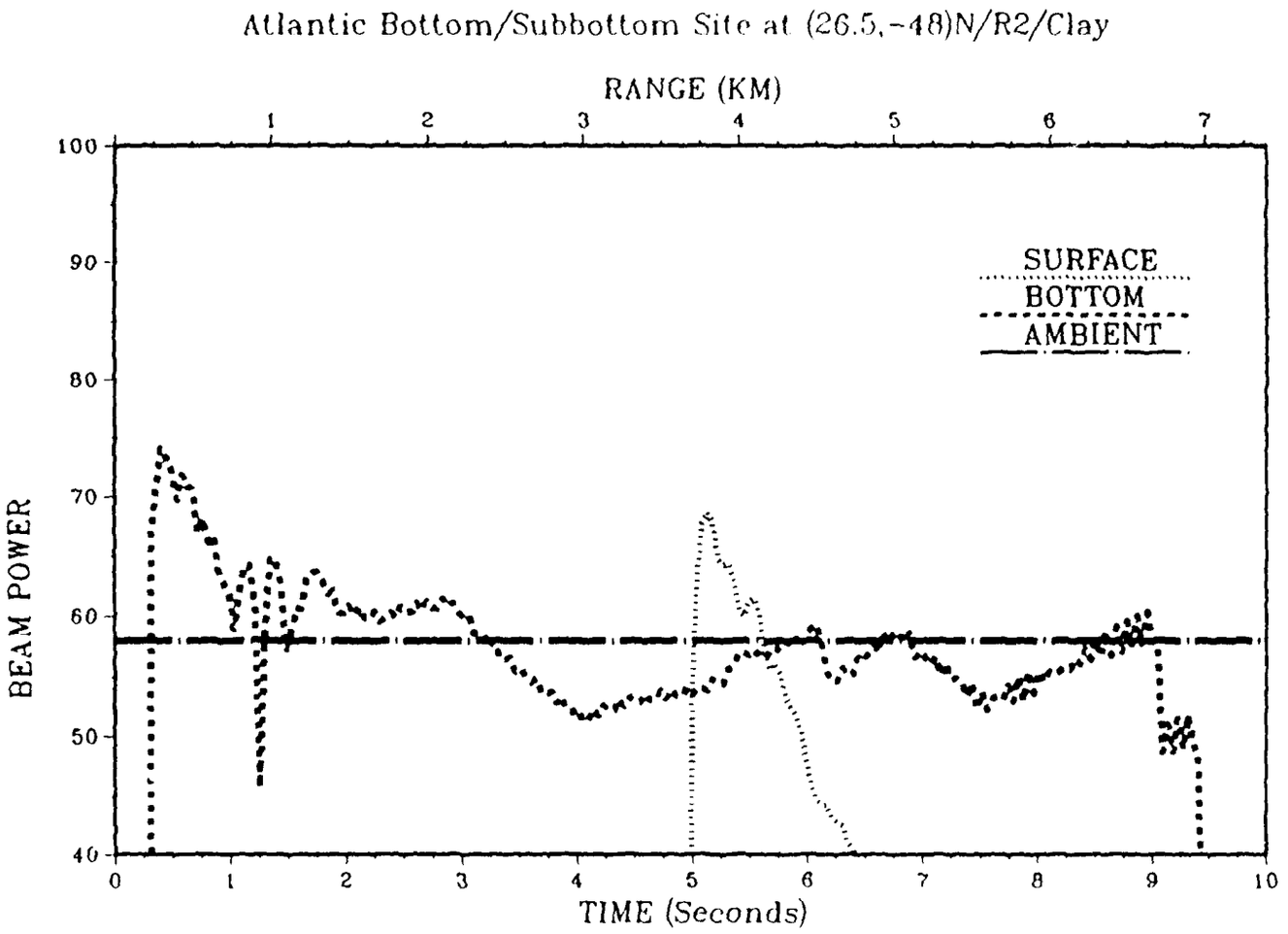
Atlantic Bottom/Subbottom Site at (26.5,-48)N/R2/Clay
RANGE (KM)
1
2
3
4
5
6
7
100
90
80
70
60
50
40
BEAM POWER
SURFACE
BOTTOM
AMBIENT
0
1
2
3
4
5
6
7
8
9
10
TIME (Seconds)

Figure 23

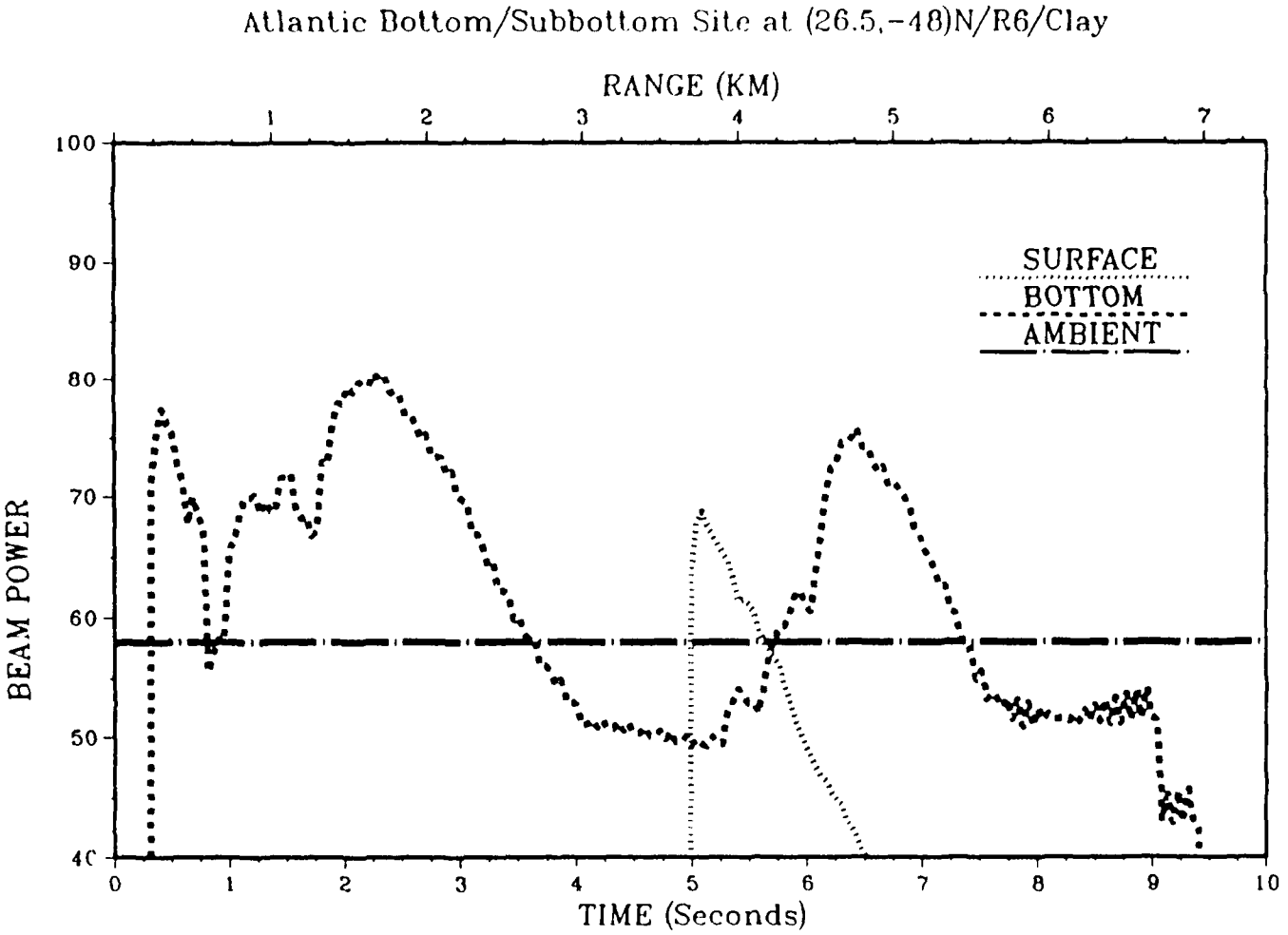
Atlantic Bottom/Subbottom Site at (26.5,-48)N/R6/Clay
RANGE (KM)
1
2
3
4
5
6
7
100
90
80
70
60
50
40
BEAM POWER
SURFACE
BOTTOM
AMBIENT
0
1
2
3
4
5
6
7
8
9
10
TIME (Seconds)

Figure 24

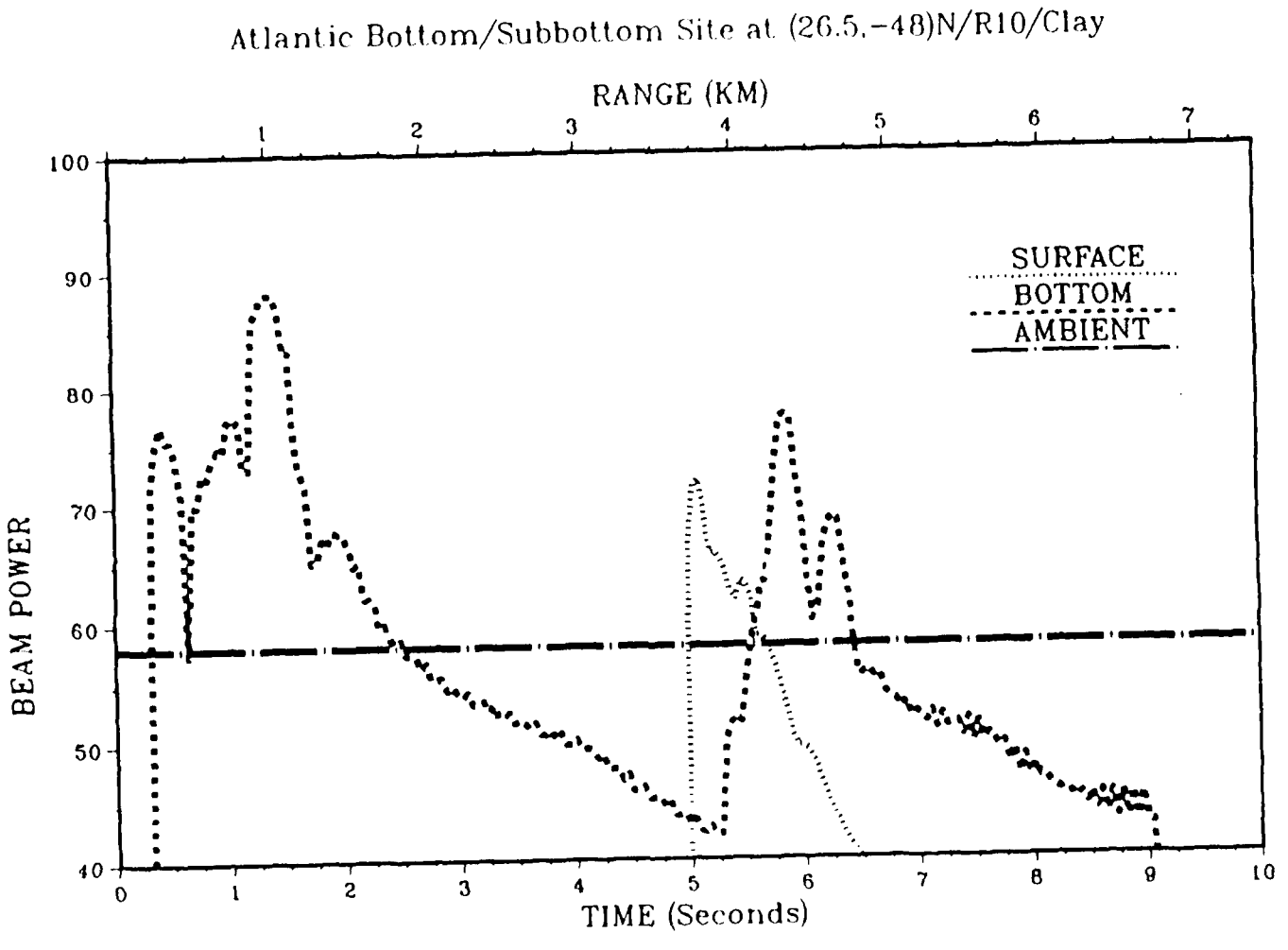
Atlantic Bottom/Subbottom Site at (26.5,-48)N/R10/Clay
RANGE (KM)
1
2
3
4
5
6
7
100
90
80
70
60
50
40
BEAM POWER
SURFACE
BOTTOM
AMBIENT
0
1
2
3
4
5
6
7
8
9
10
TIME (Seconds)

Figure 25

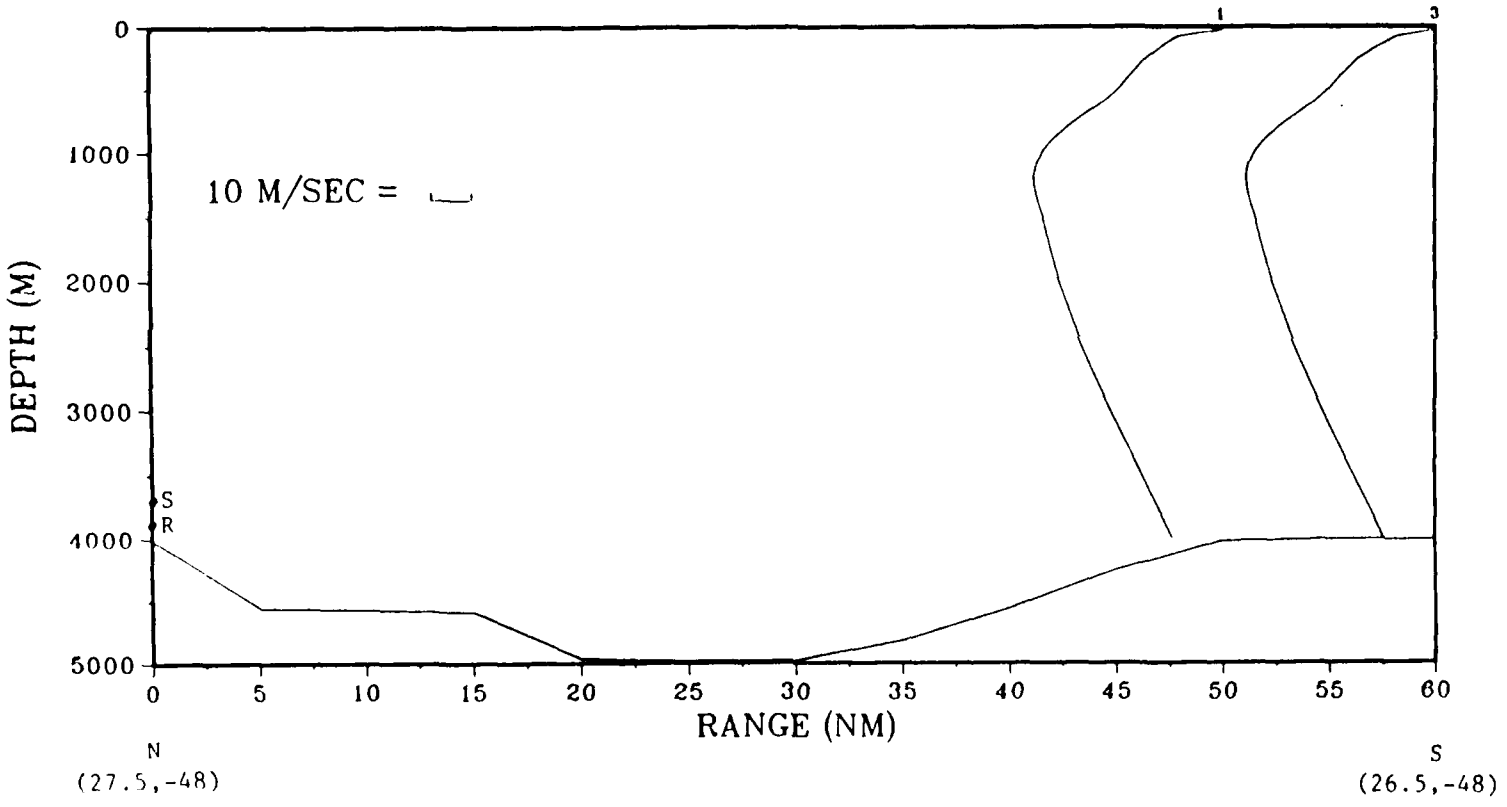
Atlantic Bottom/Subbottom Site at (27.5,-48)S
10 M/SEC =
DEPTH (M)
0
1000
2000
3000
4000
5000
S
R
1
3
0
5
10
15
20
25
30
35
40
45
50
55
60
RANGE (NM)
N
(27.5,-48)
S
(26.5,-48)

Figure 26

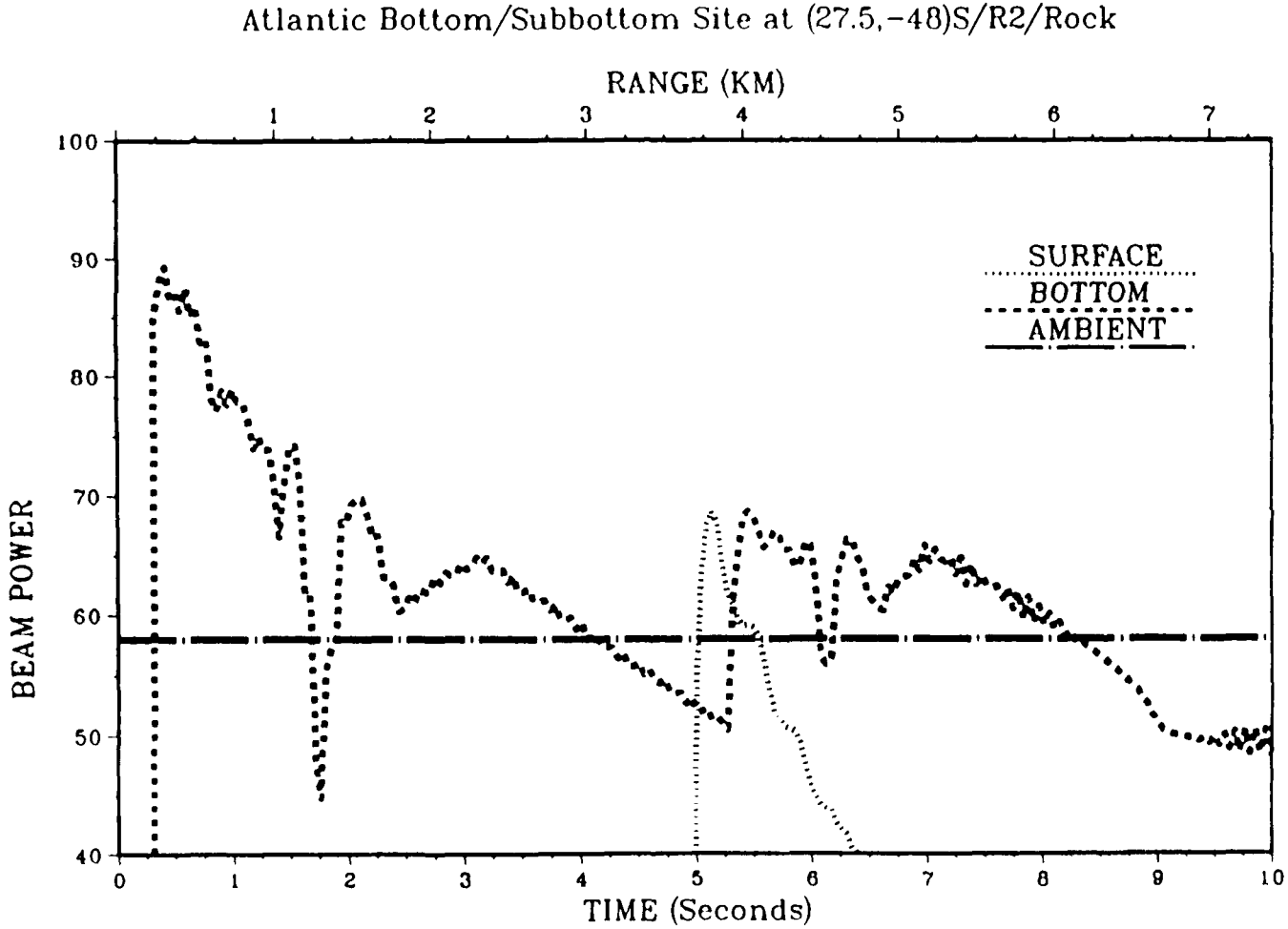
Atlantic Bottom/Subbottom Site at (27.5,-48)S/R2/Rock
RANGE (KM)
1
2
3
4
5
6
7
100
90
80
70
60
50
40
BEAM POWER
SURFACE
BOTTOM
AMBIENT
0
1
2
3
4
5
6
7
8
9
10
TIME (Seconds)

Figure 27

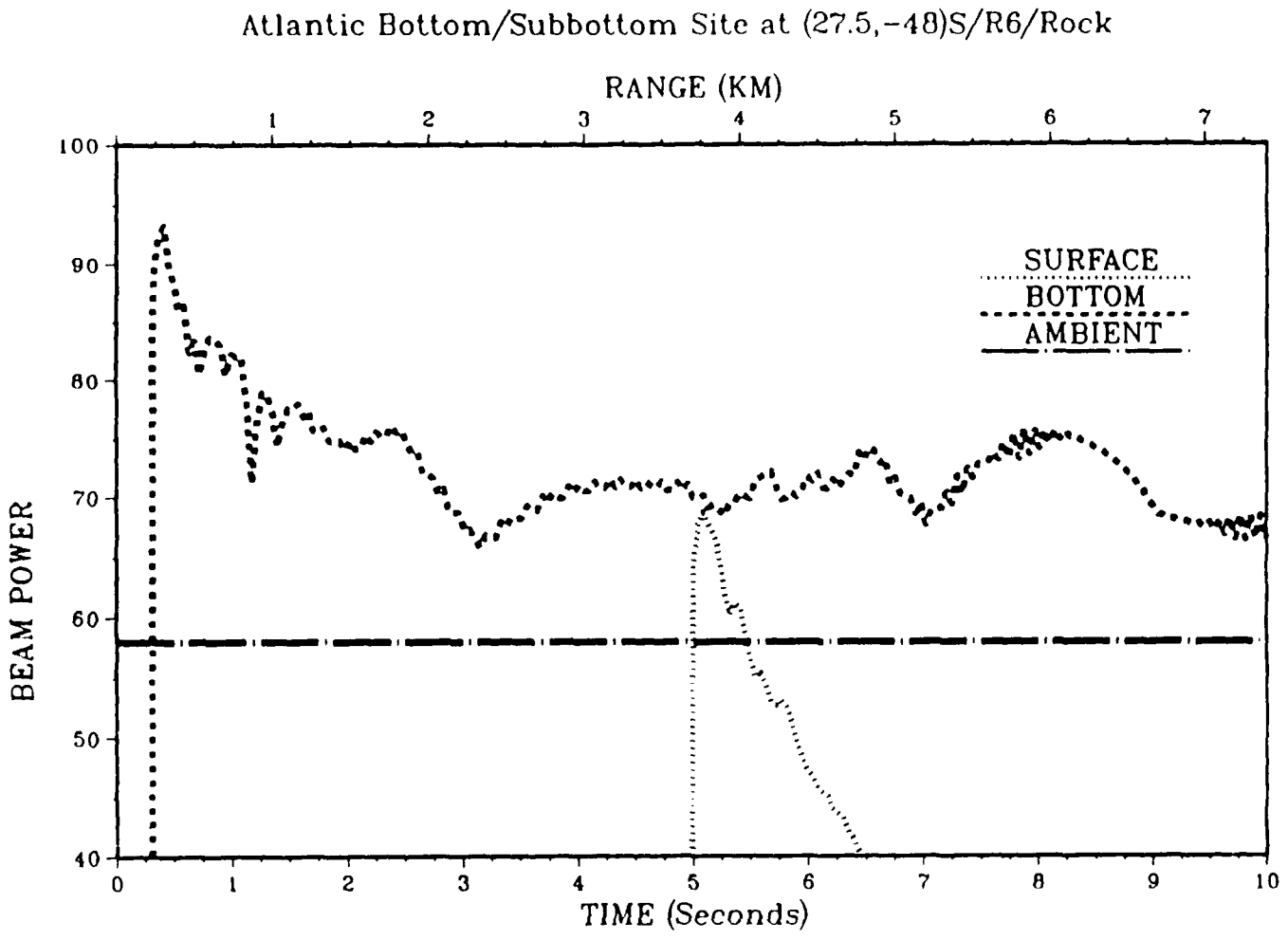
Atlantic Bottom/Subbottom Site at (27.5,-48)S/R6/Rock
RANGE (KM)
1
2
3
4
5
6
7
100
90
80
70
60
50
40
BEAM POWER
SURFACE
BOTTOM
AMBIENT
0
1
2
3
4
5
6
7
8
9
10
TIME (Seconds)

Figure 28

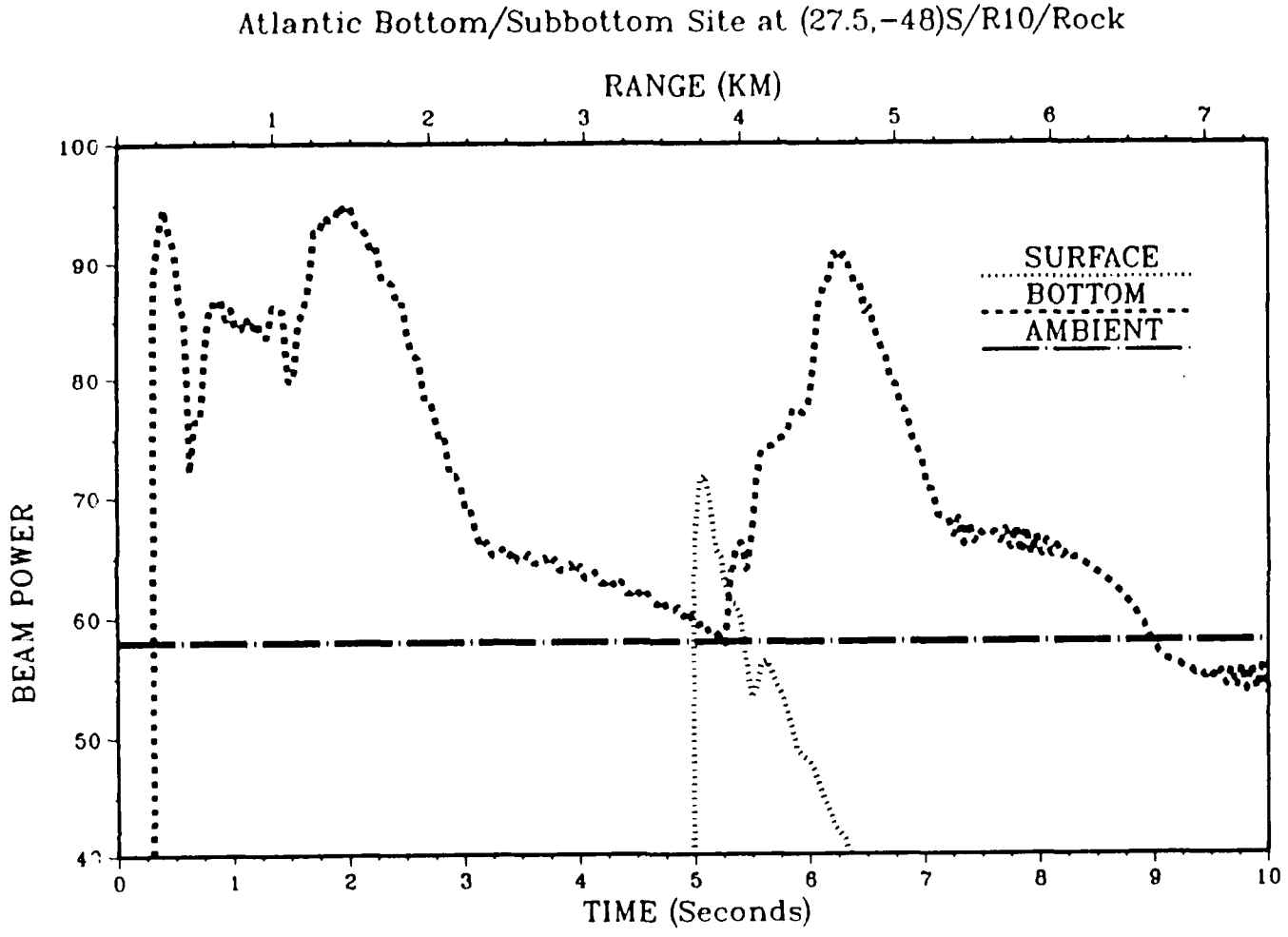
Atlantic Bottom/Subbottom Site at (27.5,-48)S/R10/Rock
RANGE (KM)
1
2
3
4
5
6
7
100
90
80
70
60
50
BEAM POWER
SURFACE
BOTTOM
AMBIENT
0
1
2
3
4
5
6
7
8
9
10
TIME (Seconds)

Figure 29

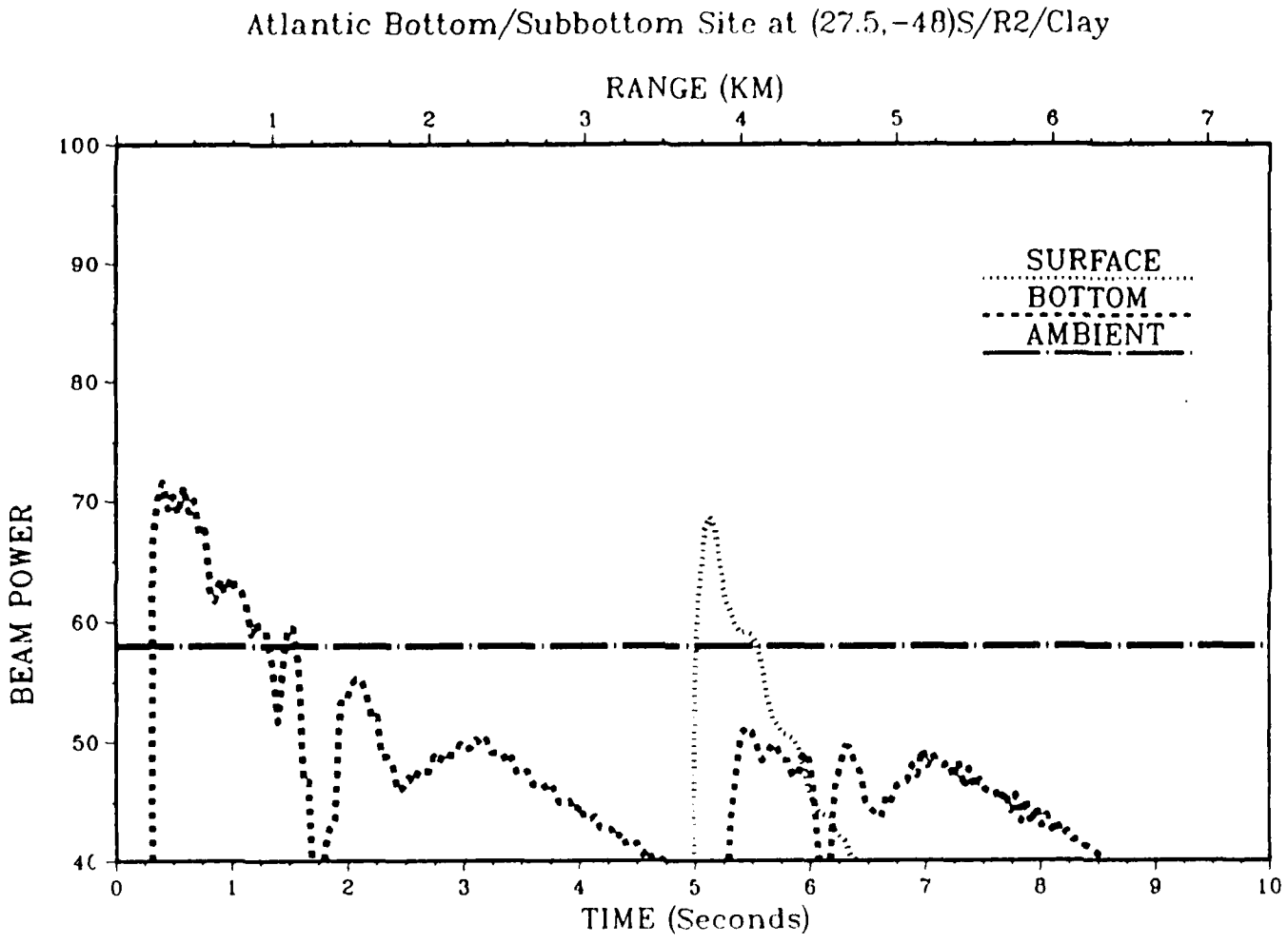
Atlantic Bottom/Subbottom Site at (27.5,-48)S/R2/Clay
RANGE (KM)
1
2
3
4
5
6
7
100
90
80
70
60
50
40
BEAM POWER
SURFACE
BOTTOM
AMBIENT
0
1
2
3
4
5
6
7
8
9
10
TIME (Seconds)

Figure 30

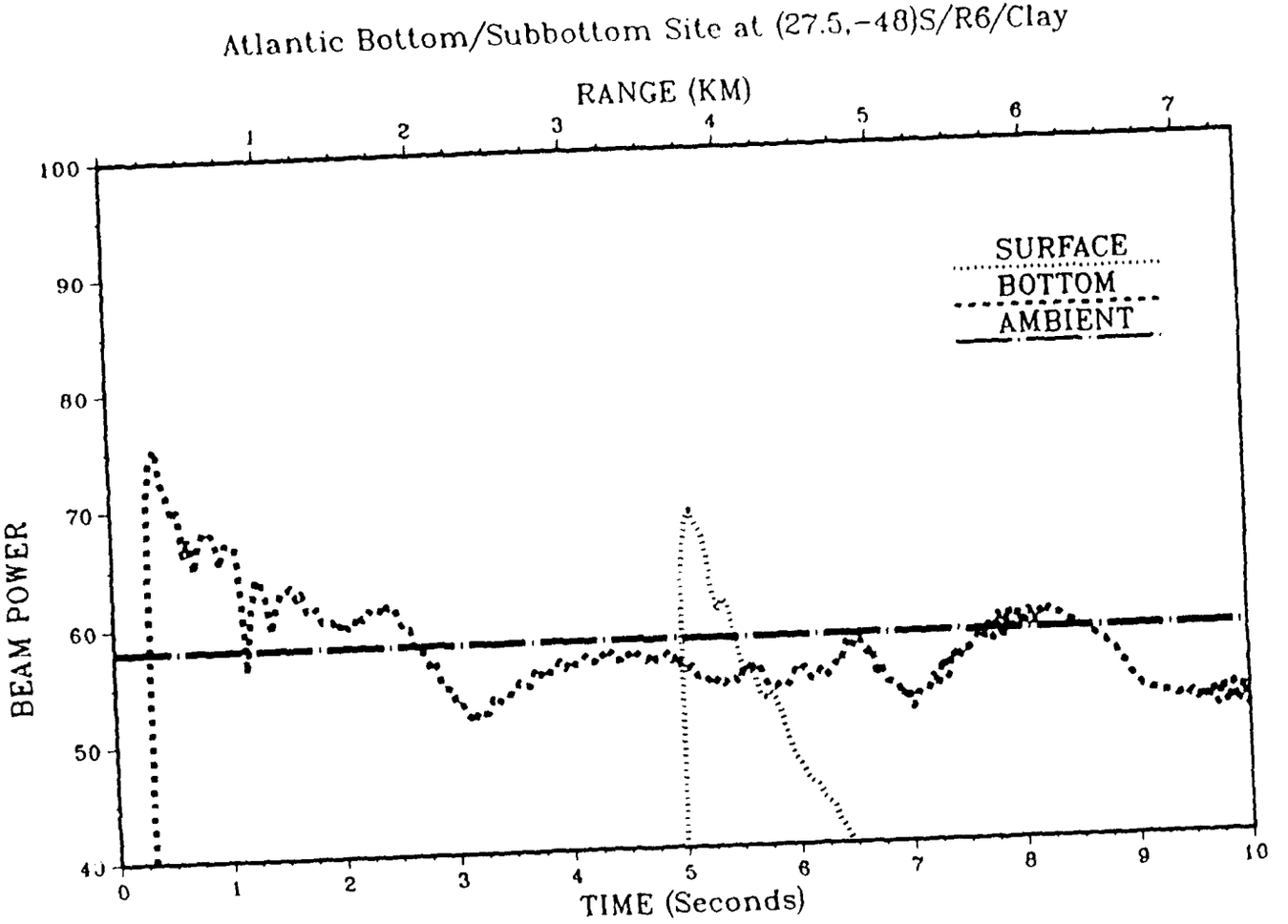
Atlantic Bottom/Subbottom Site at (27.5,-48)S/R6/Clay
RANGE (KM)
1
2
3
4
5
6
7
100
90
80
70
60
50
40
BEAM POWER
SURFACE
BOTTOM
AMBIENT
0
1
2
3
4
5
6
7
8
9
10
TIME (Seconds)

Figure 31

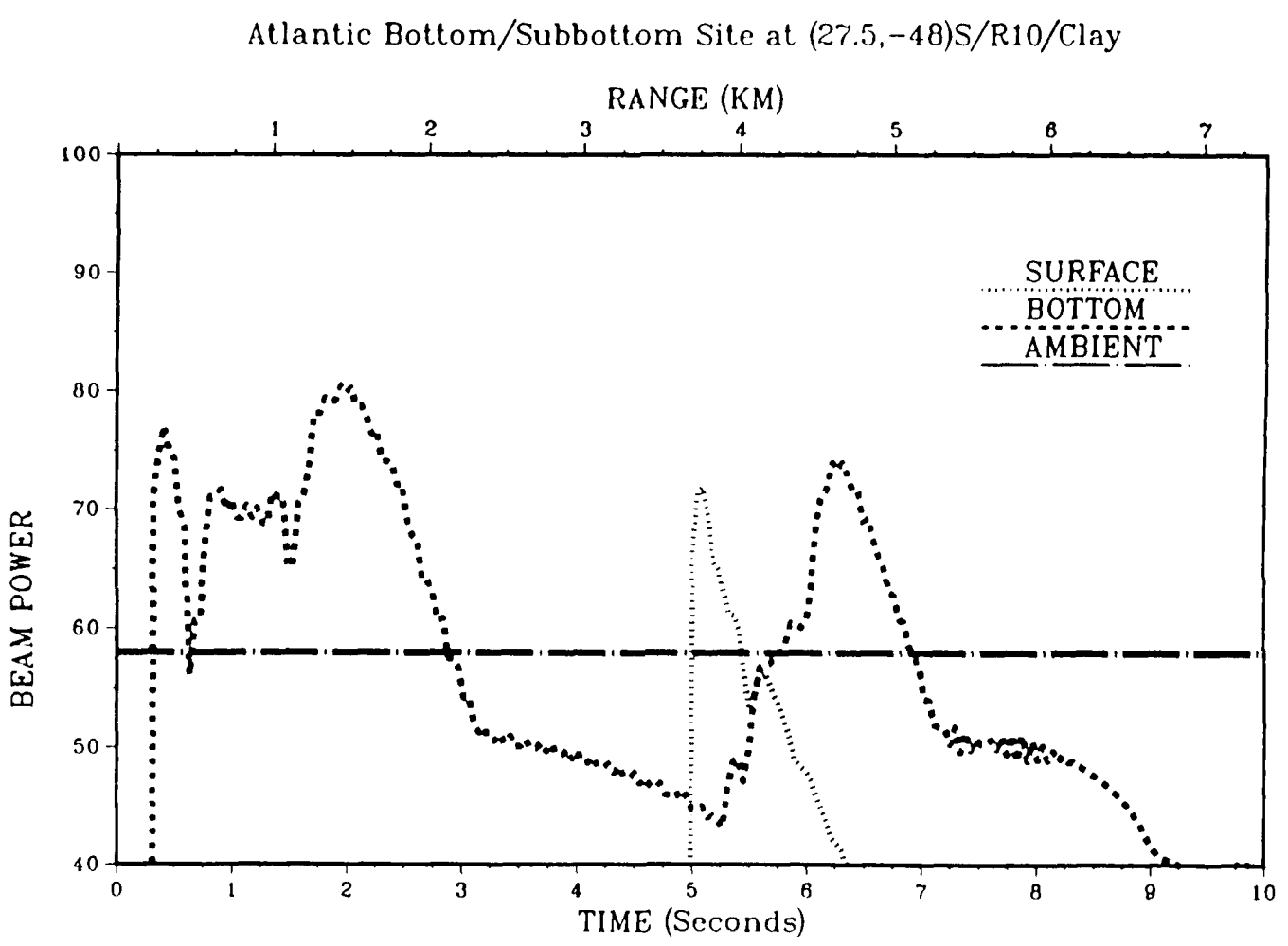
Atlantic Bottom/Subbottom Site at (27.5,-48)S/R10/Clay
RANGE (KM)
1
2
3
4
5
6
7
100
90
80
70
60
50
40
BEAM POWER
SURFACE
BOTTOM
AMBIENT
0
1
2
3
4
5
6
7
8
9
10
TIME (Seconds)

Figure 32

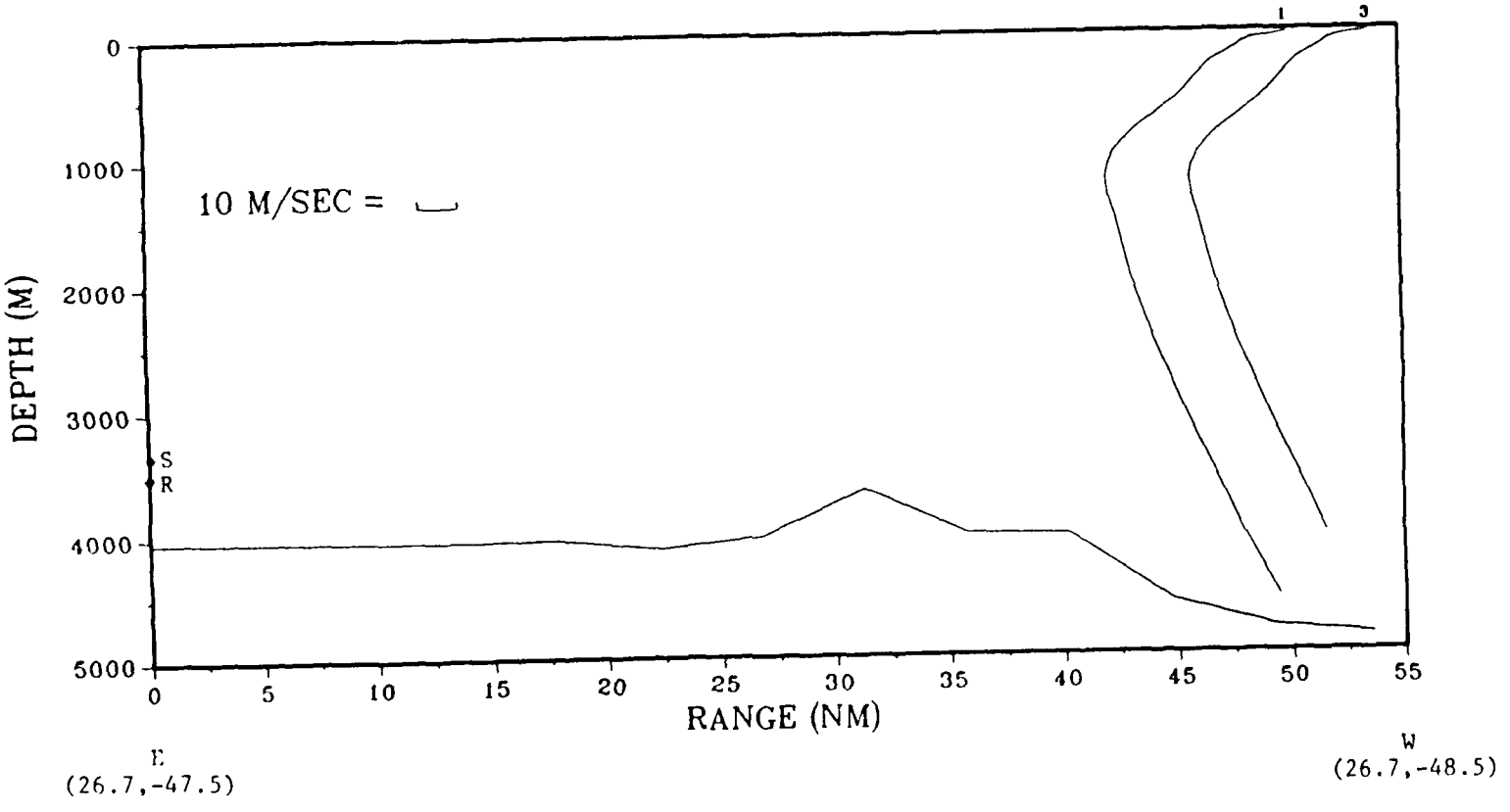
Atlantic Bottom/Subbottom Site at (26.7,-47.5)W
1
3
0
1000
2000
3000
4000
5000
10 M/SEC =
DEPTH (M)
S
R
0
5
10
15
20
25
30
35
40
45
50
55
RANGE (NM)
E
(26.7,-47.5)
W
(26.7,-48.5)

Figure 33

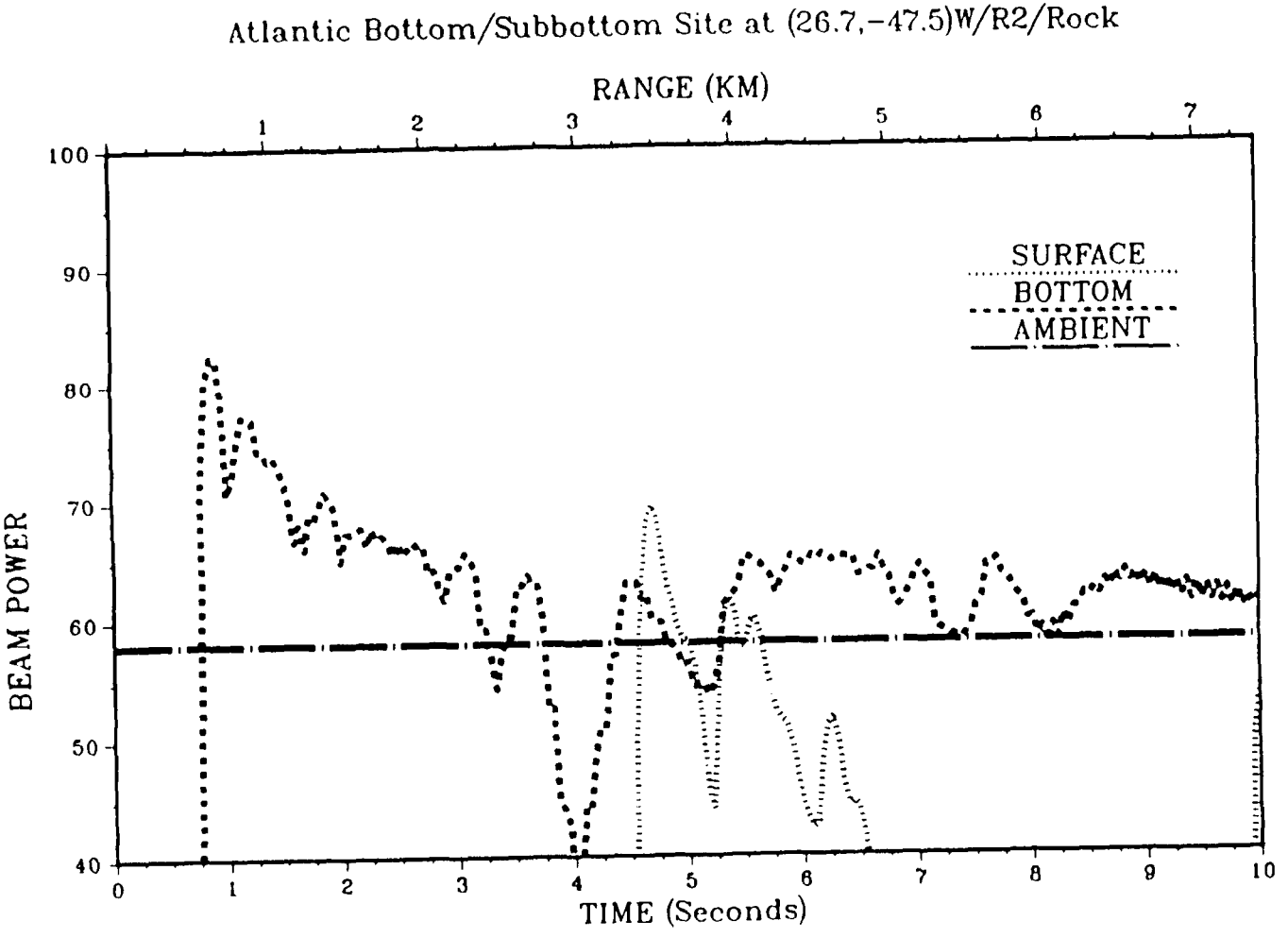
Atlantic Bottom/Subbottom Site at (26.7,-47.5)W/R2/Rock
RANGE (KM)
1
2
3
4
5
6
7
100
90
80
70
60
50
40
BEAM POWER
SURFACE
BOTTOM
AMBIENT
0
1
2
3
4
5
6
7
8
9
10
TIME (Seconds)

Figure 34

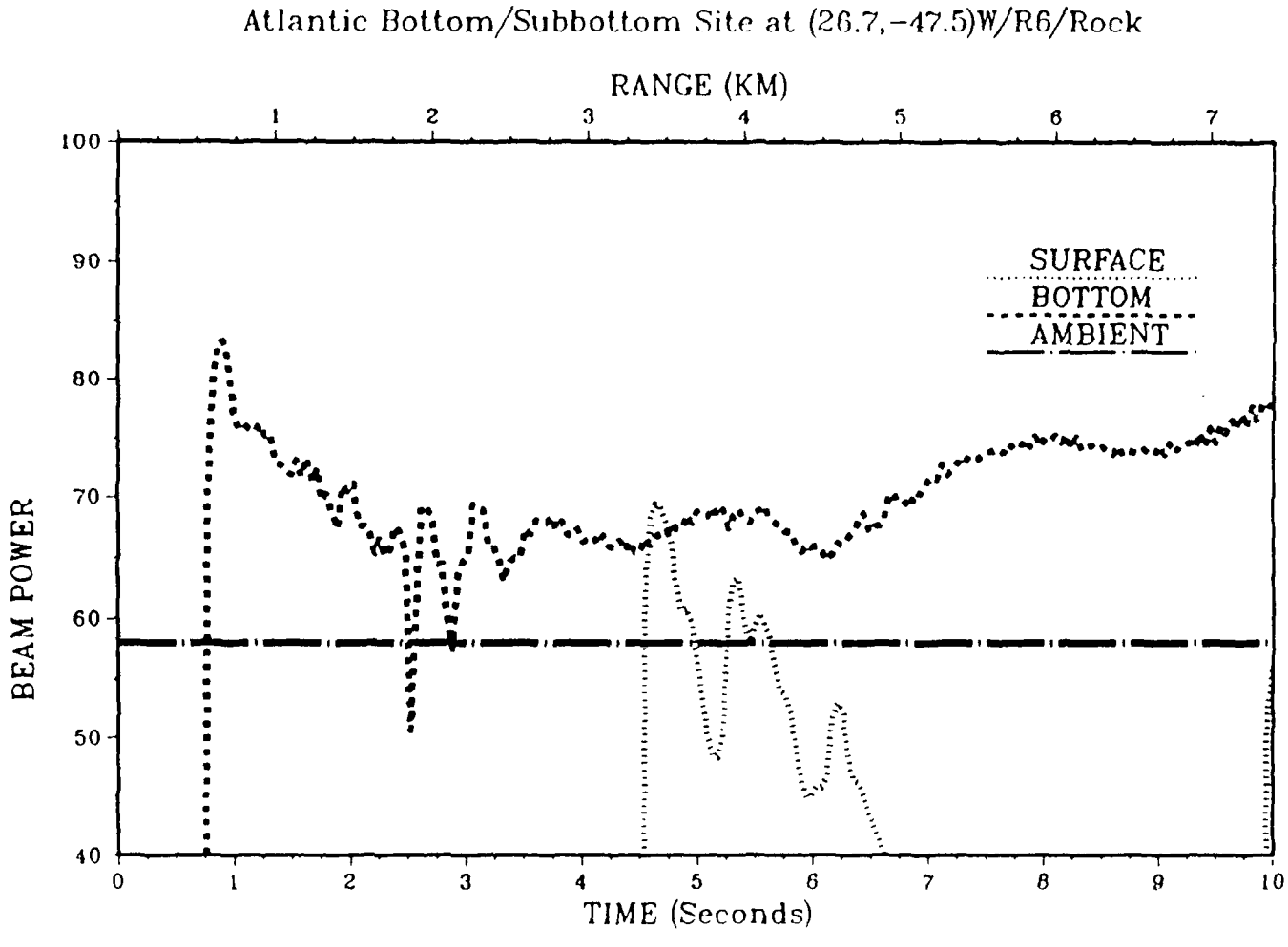
Atlantic Bottom/Subbottom Site at (26.7,-47.5)W/R6/Rock
RANGE (KM)
1
2
3
4
5
6
7
100
90
80
70
60
50
40
BEAM POWER
SURFACE
BOTTOM
AMBIENT
0
1
2
3
4
5
6
7
8
9
10
TIME (Seconds)

Figure 35

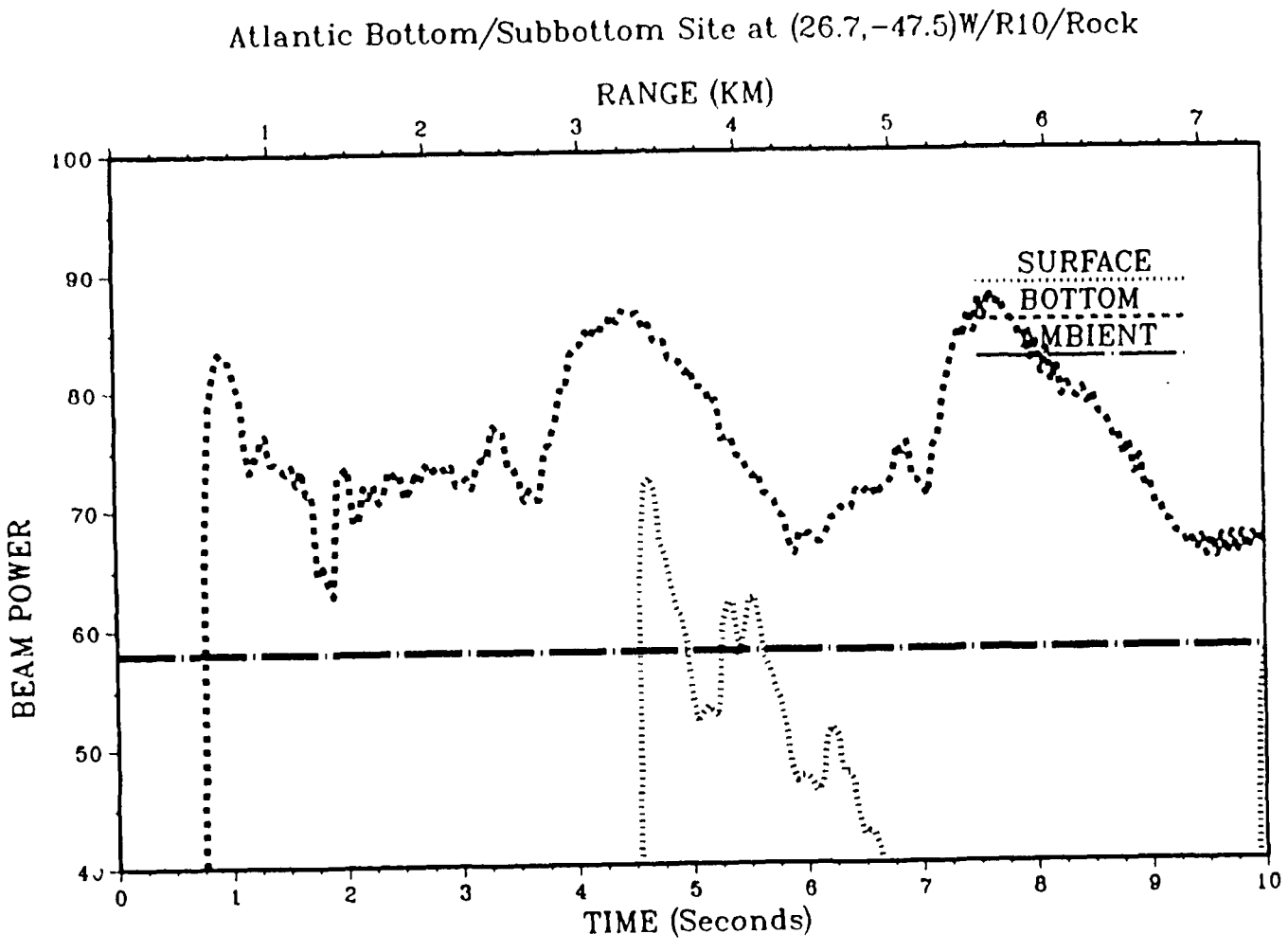
Atlantic Bottom/Subbottom Site at (26.7,-47.5)W/R10/Rock
RANGE (KM)
1
2
3
4
5
6
7
100
90
80
70
60
50
40
BEAM POWER
SURFACE
BOTTOM
AMBIENT
0
1
2
3
4
5
6
7
8
9
10
TIME (Seconds)

Figure 36

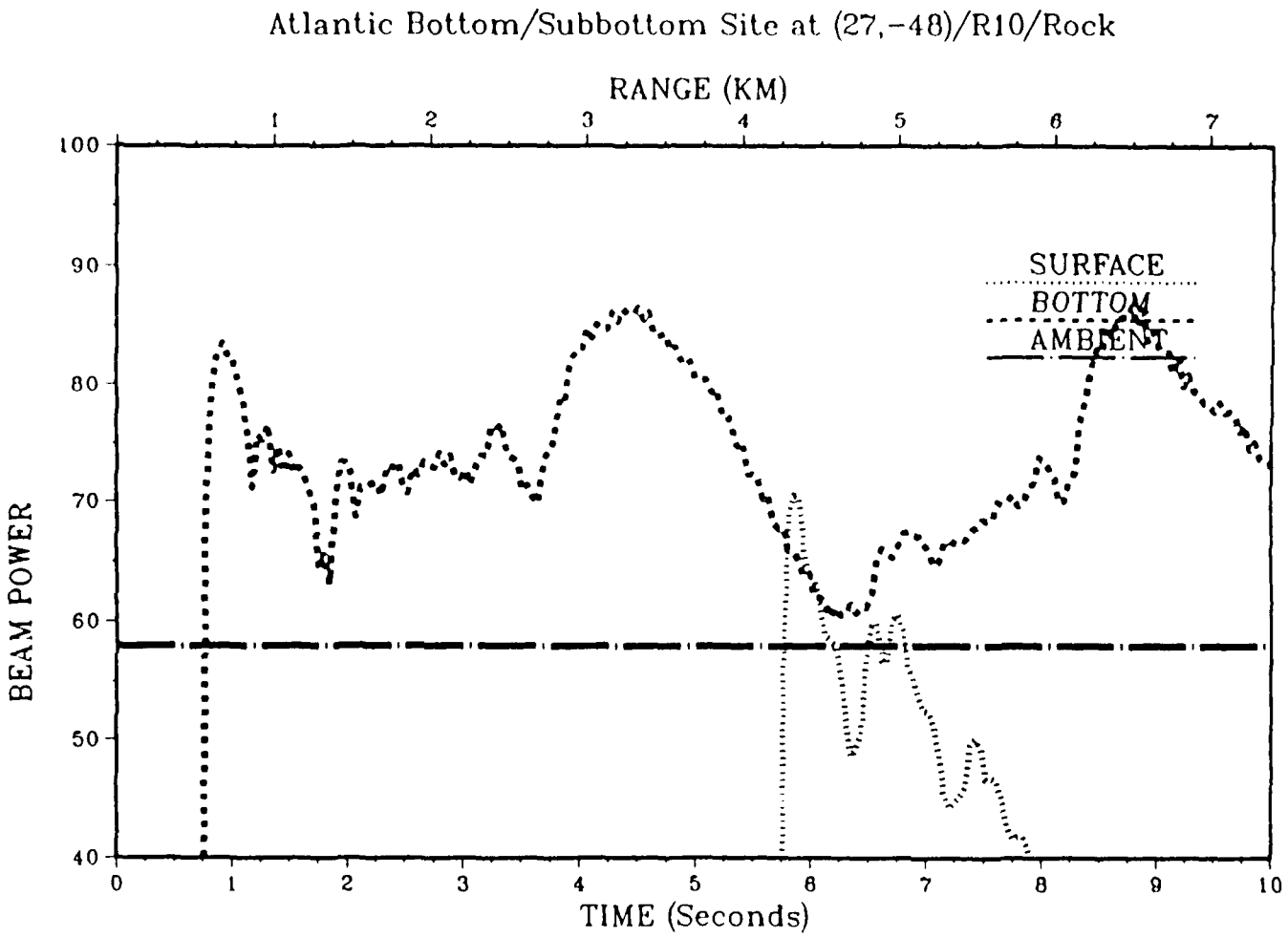
Atlantic Bottom/Subbottom Site at (27,-48)/R10/Rock
RANGE (KM)
1
2
3
4
5
6
7
100
90
80
70
60
50
40
BEAM POWER
SURFACE
BOTTOM
AMBIENT
0
1
2
3
4
5
6
7
8
9
10
TIME (Seconds)

Figure 37

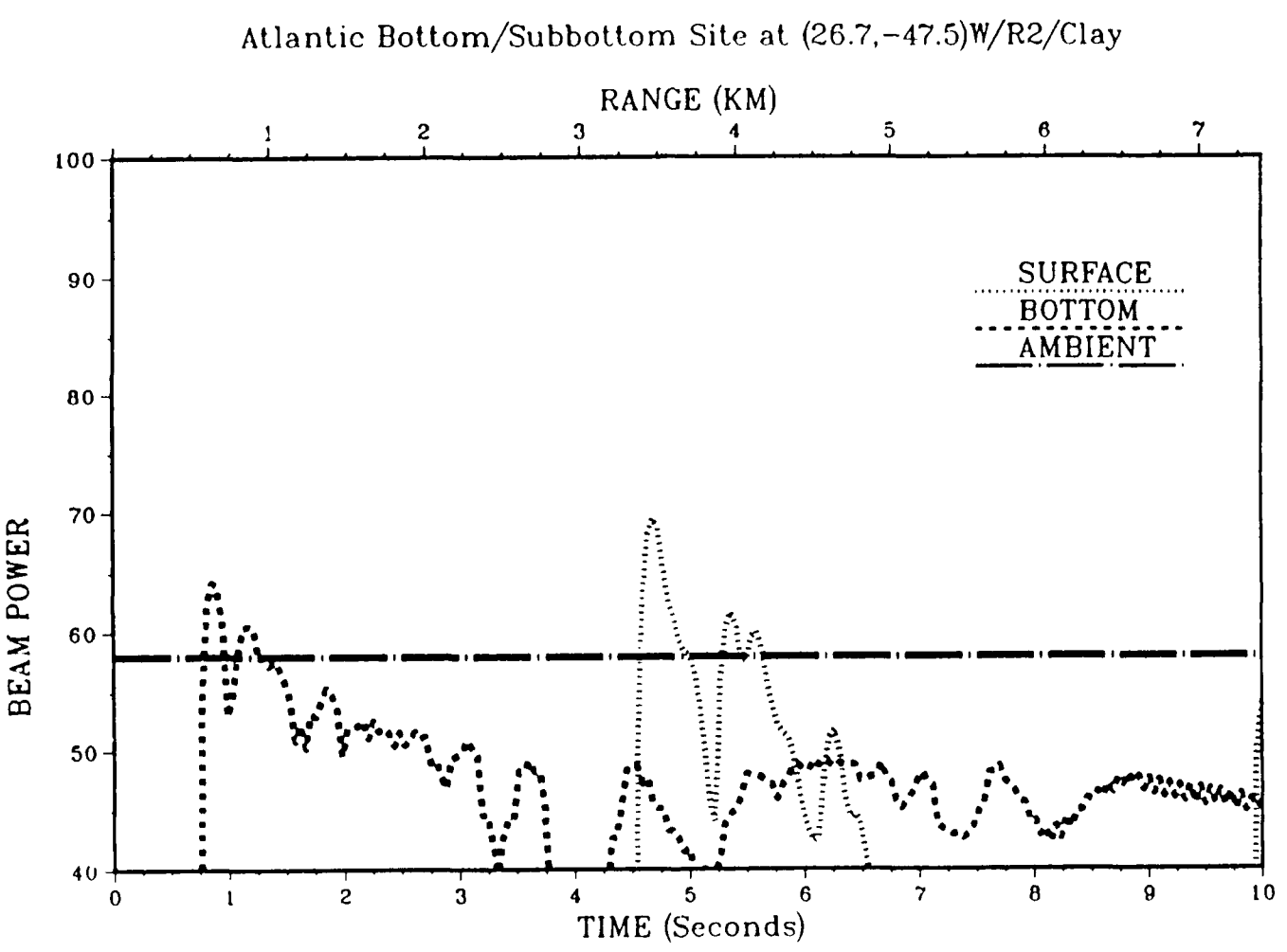
Atlantic Bottom/Subbottom Site at (26.7,-47.5)W/R2/Clay
RANGE (KM)
1
2
3
4
5
6
7
100
90
80
70
60
50
40
BEAM POWER
SURFACE
BOTTOM
AMBIENT
0
1
2
3
4
5
6
7
8
9
10
TIME (Seconds)

Figure 38

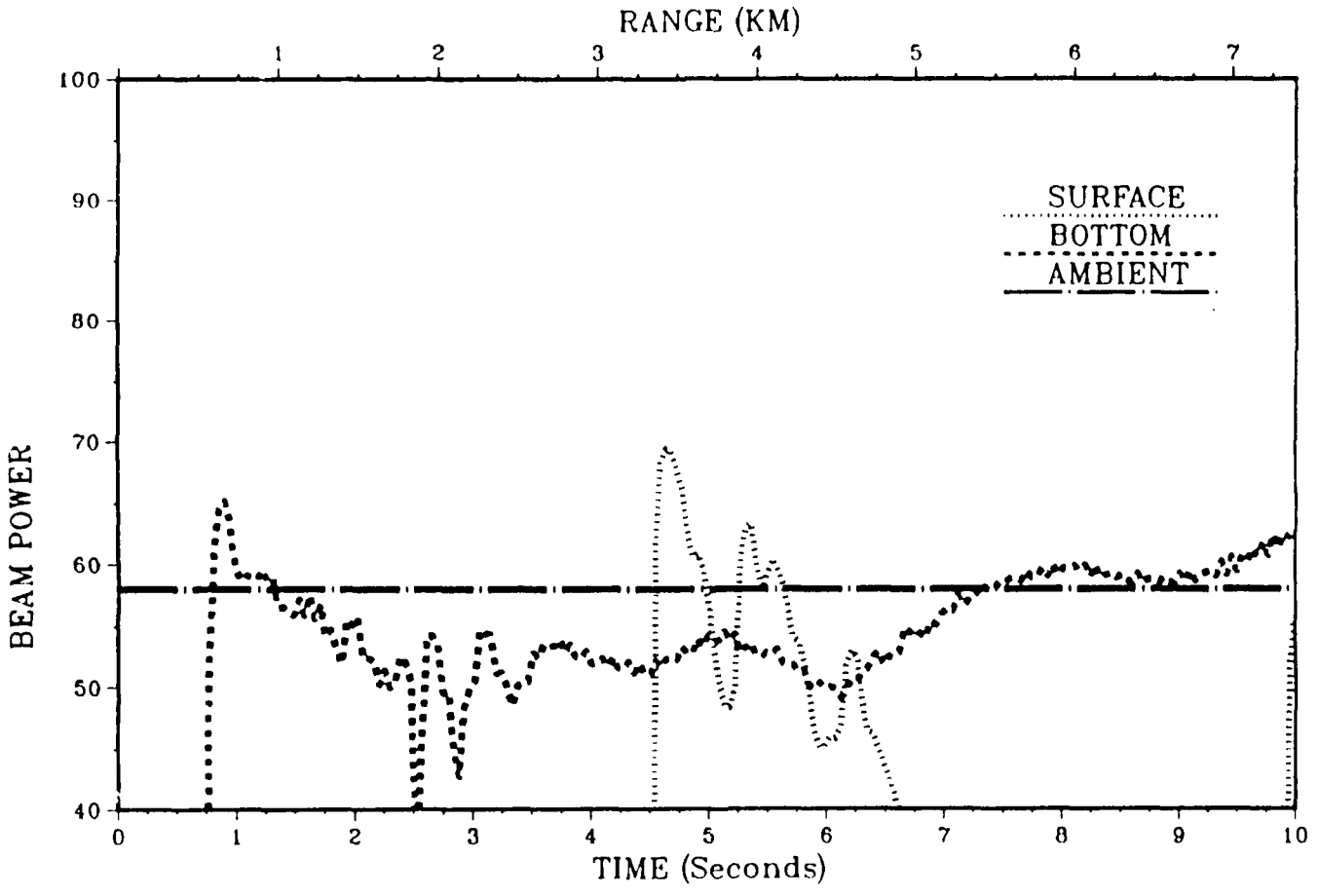
Atlantic Bottom/Subbottom Site at (26.7,-47.5)W/R6/Clay
RANGE (KM)
1
2
3
4
5
6
7
100
90
80
70
60
50
40
BEAM POWER
SURFACE
BOTTOM
AMBIENT
0
1
2
3
4
5
6
7
8
9
10
TIME (Seconds)

Figure 39

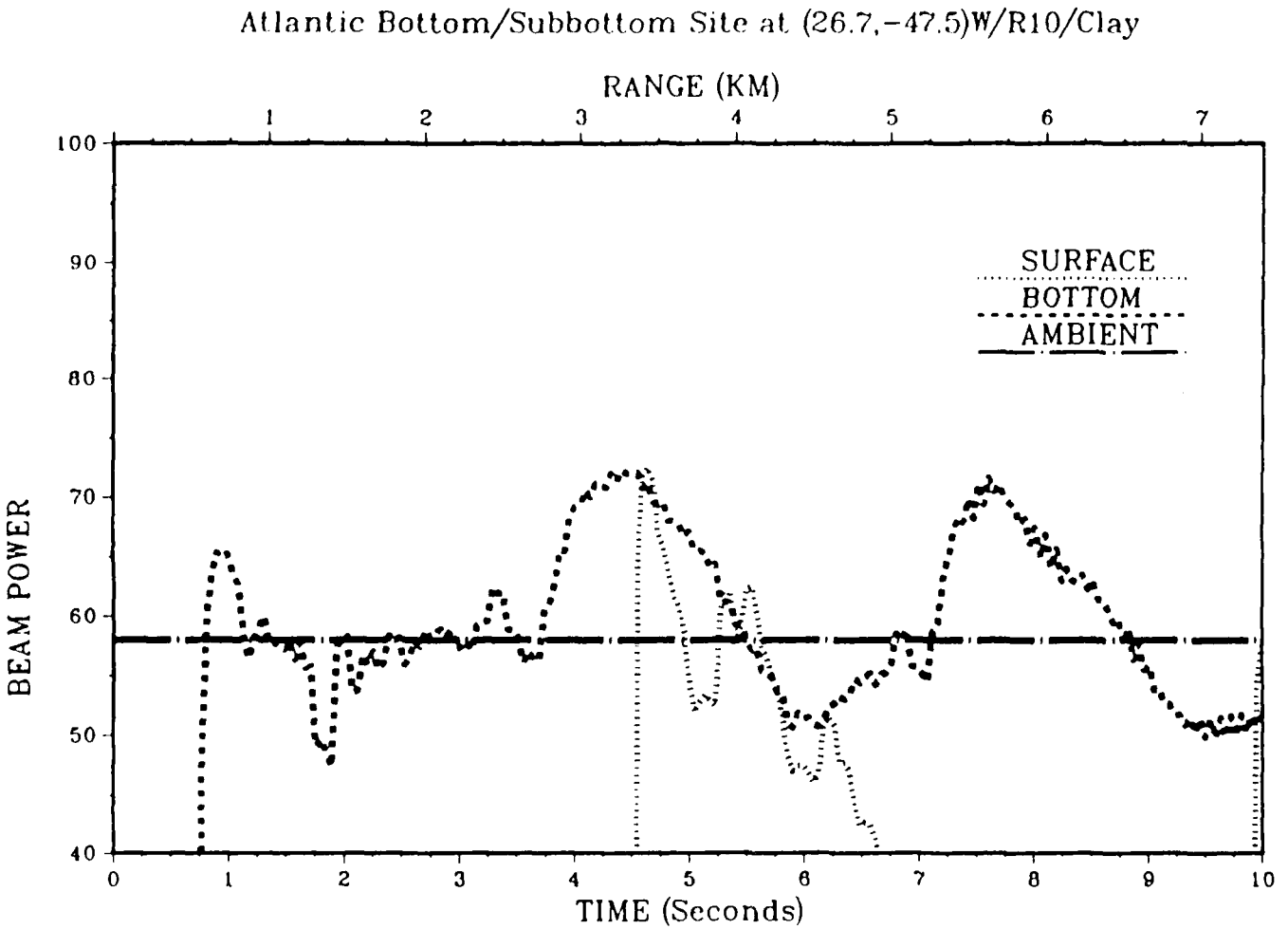
Atlantic Bottom/Subbottom Site at (26.7,-47.5)W/R10/Clay
RANGE (KM)
1
2
3
4
5
6
7
100
90
80
70
60
50
40
BEAM POWER
SURFACE
BOTTOM
AMBIENT
0
1
2
3
4
5
6
7
8
9
10
TIME (Seconds)

Figure 40

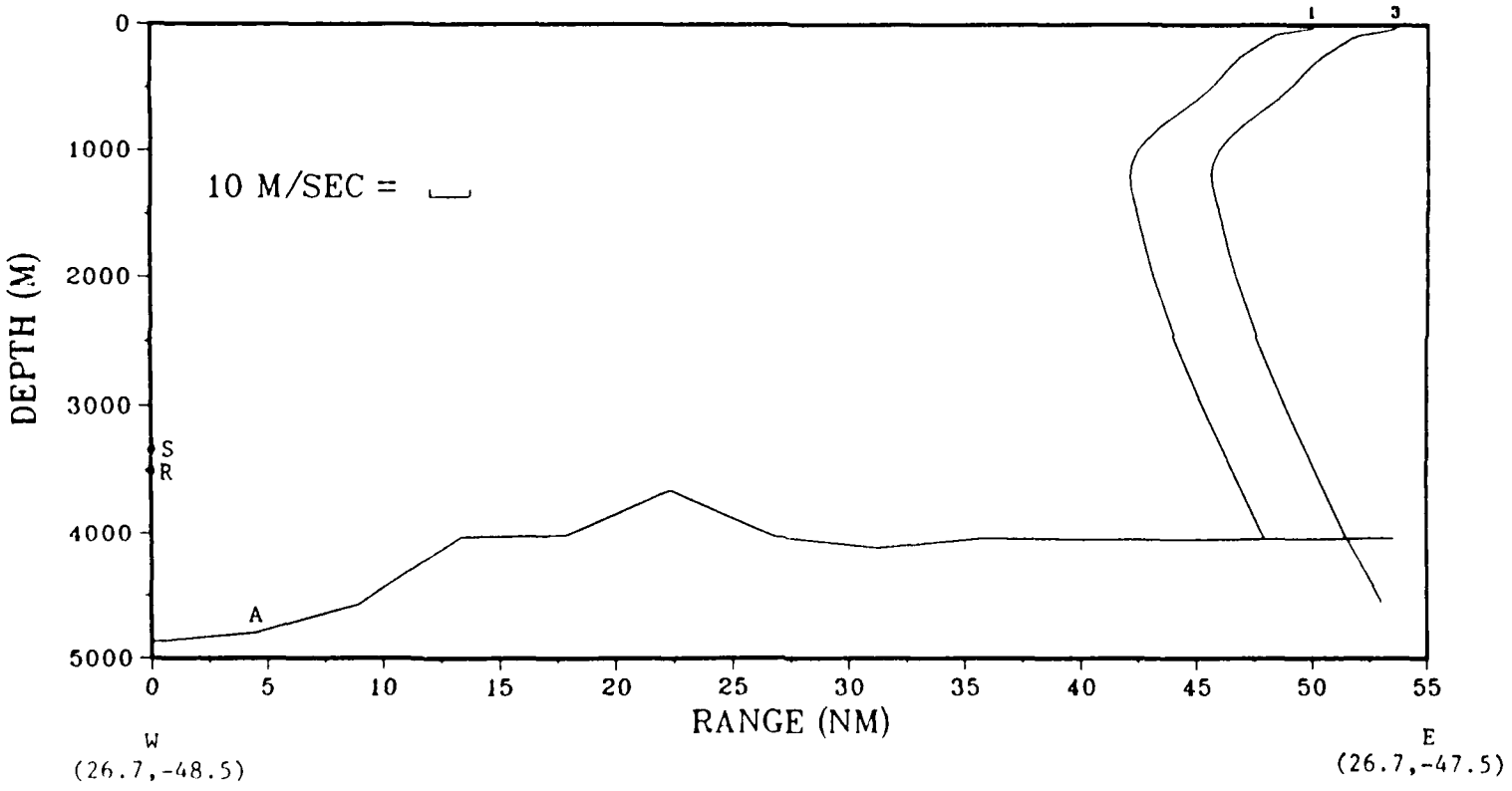
Atlantic Bottom/Subbottom Site at (26.7,-48.5)E
0
1000
2000
3000
4000
5000
DEPTH (M)
10 M/SEC =
S
R
A
1
3
0
5
10
15
20
25
30
35
40
45
50
55
RANGE (NM)
W
(26.7,-48.5)
E
(26.7,-47.5)

Figure 41

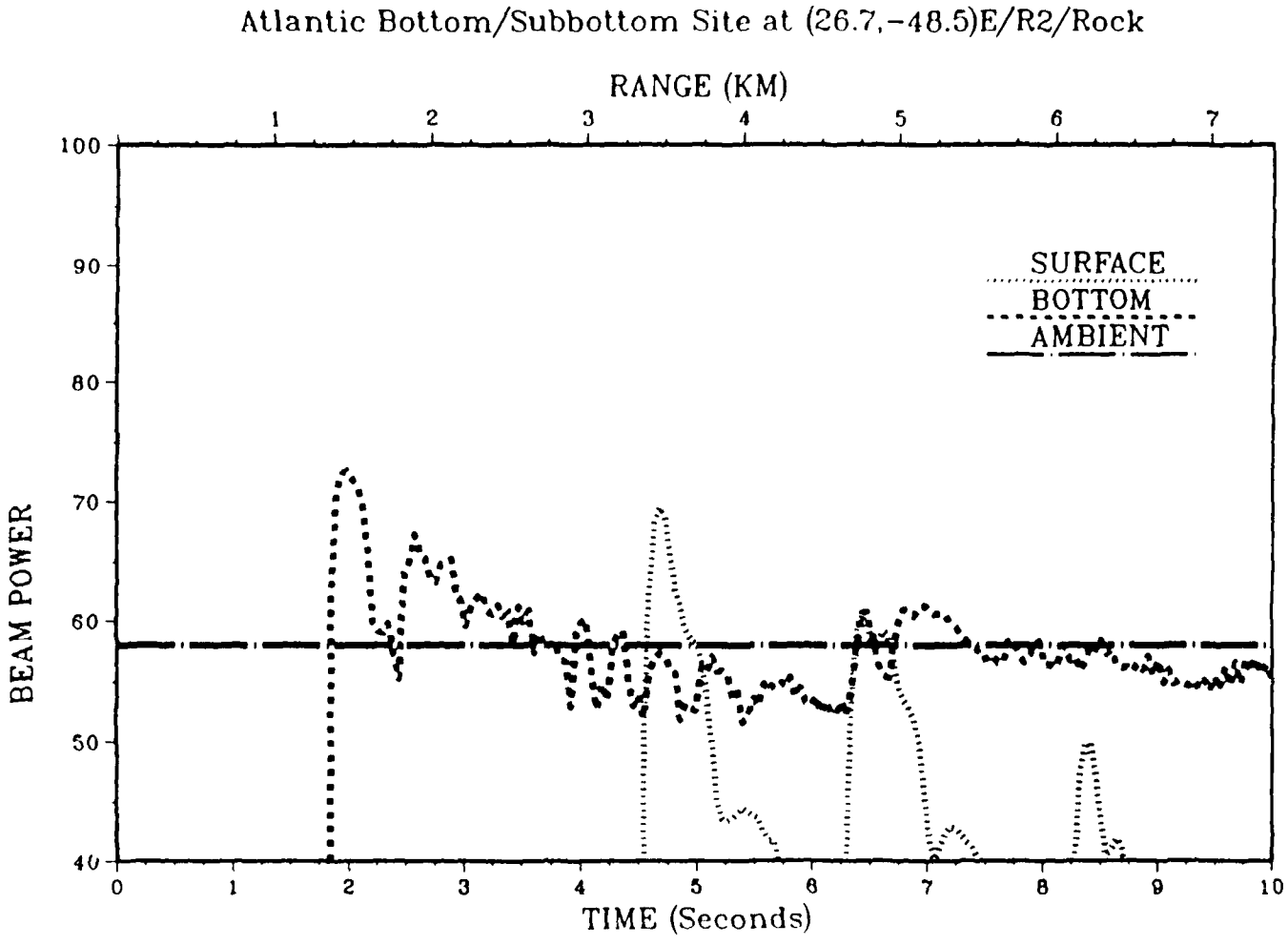
Atlantic Bottom/Subbottom Site at (26.7,-48.5)E/R2/Rock
RANGE (KM)
1
2
3
4
5
6
7
100
90
80
70
60
50
40
BEAM POWER
SURFACE
BOTTOM
AMBIENT
0
1
2
3
4
5
6
7
8
9
10
TIME (Seconds)

Figure 42

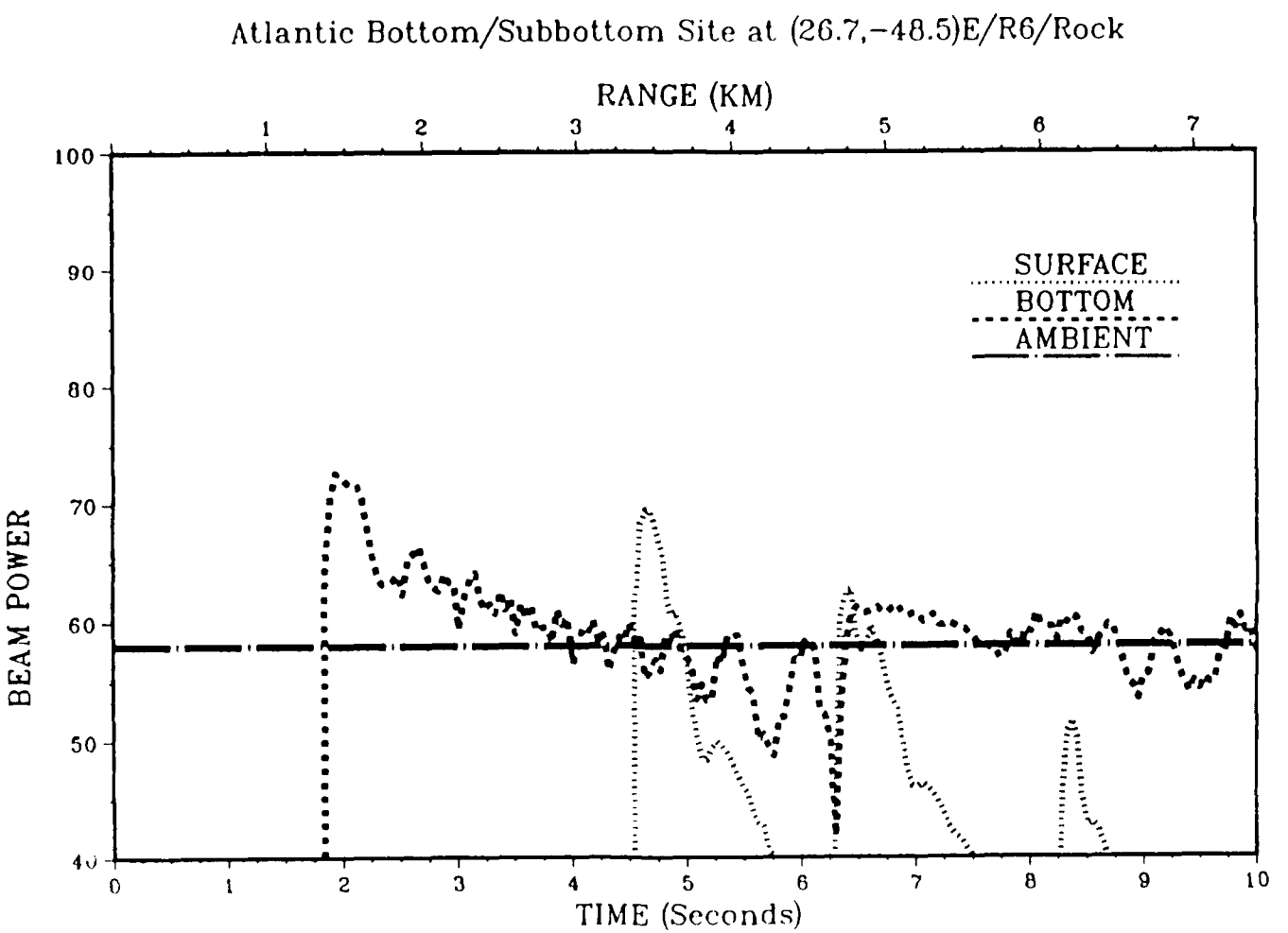
Atlantic Bottom/Subbottom Site at (26.7,-48.5)E/R6/Rock
RANGE (KM)
1
2
3
4
5
6
7
100
90
80
70
60
50
40
BEAM POWER
SURFACE
BOTTOM
AMBIENT
0
1
2
3
4
5
6
7
8
9
10
TIME (Seconds)

Figure 43

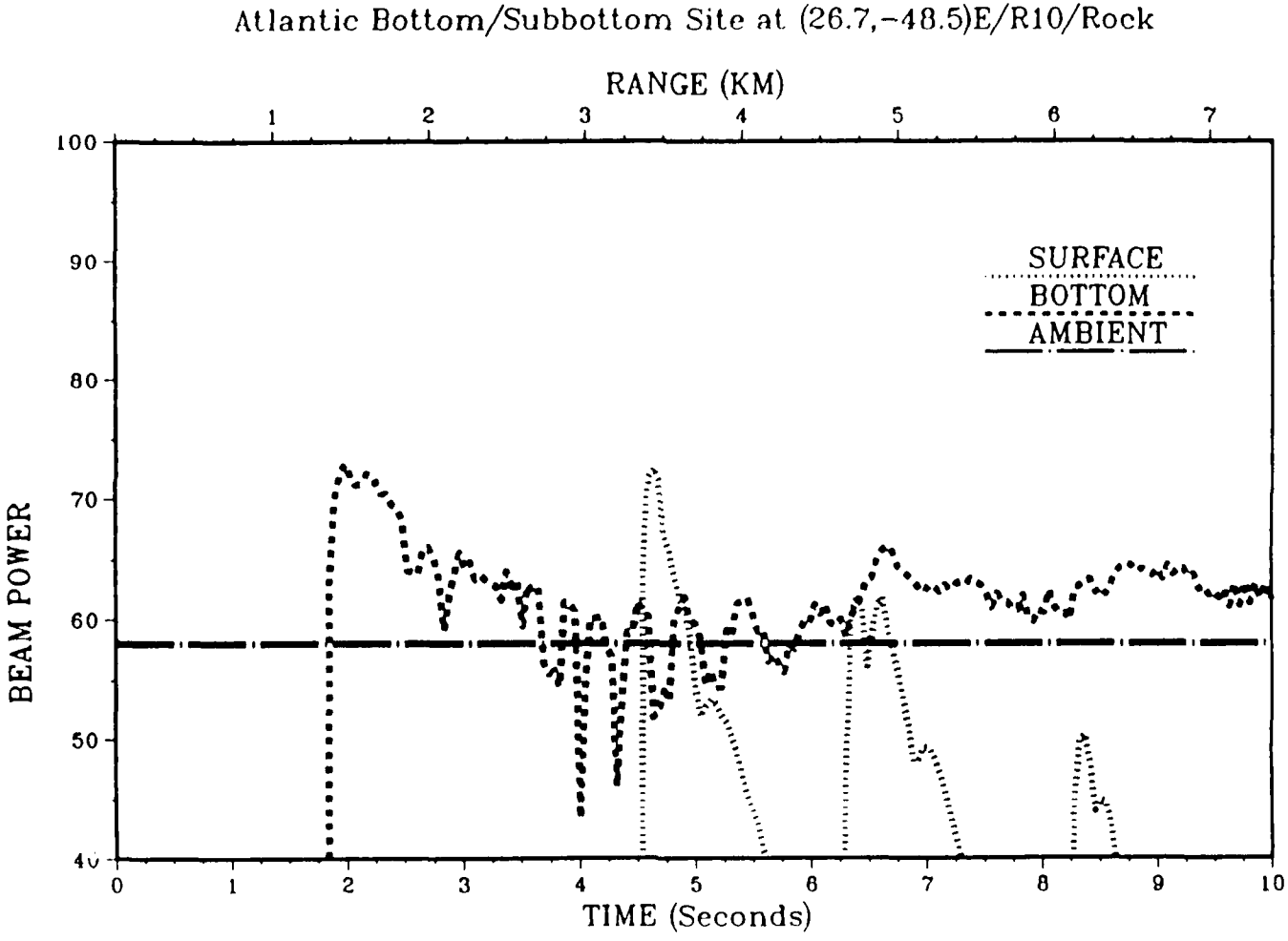
Atlantic Bottom/Subbottom Site at (26.7,-48.5)E/R10/Rock
RANGE (KM)
1
2
3
4
5
6
7
100
90
80
70
60
50
40
BEAM POWER
SURFACE
BOTTOM
AMBIENT
0
1
2
3
4
5
6
7
8
9
10
TIME (Seconds)

Figure 44

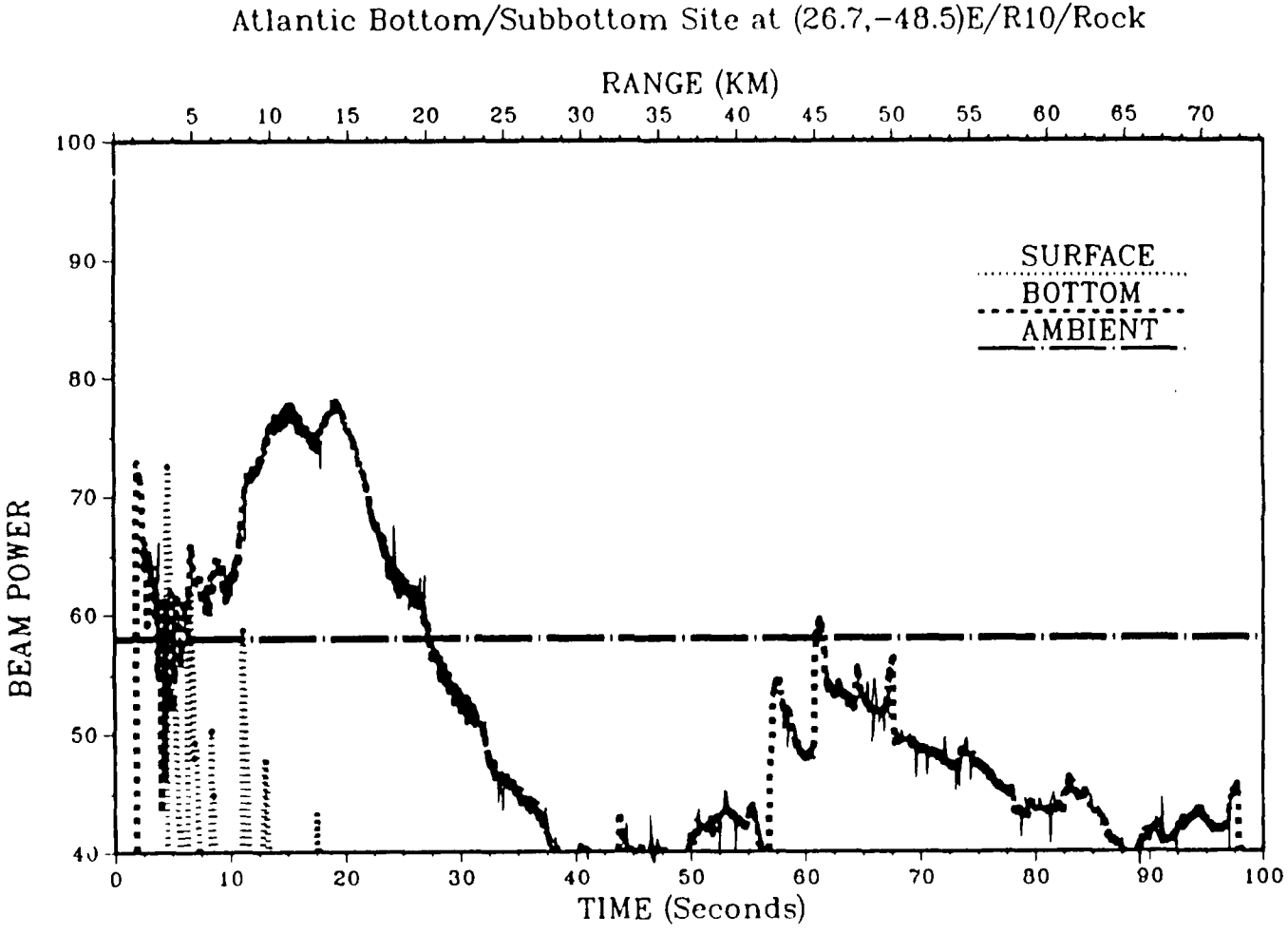
Atlantic Bottom/Subbottom Site at (26.7,-48.5)E/R10/Rock
RANGE (KM)
5 10 15 20 25 30 35 40 45 50 55 60 65 70
100
90
80
70
60
50
40
BEAM POWER
SURFACE
BOTTOM
AMBIENT
0 10 20 30 40 50 60 70 80 90 100
TIME (Seconds)

Figure 45

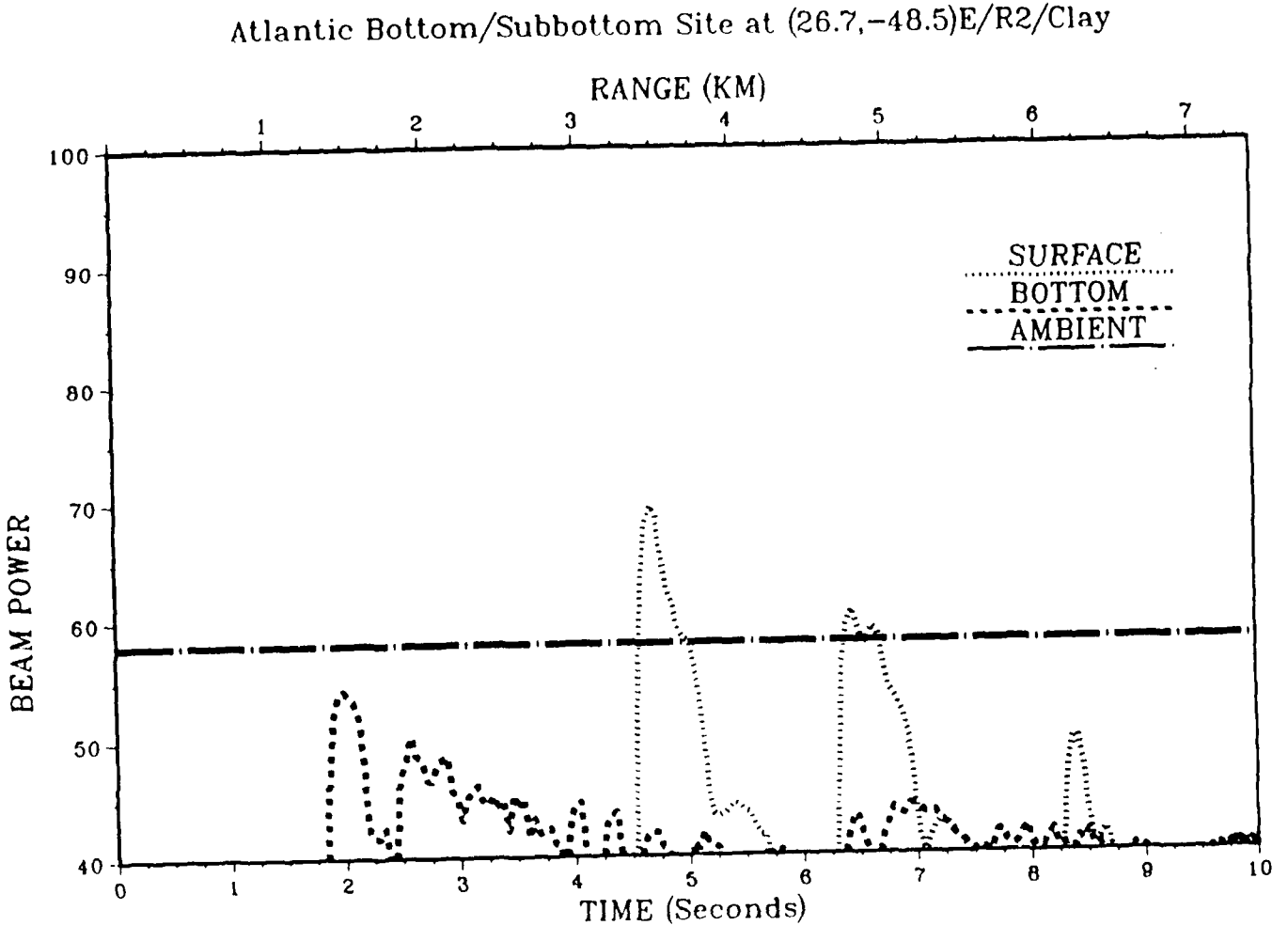
Atlantic Bottom/Subbottom Site at (26.7,-48.5)E/R2/Clay
RANGE (KM)
1
2
3
4
5
6
7
100
90
80
70
60
50
40
BEAM POWER
SURFACE
BOTTOM
AMBIENT
0
1
2
3
4
5
6
7
8
9
10
TIME (Seconds)

Figure 46

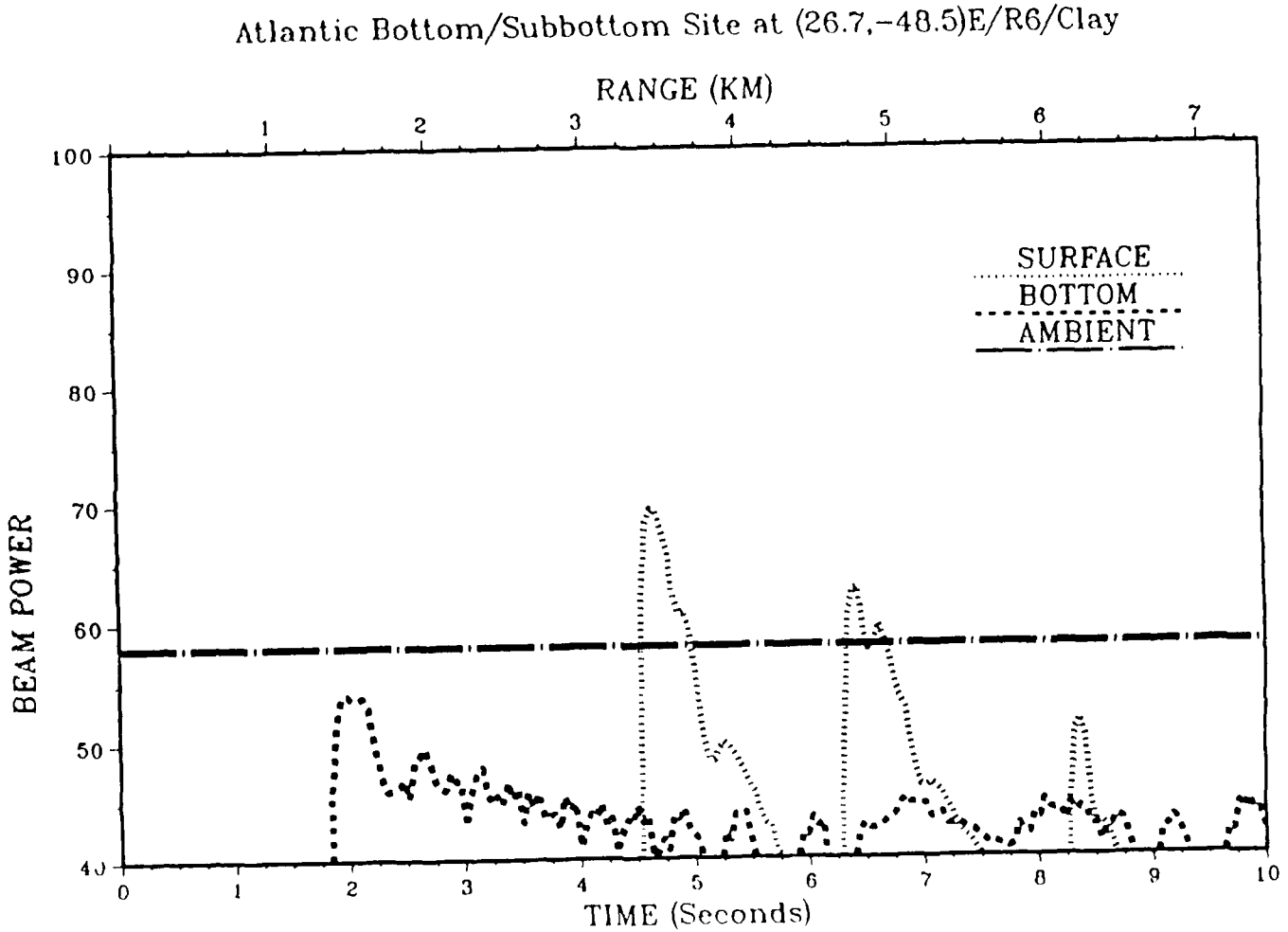
Atlantic Bottom/Subbottom Site at (26.7,-48.5)E/R6/Clay
RANGE (KM)
1
2
3
4
5
6
7
100
90
80
70
60
50
40
BEAM POWER
SURFACE
BOTTOM
AMBIENT
0
1
2
3
4
5
6
7
8
9
10
TIME (Seconds)

Figure 47

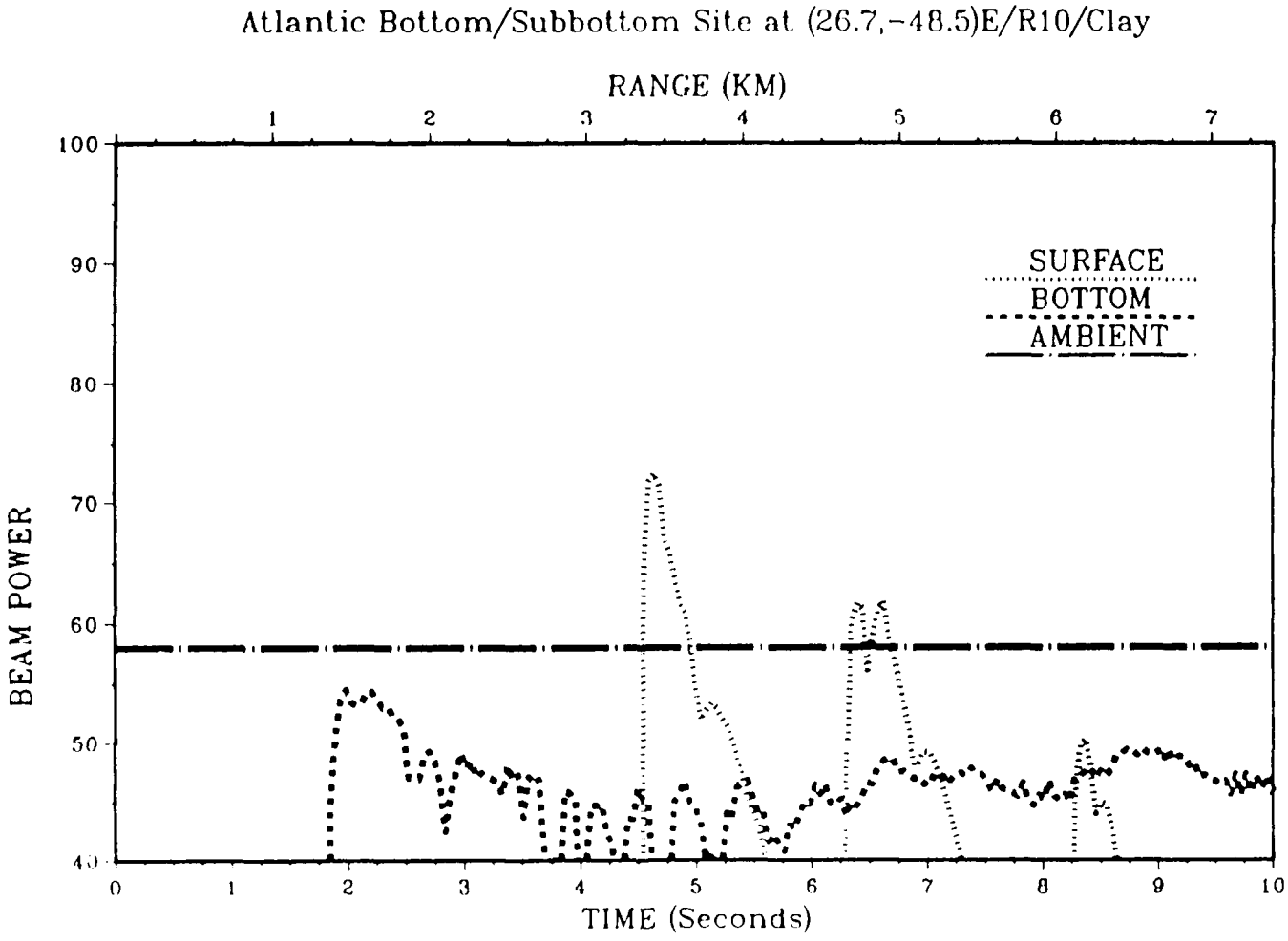
Atlantic Bottom/Subbottom Site at (26.7,-48.5)E/R10/Clay
RANGE (KM)
1
2
3
4
5
6
7
100
90
80
70
60
50
40
BEAM POWER
SURFACE
BOTTOM
AMBIENT
0
1
2
3
4
5
6
7
8
9
10
TIME (Seconds)

Figure 48

Distribution List:

NOARL Internal
Code 113 (B. Adams)
Code 125L (10)
Code 125P
Code 200 (J. Caruthers)
Code 240 (Rick Love)
Code 244 (R. Field)

Office of Naval Research
Code 11250A
ATTN: Marshall Orr
800 N. Quincy Street
Arlington, VA 22217-5000

Scripps Institute of Oceanography
IGPP, A-025
ATTN: J. Orcutt
La Jolla, CA 92093

Massachusetts Institute of Technology
ATTN: A. Baggeroer
77 Massachusetts Ave.
Cambridge, MA 02139

REPORT DOCUMENTATION PAGE

Form Approved
OBM No. 0704-0188

1. Agency Use Only *(Leave blank).*	2. Report Date.	3. Report Type and Dates Covered.
	October 1990	Final

4. Title and Subtitle.
Computer Modeling of Direct Path, Backscattered Bottom Reverberations for the Acoustic Reverberation Special Research Program (ARSRP)

5. Funding Numbers.
Program Element No. 601153N
Project No.
Task No
Accession No. DN250054

6. Author(s).
A. K. Kalra

7. Performing Organization Names(s) and Address(es).
Naval Oceanographic and Atmospheric Research Laboratory
Ocean Acoustics and Technology Directorate
Stennis Space Center, Mississippi 39529-5004

8. Performing Organization Report Number.
NOARL Technical Note 79

9. Sponsoring/Monitoring Agency Name(s) and Address(es).
Office of Naval Research
800 N. Quincy Street
Arlington, VA 22217-5000

10. Sponsoring/Monitoring Agency Report Number.
NOARL Technical Note 79

11. Supplementary Notes.

12a. Distribution/Availability Statement.
Approved for public release; distribution is unlimited.

12b. Distribution Code.

13. Abstract *(Maximum 200 words).*

Quasi-monostatic reverberations, in the general vicinity of the Atlantic natural laboratory area for the Acoustic Reverberation Special Research Program (ARSRP), are simulated using RASP (Range-dependent Active System Performance) modeling code. They are discussed in the context of the bathymetric profiles and lithology, and the short range experiment planned in FY93.

14. Subject Terms.
(U) Ocean Acoustics (U) Reverberation

15. Number of Pages.
67

16. Price Code.

17. Security Classification of Report.	18. Security Classification of This Page.	19. Security Classification of Abstract.	20. Limitation of Abstract.
Unclassified	Unclassified	Unclassified	SAR